Investigation of Phosphorylation and Ligand Binding of the Focal Adhesion Targeting Domain of Focal Adhesion Kinase

Jennifer Lynn Cable

A dissertation submitted to the faculty of the University of North Carolina at Chapel Hill in partial fulfillment of the requirements for the degree of Doctor of Philosophy in the Department of Biochemistry and Biophysics.

Chapel Hill
2011

Approved by:

Dr. Sharon Campbell

Dr. Andrew Lee

Dr. Gary Pielak

Dr. Michael Schaller

Dr. Richard Wolfenden

ABSTRACT

JENNIFER CABLE: Investigation of Phosphorylation and Ligand Binding of the Focal Adhesion Targeting Domain of Focal Adhesion Kinase
(Under the direction of Dr. Sharon Campbell)

Focal adhesion kinase (FAK) is a nonreceptor tyrosine kinase that localizes to focal adhesions upon integrin activation. FAK plays a key role in cell migration, cell cycle progression, and apoptosis. Because of its role in these processes, it is not surprising that FAK is also involved in tumor progression and metastasis. Overexpression of FAK often correlates with increased metastasis. The C-terminal focal adhesion targeting (FAT) domain of FAK is required for proper localization and subsequent activation of FAK. Phosphorylation of the FAT domain at Y926 by Src kinase is believed to delocalize FAK from focal adhesions and promote cell migration, angiogenesis, and tumor metastasis. Because of its role in such important processes, phosphorylation at Y926 is likely to be tightly regulated. Because the inherent conformation of Y926 is not favorable for Src recognition, phosphorylation of Y926 is thought to be regulated by changes in the conformation or dynamics of the region surrounding Y926. However, what regulates these conformational changes is unknown. In this study, we provide evidence that Src-mediated phosphorylation of Y926 is sensitive to pH *in vitro* and reveal a second site of Src-mediated phosphorylation in the FAT domain: Y1008. NMR studies of the FAT domain reveal pH-dependent changes in backbone dynamics in regions shown to be important for phosphorylation.

In addition to understanding how phosphorylation is regulated, we also were interested in investigating how phosphorylation itself affects the characteristics of the FAT domain. To address this issue, we characterized several Y926 mutants of the FAT domain and determined that perturbation of Y926 affects paxillin binding. Therefore, it is likely that phosphorylation is incompatible with paxillin binding, which supports the hypothesis that phosphorylation delocalizes FAK from focal adhesions.

Finally, we have investigated a possible interaction between the FAT domain and the protein talin. This interaction has been proposed as a secondary mechanism by which the FAT domain localizes FAK to focal adhesions. However, we were unable to detect an interaction under our conditions.

ACKNOWLEDGEMENTS

The next 120 pages or so attempt to describe my work over the last six years. Such an attempt is of course preposterous, and as I near the end of what can only be described as a tumultuous roller coaster ride that I hope never to repeat, I can't help but be surprised at how nicely the last six years fit into this neat little package and at how inaccurately they are represented.

This project began with the work of Dr. Kirk Prutzman, and much of what I have done is simply a continuation of his efforts. I would like to thank Dr. Sharon Campbell for taking me into her lab and providing scientific guidance and support. I would also like to thank past and present members of the Campbell Lab. In particular, I would like to thank Dr. Richard Dixon, who I could always depend on to offer his honest opinion and advice, even if I hardly ever followed it, Dr. Sean Palmer, Dr. Moriah Beck, Lauren Mitchell, Aaron Hobbs, Peter Thompson, Rachael Baker, and Kai Shen. Finally, I am deeply indebted to Min-Qi Lu. Min-Qi has helped me with countless protein preps and listened to even more tales of woe.

I would also like to thank my committee for listening to my spiel once a year. Dr. Richard Wolfenden has been a source of constancy and even-mindedness. Dr. Andrew Lee and members of the Lee lab have been instrumental in helping me collect most of the NMR data described in this paper. Dr. Michael Schaller was especially helpful in the beginning of this project as I was just learning about the system and how to do new

experiments. The Schaller lab has always provided biological insight to counter our structural approach. Dr. Gary Pielak has been a source of guidance and reassurance over the years, and I will always appreciate the time he took out of his schedule to offer advice.

I never knew whether I would successfully make it to the end of this endeavor, and while it appears to be nearing some end, success remains a matter of opinion. While I wish that I could claim that some degree of tenacity on my part helped me reach this point, in truth it was the belief that others had in me. I would like to thank my family, my mom, dad, brother, sister, and aunts and uncles for basically reminding me that there is a world outside of graduate school. I would also like to thank my fellow classmates and friends, especially Ron Jack, Grant Murphy, Chrissie Murphy, Erin Heenan, Charles Davis, and Elizabeth Pollom. Each of these people has lent an ear to listen, offered advice and encouragement, and helped me smile and laugh during times when I most needed a friend. Finally, I cannot express in words my gratitude to Doug Renfrew. To say that his support gave me a new sense of meaning in my life would be an understatement.

TABLE OF CONTENTS

LIST OF TABLES

LIST OF FIGURES

CHAPTER 1

INTRODUCTION

Focal Adhesions and Cell Migration

Cell migration plays a key role in many important cellular processes such as wound healing, embryonic development, and immune response. When left unchecked, however, cell migration can lead to tumor invasion and metastasis [2]. Therefore, understanding the mechanisms involved in and the regulation of cell migration will prove invaluable in finding treatments for cancer.

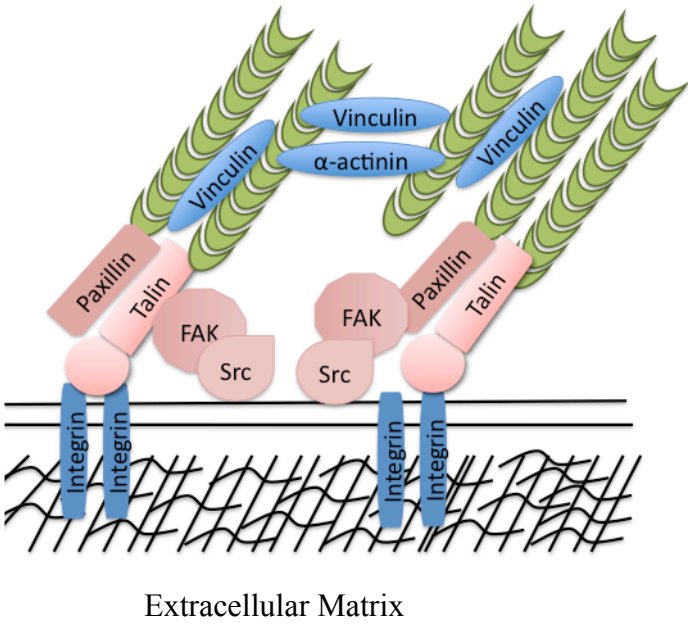

Figure 1.1: Composition of Focal Adhesions
Focal adhesions are formed when integrins engage with the ECM and cluster, causing the recruitment of a variety of proteins which link the ECM to the actin cytoskeleton.

Cells migrate via the assembly and disassembly of integrin-linked sites of attachment to the extracellular matrix (ECM), known as focal adhesions [3]. Focal adhesions are formed when integrins, a type of transmembrane receptor, attach to ECM proteins. This attachment causes integrin clustering and activation, which recruits several proteins such as paxillin, vinculin, talin, α-actinin, and

focal adhesion kinase (FAK) to focal adhesions. As shown in **Figure 1.1**, this complex of proteins links the extracellular matrix to the actin cytoskeleton [4]. The focus of this research is on FAK because it is an important component of focal adhesion organization and signaling pathways involved in cell migration, adhesion, and proliferation.

Biological Role of FAK

FAK was discovered in 1992 as a highly tyrosine-phosphorylated protein tyrosine kinase that localizes to focal adhesions [5, 6]. FAK is expressed in most tissues [6] and is highly conserved across species. Knock-out of FAK in mice results in embryonic lethality with defects that resemble those of fibronectin deficiency [7]. FAK-null cells display a more rounded phenotype than wild type cells and impaired migration. Because FAK-null cells exhibit a greater number of focal adhesions than wild type cells, the defect in cell migration in these cells has been attributed to a loss of focal adhesion turnover rather than a defect in focal adhesion formation [7, 8]. Furthermore, disruption of FAK by siRNA or anti-FAK antibodies induces apoptosis in both fibroblasts and tumor cells [9-12]. While inhibition of FAK leads to decreased migration and increased apoptosis, overexpression of FAK leads to an increase in cell migration in Chinese hamster ovarian (CHO) cells [13] and carcinoma cells [14] and increased angiogenesis in endothelial cells [15]. Therefore, there is strong evidence for a positive role for FAK in cell migration and cell survival.

FAK and Cancer

Due to its role in cell migration, cell cycle progression, and apoptosis, it is not surprising that several lines of evidence have linked FAK to cancer. FAK is overexpressed in several types of cancer including thyroid, prostate, cervix, colon,

rectum, oral epithelium, and ovarian [2, 16], and increased FAK levels are often associated with malignancy and metastasis [16, 17]. While FAK has been implicated in various processes necessary for metastasis and invasion, its precise role in malignancy is unclear. First, FAK has been implicated in the release of matrix metallo-proteinases, which degrade the basement membrane allowing cells to enter the bloodstream and invade other tissues [18]. Furthermore, FAK is linked to the release of vascular endothelial growth factor (VEGF), which controls the growth of new blood vessels necessary for growing tumors [19].

Because of the importance of FAK in cell migration and its connection to invasive, metastatic cancer, inhibition of FAK has become an attractive strategy for treating cancer. Many current cancer treatments are proapoptotic therapies; however, migrating and metastatic cells are generally resistant to apoptosis. Therefore, there is a need for the development of new, anti-migratory treatments to combat and delay metastasis of primary tumors [20]. Inhibition of FAK expression by antisense RNA reduces cell migration and invasion and increases cell death in carcinoma and melanoma cells [21, 22]. Furthermore, inhibition of FAK by siRNA in lung cancer cells decreased migration and the ability to grow in soft agar [23]. These data suggest that FAK could be a therapeutic target for treating cancer. Towards that goal, several small molecule inhibitors of FAK have been developed. Most of these compounds are ATP-competitive inhibitors, which are notoriously nonselective, although studies are underway to generate more selective FAK inhibitors based on allosteric inhibition [24].

Several phase I clinical trials investigating FAK inhibitors have either been completed or are underway (http://clinicaltrials.gov). Many of these results are not yet

public, but of the results that are available, FAK inhibitors seem to be well tolerated. Furthermore, the tyrosine kinase inhibitors dasatinib and bosutinib, which were developed to target the Bcr/Abl kinase and have been approved for the treatment of chronic myeloid leukemia, have been shown to bind to and inhibit FAK [25]. Also, the drug bortezomib, a potent proteasome inhibitor that has been approved for the treatment of multiple myeloma, suppresses FAK expression [26, 27].

The development of FAK kinase inhibitors for the use as cancer therapies is still in its infancy. As mentioned above, it is often difficult to design an inhibitor that is specific for one kinase. Such non-specificity can lead to off-target effects and potentially unwanted side effects. Therefore, it is of interest to understand the molecular mechanisms of FAK regulation, activation, and activity to determine if there are other properties of FAK that can be targeted during drug development, such as disruption of protein/protein interactions or selectively targeting a specific conformation of FAK. Such strategies could potentially target specific functions of FAK that lead to metastasis and invasion while leaving other functions unaffected. Therefore, it is important to understand the structure of FAK and to elucidate how it is regulated either via posttranslational modifications or interactions with other proteins.

Focal Adhesion Kinase

FAK is a nonreceptor tyrosine kinase involved in the assembly and disassembly of focal adhesions [28]. In addition to its kinase activity, it also functions as a scaffolding protein. **Figure 2** shows the domain structure of FAK. FAK consists of an N-terminal FERM (protein 4.1, ezrin, radixin, and moesin homology) domain, a central kinase domain, and a C-terminal focal adhesion targeting (FAT) domain. FAK is recruited to

newly forming focal adhesions upon integrin activation. Interaction of the FERM domain of FAK with integrin tails releases autoinhibitory interactions between the FERM and kinase domains allowing the FERM domain to interact with other protein tyrosine kinases and with actin-associated proteins such as ezrin (See **Figure 2**) [28-32]. The kinase domain is activated by autophosphorylation at Y397, which creates a Src-homology (SH) 2 binding site that is recognized by, among other proteins, Src kinase. After binding to Y397, Src phosphorylates FAK at Y576 and Y577 in the kinase domain, which is necessary for complete kinase activity, and at Y926 in the FAT domain [28, 33]. The FAT domain is responsible for localization of FAK to focal adhesions at least partially through its interaction with the protein paxillin [34]. Phosphorylation at Y926 in the FAT domain creates an SH2 binding site for the growth factor receptor bound protein 2 (Grb2) [28], which is believed to occlude FAK from focal adhesions and link it to the mitogen-activated protein kinase (MAPK) pathway, which is involved in cell proliferation and survival [35, 36]. This research focuses on the FAT domain of FAK as it is essential for proper FAK localization and function and plays a

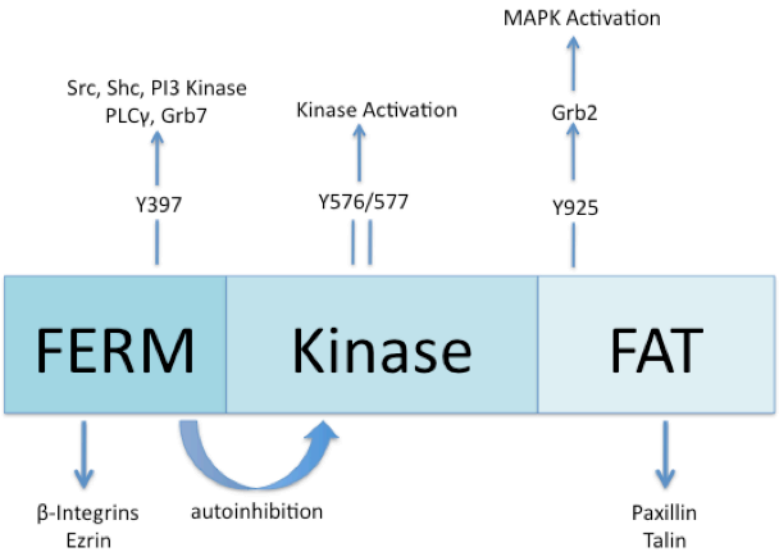

Figure 1.2: Domain Structure of FAK
The FERM domain, kinase domain, and FAT domain are indicated. Proteins that bind to a particular domain are indicated below the domain. Key sites of tyrosine phosphorylation are also shown. Proteins with SH2 domains that bind to the phosphorylated tyrosine residues are shown above the residue.

key role in FAK-mediated signaling pathways.

The FAT Domain: Targeting FAK to Focal Adhesions

The C-terminal FAT domain of FAK is necessary for proper localization of FAK to focal adhesions, which is essential for proper activation and function. Specifically, deletion mutants of FAK that do not contain the C-terminal domain of FAK do not localize to focal adhesions [37], suggesting that the FAT domain is necessary for proper localization. Furthermore, FAK-related nonkinase (FRNK), an autonomously expressed spliced variant of FAK, which contains the C-terminal domain of FAK, and chimeric proteins containing the FAT domain localize to focal adhesions, suggesting that the C-terminal domain of FAK is also sufficient for localization of FAK [37, 38].

While it seems that there are several mechanisms by which the FAT domain can direct proper localization of FAK, the major mechanism seems to be the interaction of the FAT domain with paxillin. The FAT domain is necessary for the interaction between FAK and paxillin, and mutations in the FAT domain of FAK that impair paxillin binding do not localize to focal adhesions whereas FAK constructs that can bind to paxillin do localize to focal adhesions [34].

Paxillin binds to the FAT domain via its LD motifs, named because of the presence of several leucine residues and a key aspartate residue (consensus sequence: LDXLLXXL). Paxillin contains five LD motifs in its N-terminus (LD 1-5), and LD2 and LD4 have been shown to bind the FAT domain. Furthermore, there are two paxillin-binding sites on the FAT domain, termed the 1,4 and 2,3 sites, described in more detail below. While structures of FAT bound to paxillin peptides have been solved, it is unclear how the proteins interact in a larger context, i.e., whether paxillin binds to two FAK

molecules via its LD2 and LD4 motifs or whether the LD2 and LD4 motifs of one paxillin molecule bind simultaneously to one FAK molecule. However, it has been shown that the LD2 and LD4 motifs can simultaneously bind to one FAT molecule *in vitro* and that the 2,3 site in the FAT domain can bind to both LD2 and LD4 whereas the 1,4 site has a stronger preference for LD2 [39, 40]. A model has been proposed in which the LD2 motif binds to the 1,4 site in the FAT domain, paxillin wraps around helices-3 and -4, and the LD4 motif binds to the 2,3 site [40].

While both paxillin binding sites in the FAT domain are necessary for maximal activity of FAK, only one site is required to target FAK to focal adhesions [39]. However, it appears that the two paxillin binding sites are not completely redundant as mutation of the 1,4 site has a more drastic effect on FAK localization than mutation of the 2,3 site, suggesting that the 1,4 site is more important for proper localization of FAK. Interestingly, FAK is still able to localize to focal adhesions upon mutation of both paxillin binding sites, albeit to a lesser extent (~10% of wild type), suggesting that there is a secondary mechanism for FAK localization that is independent of its interaction with paxillin [39].

One possibility for this paxillin-independent mechanism of localization is the interaction of the FAT domain with talin. Talin co-immunoprecipitates with FAK, suggesting an interaction *in vivo* [41, 42], and deletion of residues 965-1012 of FAK, which are in the FAT domain, abrogates binding to talin, suggesting that talin binds to the FAT domain of FAK [41]. Interestingly, Pyk2, a close homolog of FAK that does not localize to focal adhesions does not bind to talin. However, a chimeric protein containing the N-terminal domains of Pyk2 and the C-terminal domain of FAK is able to bind talin

and localize to focal adhesions [42]. These data suggest that talin binding to the FAT domain of FAK may be involved in localization to focal adhesions. However, more recent studies have had difficulties detecting an interaction between FAK and talin [39], and the role for a FAK/talin interaction remains elusive and controversial.

Phosphorylation of Y926

In addition to its role in localization, the FAT domain also plays an important role in FAK signaling via Src-mediated phosphorylation of Y926. Phosphorylation of Y926 has been linked to delocalization of FAK from focal adhesions and focal adhesion turnover due to reports that phosphorylation of a membrane-anchored construct of FAK was shown to exclude FAK from focal adhesions whereas a Y926F variant of FAK remained at focal adhesions [28, 35]. While the mechanism by which phosphorylation occludes FAK from focal adhesions is unclear, it has been proposed that phosphorylation at Y926 disrupts FAK/paxillin interactions leading to delocalization of FAK from focal adhesions and subsequent focal adhesion disassembly [34, 43-45].

Y926 exists in a canonical Grb2 SH2 domain binding motif (YXNX) [46], and phosphorylation at this site creates an SH2 domain binding site for Grb2, linking FAK to the MAPK/ERK pathway [33, 36]. Mutation of Y926 to phenylalanine suppresses ERK activation, which leads to a decrease in VEGF expression and tumor growth and vascularization in breast carcinoma cells [19] as well as decreased metastasis and invasion in melanoma cells [47]. These studies suggest that phosphorylation of Y926 is intimately involved in FAK's role in cancer progression and metastasis and that targeting this site could represent a potential strategy in designing cancer therapeutics.

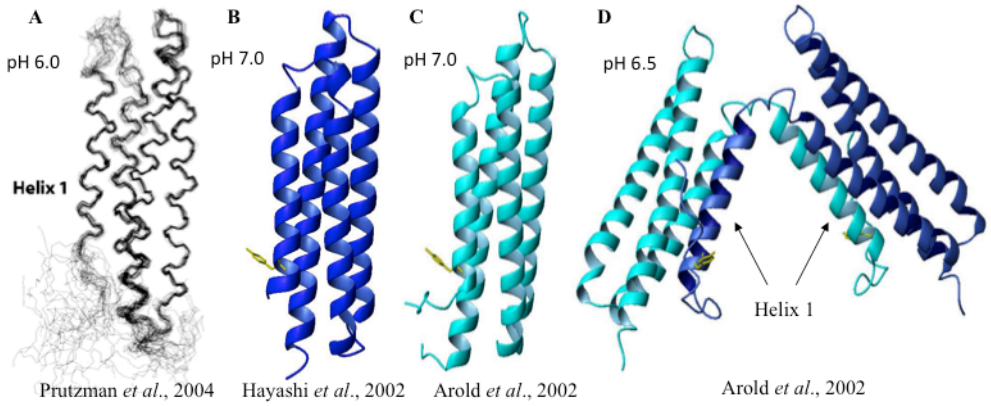

Figure 1.3: Structure of the FAT Domain
Both NMR (A) and crystal (B,C) structures of the FAT domain indicate that it is a four-helix bundle. One crystal structure (D) has been solved in which helix-1 forms a domain-swapped dimer with a second molecule. The site of phosphorylation (Y926) is shown in yellow.

Structure and Dynamics of the FAT Domain

Because of the importance of the FAT domain in FAK localization and signaling, understanding the mechanisms by which the FAT domain is regulated at the molecular level will provide insight into FAK's role in cancer. Both solution state and crystal structures of the FAT domain, shown in **Figure 1.3**, indicate that it forms an anti-parallel four-helix bundle [44, 48, 49]. However, the crystal structure of a domain swapped dimer **(Fig. 1.3D),** in which helix-1 partitions away from the four helix bundle and packs against the other three helices of a second FAT molecule, has also been reported [48]. The observation of the domain-swapped dimer caused the authors to speculate that the mechanism involved in forming the dimer, i.e., the opening of helix-1, would result in exposure of Y926, rendering this residue more accessible for phosphorylation by Src and for binding to Grb2.

While it is unclear whether the domain-swapped dimer represents a biologically-relevant species, there is evidence that helix-1 has a propensity to partition from the four-helix bundle in solution. NMR studies of the FAT domain indicate that residues in the

loop between helix-1 and helix-2 are broadened at 25°C and become more narrow at 37°C, indicating that this region is in exchange between two or more conformations on the NMR timescale and that helix-1 may be conformationally flexible in solution [49]. To further investigate the conformational flexibility of helix-1 in the FAT domain, our lab used a combination of hydrogen exchange (HEX) and discrete molecular dynamics (DMD) to visualize intermediate conformations that may only be weakly populated in solution. **Figure 1.4** shows the folding intermediate observed in the DMD simulations in which helix-1 partitions from the four-helix bundle [50]. For comparison, the monomer from the domain-swapped dimer is also shown. In both of these species, helix 1 has partitioned away from the four-helix bundle. In addition, a "hidden folding intermediate" similar to that detected in the wild type FAT domain [50] has been detected in a Y926E mutant of the FAT domain, which was used to mimic the phosphorylated form. These studies included hydrogen exchange experiments as a function of denaturant to detect the presence of folding intermediates and stopped-flow fluorescence to investigate the kinetics of folding. The intermediate state was determined to be ~4 kcal/mol more stable than the unfolded states and represents ~0.1% of the population [51]. The domain-swapped dimer, solution structure, and hydrogen exchange and molecular dynamics data support the idea that the FAT domain can adopt two conformations: a closed form with helix-1 packed in the helix bundle and an open form with helix-1 partitioned away from the bundle.

The partitioning of helix-1 is likely facilitated by strain caused by a series of proline residues (PAPP) in the loop between helices-1 and -2; the partitioning of helix-1 serves to relieve this strain. Proline residues are often found in the hinge regions of

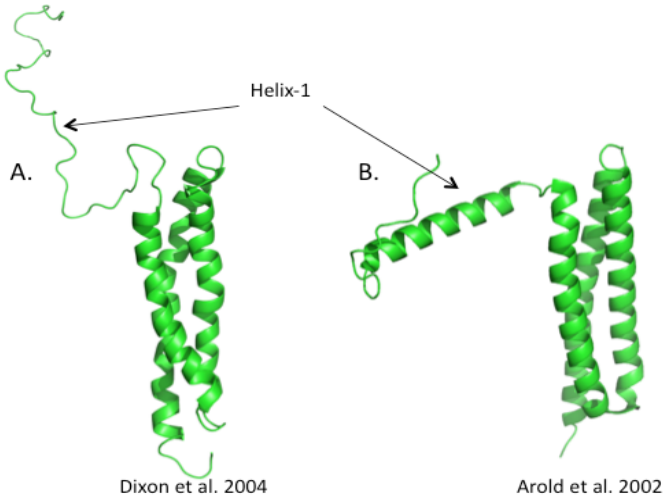

Figure 1.4: Intermediate of the FAT Domain:
A. Intermediate of the FAT domain detected by HEX-directed DMD. In this intermediate, helix 1 is partitioned away from the four-helix bundle. **B.** One of the monomers from the crystal structure of the domain-swapped dimer (See Figure 1.3). In this structure as well, helix 1 is partitioned away from the four-helix bundle.

domain swapped dimers due to their unique characteristics. First, because the proline side chain is covalently bonded to the backbone, it can adopt a limited number of phi/psi angles. Second, because prolines lack an amide hydrogen, it cannot participate in hydrogen bonds and is often excluded from normal secondary structural elements. Finally, proline is the only amino acid that restricts the conformation of the residue preceding it, thus introducing conformational flexibility in two consecutive residues [52]. Proline-induced domain swapping has been observed in $p13^{suc1}$ [53], RNaseA [54], and bleomycin resistance protein [52]. Therefore, it seems likely that the series of proline residues in helix-1 of the FAT domain could promote the partitioning of helix-1 from the four-helix bundle. We have dubbed the loop between helices-1 and -2 a putative "hinge region" and speculated that dynamics in the hinge region may regulate the partitioning of helix-1 from the four-helix bundle.

Functional Consequences of Conformational Dynamics

If the FAT domain can exist in two distinct conformations (open and closed), the question remains whether these two conformations are distinct functionally. Several

structures of the FAT domain bound to peptides mimicking the paxillin LD motifs have been solved [43, 55, 56]. **Figure 1.5** shows the NMR structure of the FAT domain bound to a 28-mer peptide that mimics the LD2 motif of paxillin. One of the paxillin binding sites is in a hydrophobic groove between helices-1 and -4 while the other site is in a hydrophobic groove between helices-2 and -3.

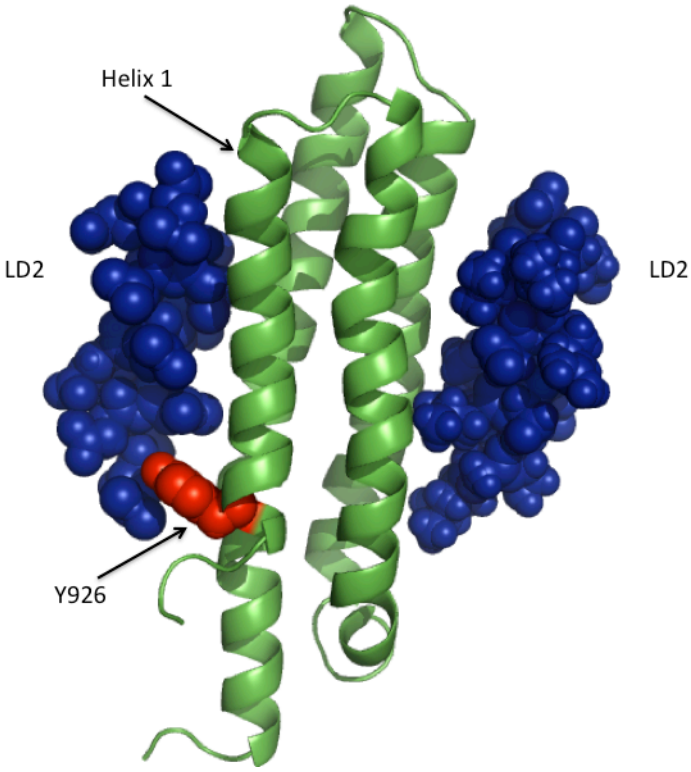

Figure 1.5: Solution Structure of FAT Bound to LD2 peptides
The FAT domain (green) bound to two LD2 peptides (blue, spheres) (PDB 1QVX). LD2 binds to the 1,4 site (left) and 2,3 site (right) on the FAT domain. Y926 is shown in red to demonstrate how paxillin binding is expected to occlude phosphorylation at Y926.

If helix-1 partitions away from the bundle to form the open conformation, as has been suggested based on NMR and DMD [50, 51] data as described above, this would likely disrupt paxillin binding. Therefore, the closed form of the FAT domain is likely the form that is involved in paxillin binding. On the other hand, the open form of the FAT domain would be expected to expose Y926. Previous studies have indicated that Y926 is difficult to phosphorylate *in vitro* [48], suggesting that this residue is not in a conformation that is easily recognized by Src kinase. Indeed, crystal structures of kinases bound to substrate peptides indicate that the substrate is in an extended conformation. For example, crystal

structures of the tyrosine kinases insulin receptor tyrosine kinase (IRK), epidermal growth factor receptor (EGFR), and Abelson leukemia tyrosine kinase (Abl) bound to substrate peptide analogs reveal that the substrate adopts an extended β-strand conformation that forms an antiparallel β-strand interaction with the activation loop of the kinase [57, 58]. Perhaps more relevant, an NMR structure of the substrate peptide immunoreceptor tyrosine-based activation motif (ITAM) bound to Lyn kinase, a Src-family kinase, reveals that ITAM adopts an irregular helix conformation in which the side chains are oriented in the same direction [59]. The site of phosphorylation in the FAT domain is in a helix, which, based on the previous structural data mentioned above, is not conducive to recognition and phosphorylation by Src kinase. One hypothesis for how Y926 is phosphorylated is that the partitioning of helix-1 causes the helix to become disordered and thus a better substrate for Src. Therefore, based on the structural data described above, it appears that when in the closed form, the FAT domain is able to bind paxillin and localize to focal adhesions whereas in the open form, the FAT domain is more readily phosphorylated at Y926, which results in delocalization from focal adhesions.

Once the FAT domain is phosphorylated, conformational dynamics are also expected to play a role in its function. Phosphorylation at Y926 creates a binding site for the SH2 domain of Grb2; however, this site is not in a conformation that is easily recognizable by Grb2. Structures of peptides bound to Grb2 indicate that the peptide exists in a compact, type I β-turn conformation [60-62]. The SH2 domain of Grb2 is unique among SH2 domains in that a tryptophan residue in the specificity-determining loop closes the binding cleft and forces the substrate to adopt a β-turn conformation in

which the pY and the N+2 are near each other. In addition, difficulties in observing a direct interaction between Grb2 and the FAT domain have been reported, and an interaction was only observed upon denaturation of the phosphorylated FAT domain, suggesting that Y926 is not inherently in a conformation that is conducive to Grb2 binding [48]. Therefore, while it appears that helix-1 must adopt an extended conformation to be phosphorylated by Src, the phosphorylated form must also adopt a distinct conformation to bind Grb2.

In summary, several lines of evidence suggest that inherent conformational dynamics of the FAT domain regulate phosphorylation and ligand binding. The conformation of the FAT domain that is likely to be conducive to phosphorylation and Grb2 binding (open form) is a minor species in solution. Therefore, we postulate that the cell has a mechanism that promotes a distinct or open form of the FAT domain to facilitate phosphorylation by Src or Grb2 binding. However, the identity of this mechanism remains a mystery. We postulate that pH may be a mechanism for regulating conformational dynamics of the FAT domain, which in turn modulates phosphorylation and ligand binding. To test this hypothesis, we have examined the role of pH on the dynamics of the FAT domain and how pH-dependent dynamics affect the stability and phosphorylation of the FAT domain.

pH and Cell Migration

Cells must establish a spatial and temporal polarity to achieve directed migration. One of the suggested mechanisms by which the cell achieves this is the establishment of a pH gradient. Both extracellular and intracellular pH gradients have been observed in migrating cells [63, 64]. Depending on the cell type, the intracellular pH of the leading

edge of the cell was found to be more basic than the trailing edge by 0.05 to 0.16 pH units [63], and the extracellular pericellular proton concentration increased by a factor of two at the leading edge of cells compared to the trailing edge [64]. These gradients are achieved by localization of the sodium/proton exchanger 1 (NHE1) to the leading edge of migrating cells. NHE1 regulates intracellular pH by exchanging intracellular protons for extracellular sodium ions. Its ion-transport activity is essential for establishing cell polarization, protrusion, and adhesion [65]. Furthermore, NHE1 co-localizes with vinculin and talin, common focal adhesion markers [66], and FAK has been implicated in regulating proper localization of NHE1 [67].

Changes in intracellular pH have been proposed to promote cell proliferation [68], to initiate and direct cell migration [65], and to trigger apoptosis [69], though the exact role of pH changes in these processes remains controversial [70]. An increase in cytosolic pH (0.3-0.5 units) has been shown to promote directed cell migration by promoting focal adhesion remodeling through the regulation of actin filament assembly, bundling, and cell adhesion [71, 72] and is a hallmark of transformed cells and a common characteristic of many different cancers. In contrast, a decrease in cytosolic pH (0.3-0.4 units) promotes apoptosis [71].

The processes by which pH regulates cell migration remain to be fully elucidated. However, the activities and interactions of several proteins associated with migration have been shown to be pH dependent, and the structural mechanisms for these pH dependencies have been investigated. For example several proteins that localize to actin-rich structures, such as cofilin, villin, and talin, have been shown to be sensitive to changes in pH. In the case of cofilin, its actin-severing activity increases whereas it

ability to bind phophoinositides decreases as the pH increases. Its sensitivity to pH is thought to result from disruption of a salt bridge between His 133 and Asp 98 between pH 6.9 and 7.2. Because NMR data and MD simulations indicate that any pH-dependent structural changes are subtle and localized, it is believed that de/protonation of His 133 directly affects actin binding because this residue lies in the actin binding site [64, 71]. Another actin-associated protein that is sensitive to pH is villin. At pH 6.5, CD, NMR, and hydrogen-exchange data indicate that the N-terminus of villin is unstructured. Raising the pH causes the N-terminus to fold, which stabilizes the C-terminal actin-binding domain. It is thought that a positive charge on H41 at low pH destabilizes hydrophobic packing, causing the N-terminus to become unstructured. When the histidine is deprotonated, this instability is relieved, and the domain can fold [71]. Finally, the talin has been shown to bind to actin in a pH-dependent manner. It has a lower affinity for actin at higher pH. Molecular dynamics and NMR have revealed a region of titratable amino acids with upshifted pK_a values in a region distal from the actin binding site. It is believed that protonation of H418 in this region changes the conformation and dynamics of the actin binding site, thus affecting the binding affinity. The pH-dependent talin-actin interaction could play a role in focal adhesion remodeling and therefore in cell migration.

pH and the FAT Domain

Due to the role of intracellular pH in cell migration and adhesion and the link between NHE1 and focal adhesion proteins, including FAK, it is possible that pH plays a role in FAK regulation *in vivo*. While it is unclear if pH plays a role in the regulation of

the FAT domain *in vivo*, we have *in vitro* data that suggest that the structure, dynamics, and function of the FAT are sensitive to pH within physiological limits.

One of the main differences between the solution structure of the FAT domain and current crystal structures is pH. The solution structure of the FAT domain was solved at pH 6.0 while the crystal structures were solved at pH 7.0 for the monomer and at pH 6.5 for the domain swapped dimer (See **Figure 1.3)**. While the solution and crystal structures are very similar, there are some differences. The main structural difference between the solution and crystal structures lies in helix-1; there is an extra turn in helix-1 between helices-1 and -2 in the crystal structure. Whether this difference is a result of crystal packing or of a pH dependent conformational change is unclear. However, as described above, the loop between helix-1 and -2 has been shown to be conformationally flexible, and this flexibility has been implicated in regulating phosphorylation of Y926 [49, 50]. Therefore, if the region between helices-1 and -2 in the FAT domain is sensitive to pH, then it is possible that phosphorylation of Y926 could be regulated by pH. Understanding how phosphorylation of Y926 is regulated *in vitro* could lead to insights regarding how this site is regulated *in vivo* and help elucidate how FAK and specifically phosphorylation at Y926 is involved in cell migration and metastasis.

Conclusion

In conclusion, several lines of evidence confirm that conformational dynamics of the FAT domain are important for the regulation of FAK function. While it is currently unclear how these dynamics are regulated in the cell, we have characterized pH-dependent conformational dynamics *in vitro* and provide evidence that pH-induced changes in dynamics promote changes in phosphorylation of the FAT domain. A second

goal of this work is to understand how phosphorylation itself affects the structure and dynamics of the FAT domain. Due to complications arising from a secondary phosphorylation site, we could not isolate and characterize conformational and dynamic properties of FAT singly phosphorylated at Y926. However, we have been able to characterize how changes via mutation at position 926 affect the stability of the FAT domain and its ability to bind paxillin. Amino acid substitution of asparate or glutamate at this position was used to mimic the phosphorylated form of FAT whereas a Y926F mutant was employed to determine how a non-phosphorylatable mutant affects FAT function *in vitro*. We discovered that mutation of Y926 to any of several residues disrupts paxillin binding, suggesting that any perturbation at this site, for example phosphorylation, is likely to disrupt paxillin binding as well. Because paxillin binding is important for proper localization of FAK, disruption of paxillin binding could lead to delocalization of FAK from focal adhesions. Finally, we have also investigated interactions between the FAT domain of FAK and the F3 domain of talin as binding to talin has been proposed as a paxillin-independent mechanism for FAK localization.

CHAPTER 2

pH AND THE FAT DOMAIN

Introduction

All proteins depend on pH to maintain their proper structure and function. It is therefore not surprising that the cytosolic pH is tightly regulated by several ion pumps that pump protons into and out of the cell. While the main purpose of these pumps may be to maintain pH homeostasis, they also create localized pH gradients and fluctuations, which could act as a signal by altering the structure, activity, and interactions of proteins. In fact, the activities of several proteins involved in actin-mediated cell migration such as cofilin [64, 71], villin [71], and talin [72] are sensitive to pH. While the biological consequences of these proteins' sensitivity to pH remain to be fully elucidated, changes in intracellular pH have been proposed to promote cell proliferation [68], to initiate and direct cell migration [65], and to trigger apoptosis [69].

pH gradients are proposed to be one of the mechanisms by which cells establish the spatial and temporal polarity necessary for directed migration. Both extracellular and intracellular pH gradients have been observed in migrating cells [63, 64]. These pH gradients are achieved by localization of the sodium/proton exchanger 1 (NHE1) to the leading edge of migrating cells [63]. At the leading edge, NHE1 co-localizes with vinculin and talin, common focal adhesion markers [66], and regulates intracellular pH

by exchanging intracellular protons for extracellular sodium ions. Its ion-transport activity is essential for establishing cell polarization, protrusion, and adhesion [65].

Due to the role of intracellular pH in cell migration and adhesion, the link between NHE1 and focal adhesion proteins, and the pH sensitivity of several proteins involved in migration, we investigated the pH sensitivity of the focal adhesion targeting (FAT) domain of focal adhesion kinase (FAK). FAK is a non-receptor tyrosine kinase that localizes to focal adhesions upon integrin activation, and the C-terminal FAT domain is necessary for proper localization and subsequent activation of FAK [37, 38]. The FAT domain localizes FAK to focal adhesions at least partially via its interaction with the protein paxillin. Phosphorylation of Y926 in the FAT domain has been linked to delocalization of FAK from focal adhesions. In addition to its role in localization, the FAT domain is also involved in FAK-mediated signaling pathways. In particular, phosphorylation of Y926 in the FAT domain has been shown to activate the MAPK pathway [19], which promotes angiogenesis [19] and tumor invasion and metastasis [47]. Several labs have proposed that Y926 is not conducive to phosphorylation by Src based on its conformation [48, 49]. Therefore, the cell likely has a mechanism to promote phosphorylation of Y926, presumably by regulating the conformation of the region surrounding Y926. In this paper, we investigate the role of pH on the conformation and dynamics of the FAT domain and how changes in pH affect phosphorylation. While it is unclear if pH plays a role in regulation of the FAT domain *in vivo*, we have *in vitro* data that suggests that the structure, dynamics, and function of the FAT are sensitive to pH within physiological limits.

In this study, we investigated the role of pH on the phosphorylation, structure, and dynamics of the FAT domain *in vitro*. Our data indicate that there are two sites of Src-mediated phosphorylation *in vitro*: Y926, which has been shown to modulate FAK function by linking FAK to the MAPK pathway [19], and Y1008, which has no known biological function. Interestingly, the pH-dependent phosphorylation profiles of these two sites are different. Furthermore, Src-mediated phosphorylation of two synthetic peptides containing the sites of phosphorylation differ do not show a pH dependence, suggesting that it is the structure of the FAT domain and not Src activity that is affected by pH. To explore the mechanism by which pH affects the FAT domain, we investigated the effect of pH on the structure and dynamics of the FAT domain using circular dichroism (CD) and NMR. CD analyses reveal that the stability of the FAT domain is sensitive to pH; the FAT domain becomes less stable as the pH is increased from pH 5.5 to pH 7.5. NMR-derived short-range distance (NOE) and long-range orientation (residual dipolar coupling (RDC)) constraints do not support a pH-dependent structural change in the FAT domain; however, analysis of the ^{1}H-^{15}N HSQC spectra reveals pH-dependent changes in backbone dynamics near the two sites of phosphorylation. These data indicate that the backbone dynamics of the FAT domain are sensitive to pH and that pH-dependent changes in dynamics could lead to the observed changes in phosphorylation of the FAT domain *in vitro*. It will be interesting to examine whether pH changes *in vivo* could regulate phosphorylation of the FAT domain and modulate FAK function.

Results/Discussion

Phosphorylation as a function of pH

Phosphorylation of Y926 in the FAT domain has been implicated in excluding FAK from focal adhesions [73] and has been linked to promoting cell adhesion, migration, and invasion *in vitro* and metastasis *in vivo* [47]. Therefore, understanding how phosphorylation of Y926 affects FAK signaling on a molecular level may provide key insights into how this site is involved in FAK-mediated cancer progression. We were interested in characterizing the phosphorylated species of the FAT domain because previous data from our lab and others have suggested that a structural rearrangement is necessary for recognition of the phosphorylated species by Grb2 [44, 49, 51]. We phosphorylated the FAT domain *in vitro* using purified Src kinase domain varying several conditions, one of which was pH, to optimize the levels of *in vitro* phosphorylation. Levels of phosphorylation were detected by Western blot, and the site of phosphorylation was verified by mass spectrometry (MS). As shown in **Figure 2.1**, the levels of FAT phosphorylation, as detected by both a general tyrosine and a phospho-Y926-specific antibody increase as the pH is raised from 5.5 to 7.5. This result is not surprising as the level of Src activity also increases from pH 5.5 to 7.5 as indicated by the increased levels of Src autophosphorylation (**Figure 2.1**).

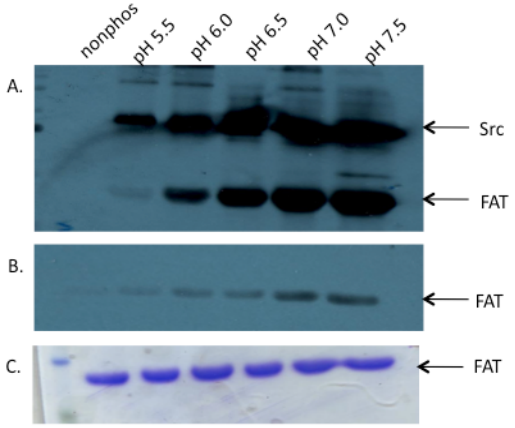

Figure 2.1: Detection of Phosphorylation by Western Blot
The FAT domain was phosphorylated *in vitro* by Src kinase at pH 5.5, 6.0, 6.5, 7.0, and pH 7.5. **A.** Detection of phosphorylation with a general phosphotyrosine antibody. **B.** Detection of phosphorylation with a pY926 antibody. **C.** Coomassie-stained gel showing consistent loading of the FAT domain. Both the pTyr and the pY926 antibodies indicate higher levels of phosphorylation as the pH is increased.

We verified the site of phosphorylation by MS. Several MS techniques were employed to find a technique that was appropriate for determining the site of phosphorylation. First, the full-length protein was analyzed by microelectrospray fourier transform ion cyclotron resonance mass spectrometry (μFTICR ECD MS) by Dr. Li Zhou in the laboratory of Dr. Xian Chen at UNC-CH. After incubation with Src, the mass of the FAT domain increased by 80 Da, consistent with a single phosphorylation event. A representative spectrum is shown in **Figure 2.2A**. Typically, we observe approximately 30% phosphorylation after overnight incubation with Src. We used both bottom-up and top-down approaches to verify the site of phosphorylation. For the bottom-up approach, the sample was subjected to trypsin digestion and analyzed by matrix-assisted laser desorption/ionization (MALDI) by Dr. Viorel Mocanu at the UNC Proteomics Core Facility. For the top-down approach, the sample was analyzed by μFTICR ECD MS/MS by Dr. Li Zhou in the laboratory of Dr. Xian Chen (data not shown). In both of these approaches, two phosphorylation sites were detected: Y926 and Y1008. **Figure 2.2B** shows a representative spectrum from the MALDI analysis showing peptides that correspond to phosphorylation at Y926 and Y1008. As stated above, analysis of the full-length FAT domain by MS indicates a single phosphorylation event. Therefore, even though there are two sites of phosphorylation, it appears that, under our conditions, the occurrence of a doubly phosphorylated FAT molecule is quite rare. We currently do not have an explanation for this observation as the two phosphorylation sites are on opposite ends of the molecule, and it isn't apparent why phosphorylation at one site should preclude phosphorylation at the other. Alternatively, the fact that we detect only a singly

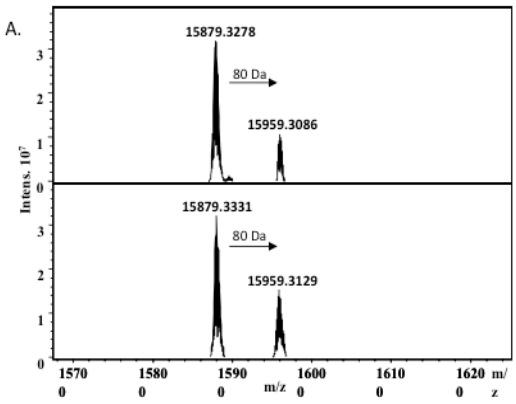

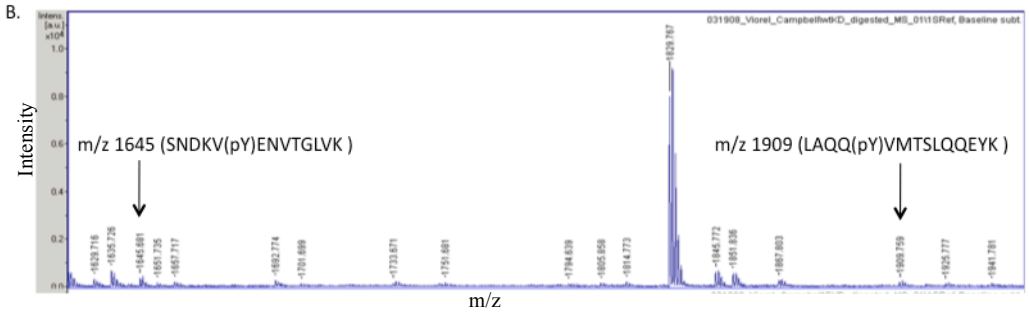

Figure 2.2: Detection of Phosphorylation by Mass Spectrometry
A. The FAT domain was phosphorylated *in vitro* at pH 5.5 (top) and pH 7.5 (bottom). Phosphorylation was detected by μFTICR ECD MS. **B.** The phosphorylated FAT domain was subjected to trypsin digestion and analyzed by MALDI MS. Two phosphorylated peptides were detected, one containing Y926 (m/z 1645) and one containing Y1008 (m/z 1909). These peptides were not detected in the unphosphorylated protein (data not shown).

phosphorylated species could simply be a statistical phenomenon. After incubation with Src overnight, only about 30% of the FAT domain is phosphorylated. Therefore, one can imagine that, during the reaction, it is more likely for Src to encounter a non-phosphorylated species than a phosphorylated species. Furthermore, there are two ways to phosphorylate the non-phosphorylated species (at Y926 and at Y1008) whereas there is only one way to phosphorylate a singly phosphorylated species. Therefore, phosphorylation of a previously phosphorylated species would be a rare event.

Because there were two sites of phosphorylation *in vitro*, we decided to quantify the relative levels of each site to determine whether Y926 was the major site of phosphorylation. We subjected the phosphorylated samples to trypsin digestion and analyzed the peptides by reverse-phase LC/MS/MS. To quantify the relative and absolute levels of phosphorylation at Y926 and Y1008, we spiked each sample with an internal standard: a synthetic phosphorylated peptide that mimics the tryptic peptide of each

phosphorylation site and contains a ^{13}C-labeled valine residue in order to distinguish it from the sample peptide. Because we observed missed-cleavage peptides by LC/MS, two tryptic peptides were synthesized for each phosphorylation site: Y926: SNDKV(pY)ENVTGL(V^{13}C5)K-OH and V(pY)ENVTGL(V13C5)K-OH, Y1008: LAQQ(pY)(V^{13}C5)MTSLQQEYK-OH and MKLAQQ(pY)(V13C5)MTSLQQEYK-OH. We phosphorylated the FAT domain *in vitro* at pH 5.5, 6.0, 6.5, 7.0, and 7.5 and analyzed the reactions by LC/MS using the synthesized peptides described above as internal standards at concentrations of 0.1, 0.2, 1, and 2 μg/mL. **Figure 2.3A-D** shows the spectra of the peptide SNDKV(pY)ENVTGLVK-OH in the +2 charge state (m/z 823) and corresponding heavy internal standard (m/z 826) at different concentrations for the phosphorylation reaction at pH 5.5. **Figure 2.3E** shows the calibration curve generated by plotting the log of the normalized peak area (area of sample/area of standard) versus the concentration of the internal standard for the +2 charge state of the peptide containing Y926 at pH 5.5. The x-intercept of this graph represents the amount of phosphorylation in this sample.

A standard curve similar to the one shown in **Figure 2.3E** was generated for the +2 and +3 charge states for peptides phosphorylated at Y926 and Y1008 at pH 5.5, 6.0, 6.5, 7.0, and 7.5 to calculate the levels of phosphorylation at each site. Figure **2.4** shows the level of phosphorylation as a function of pH for Y926 (red) and Y1008 (blue). At pH 5.5, phosphorylation of Y926 is low (0.75 ± 0.04 μg/mL). At pH 6.0, the levels of phosphorylation have increased to 1.6 ± 0.2 μg/mL. The level of phosphorylation stays relatively constant from pH 6.0 to 6.5 before decreasing to 0.9 ± 0.5 μg/mL at pH 7.0 and 0.4 ± 0.2 μg/mL at pH 7.5. The pH profile for phosphorylation of Y1008 is slightly

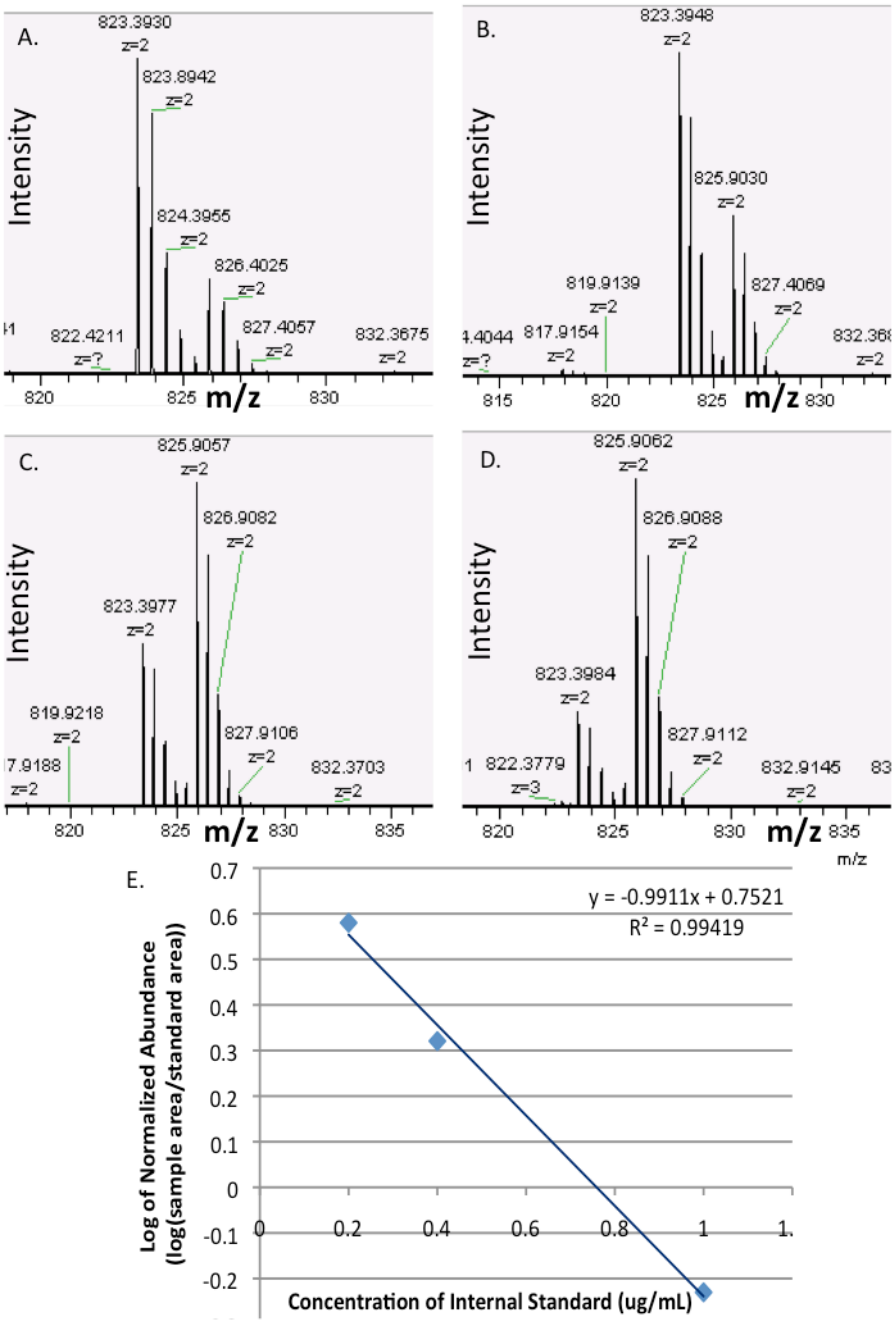

Figure 2.3: Site-specific quantitation of phosphorylation using internal standards
A-D. Spectra of the +2 charge state of the peptide containing phosphorylated Y926 (m/z 823) and the heavy internal standard (m/z 826) at **A.** 0.1 µg/mL, **B.** 0.2 µg/mL, **C.** 1 µg/mL, and **D.** 2 µg/mL of the internal standard for the phosphorylation reaction at pH 5.5 **E.** Calibration curve used to calculate the level of phosphorylation of Y926 at pH 5.5. The log of the normalized peak area (area of sample/area of standard) is plotted against the concentration of the internal standard. The x-intercept of this graph represents the amount of phosphorylation in the sample.

different. As seen for phosphorylation of Y926, phosphorylation of Y1008 increases as the pH is raised from 5.5 to 6.0 (from 0.5 ± 0.2 to 2.3 ± 0.1 µg/mL). However, whereas phosphorylation of Y926 remains constant from pH 6.0 to 6.5, phosphorylation of Y1008 increases to 2.85 ± 0.06 µg/mL. As seen for Y926, phosphorylation of Y1008 decreases from pH 6.5 to 7.5 (0.5 ± 0.1 µg/mL at pH 7.5).

To distinguish whether the observed pH-dependent phosphorylation of the FAT domain is a result of the sensitivity of Src activity to pH or to pH-dependent changes in the FAT domain, we phosphorylated two synthetic peptides *in vitro*, one of which contains Y926 whereas the other contains Y1008, (SNDKV^{926}YENVTGLVK-OH and MKLAQQ^{1008}YVMTSLQQEYK-OH) at pH 5.5, 6.0, 6.5, 7.0, and 7.5 and subjected them to the same analysis as the full-length protein. These peptides are expected to be unstructured, and therefore their structure should not be influenced by pH. **Figure 2.5** shows the pH profile of phosphorylation of the synthetic peptides. The phosphorylation of Y926 is relatively insensitive to pH whereas phosphorylation of Y1008 has a maximum value at pH 7.0. It is unclear why the two peptides show different pH profiles. One reason may be that the phosphorylation levels for Y926 are so much greater than those of Y1008 (~100 fold) that any pH dependence is effectively masked. For both peptides, we detected the nonphosphorylated peptide, indicating that the reaction did not go to completion; however, it is possible that the phosphorylation reaction with the Y926 peptide reached a maximum value and that, if we had taken samples at an earlier time point, pH-dependent changes in phosphorylation would have been observed. However, one must also be careful not to read too much into the pH-dependence of Y1008. The levels of phosphorylation are very low, and because we only conducted a one-point calibration, the quantitation of the of the peptides may not be as accurate as that of the full-length protein (**Figure 2.4**). Therefore, we contend that the pH dependent phosphorylation of the peptides is negligible, and even if one were to propose that Y1008 shows a pH optimum of 7.0, this value is different than the optimum pH in the context of the full-length protein (pH 6.5). Therefore, we conclude that the pH-dependent phosphorylation observed in the full-length FAT

domain is a result of a pH-dependent change in the conformation or dynamics of the FAT domain and not Src activity.

Interestingly, in the context of the peptide, Y926 is phosphorylated to a greater extent than Y1008 (~100 fold). This result differs from the full-length protein in which levels of phosphorylation of the two sites were either comparable or Y1008 was the major site, depending on pH. The fact that the Y926 peptide is phosphorylated to a greater extent

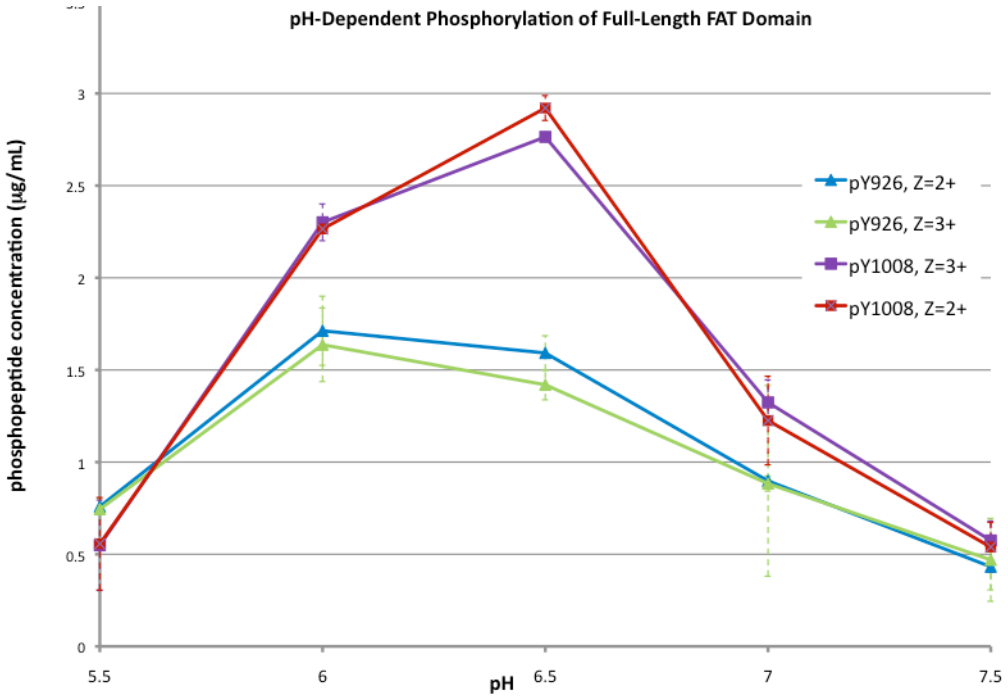

Figure 2.4: Site-Specific Quantitation of Phosphorylation
The FAT domain was phosphorylated *in vitro* with Src kinase at pH 5.5, 6.0, 6.5, 7.0, and 7.5. The levels of phosphorylation at Y926 and Y1008 were quantified as described in the text. In the context of the full-length protein, Y1008 is a better substrate for Src than Y926 as the levels of phosphorylation at Y1008 are either similar to or higher than the levels of phosphorylation at Y926 for all the pH values tested. Optimum phosphorylation of Y926 occurs at pH 6.0 whereas optimum phosphorylation of Y1008 occurs at pH 6.5.

than the Y1008 peptide is consistent with the fact that Y926 is the biologically relevant site of phosphorylation and that, in the absence of structure, the sequence surrounding Y926 is a better substrate for Src than the sequence surrounding Y1008.

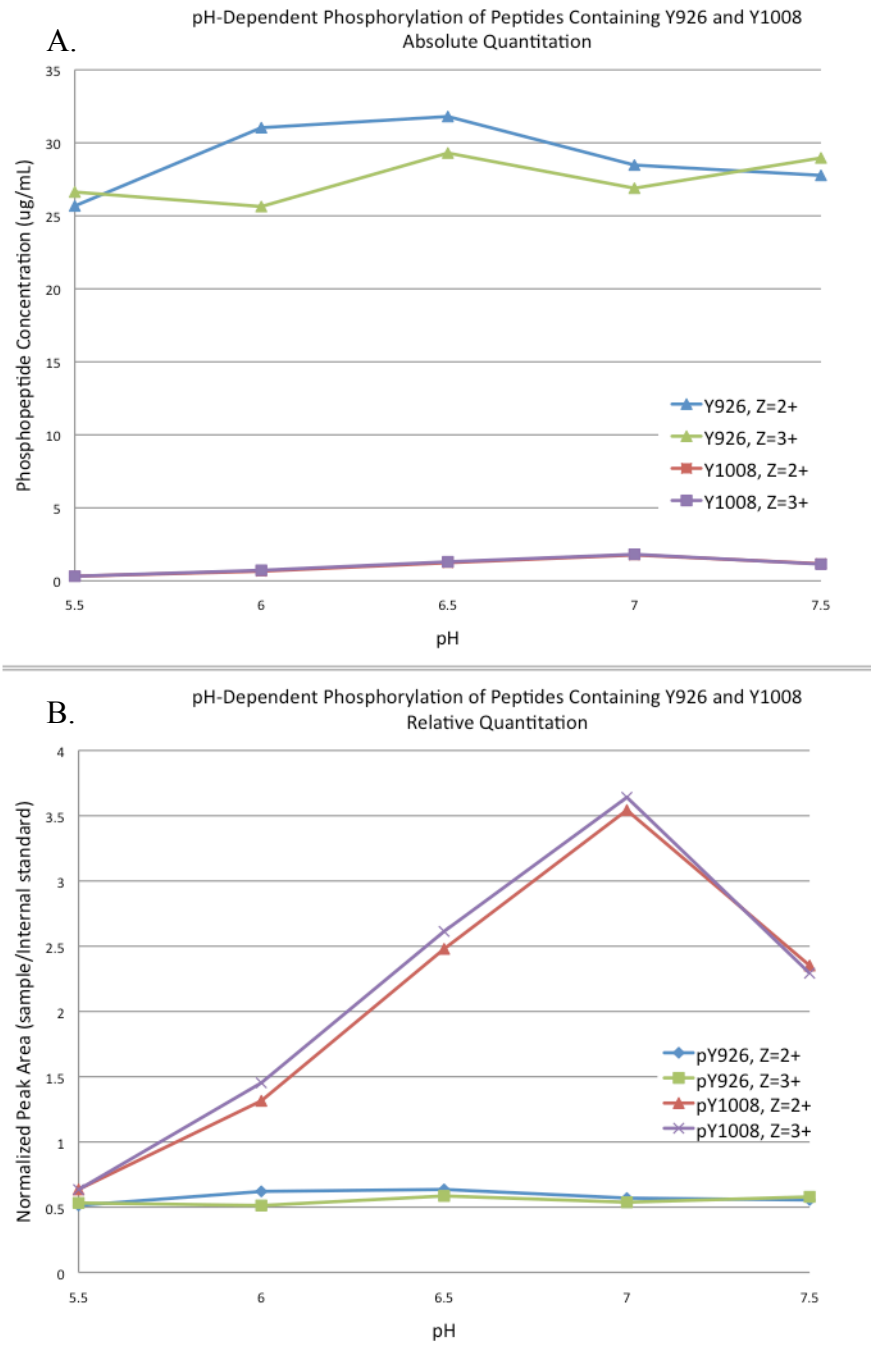

Figure 2.5: Phosphorylation of Synthetic Peptides as a Function of pH
Synthetic peptides containing Y926 and Y1008 of the FAT domain were phosphorylated *in vitro* as a function of pH and analyzed by mass spectrometry as described in the text. **A.** Absolute quantitation of phosphorylation at Y926 and Y1008. Absolute concentrations of phosphorylation at each site were calculated based on a one-point calibration with an internal heavy standard (0.5 µg/mL) and are reported as µg/mL. **B.** Relative levels of phosphorylation were determined based on the relative area of the sample peak and the internal standard peak and are reported as the fraction of sample area/standard area.

Y926 is the only site of tyrosine phosphorylation in the FAT domain reported to modulate FAK function. Whereas phosphorylation of Y1008 has been observed by mass spectrometry in full-length FAK purified from Sf9 cells [74], it is unclear whether phosphorylation of Y1008 is physiologically relevant. As described above, we detected phosphorylation at Y926 using a commercially available phospho-Y926-specific antibody, as shown in **Figure 2.1**. This antibody shows increasing levels of phosphorylation as the pH is increased from pH 5.5 to 7.5, which is similar to the trend observed with the general phosphotyrosine antibody. These results contradict the MS results, which show that phosphorylation of Y926 reaches a maximum at pH 6.0. Attempts to assess the specificity of pY926-specific antibodies using the phosphorylated peptides were unsuccessful, likely because the pY926 peptide did not bind to the nitrocellulose membrane. It is possible that phosphorylation of Y1008 has been missed by previous studies that have used phospho-Y926-specific antibodies. Further experiments are necessary to determine whether phosphorylation of Y1008 is relevant *in vivo*.

Circular Dichroism as a function of pH

Regardless of whether Y1008 is phosphorylated *in vivo*, the fact that the pH profile of phosphorylation of the full-length FAT domain differs from phosphorylation of a short peptide *in vitro* suggests a change in structure and/or dynamics between pH 5.5 and 7.5 in the FAT domain that affects the accessibility of Y926 and Y1008 to Src kinase. We therefore investigated the effects of pH on the secondary structure of the FAT domain by CD. **Figure 2.6** shows the far-UV CD spectra at pH 5.0, 5.5, 6.0, 6.5, 7.0, and 7.5. Each spectrum shows the minima at 222 and 208 nm characteristic of a helical protein. While there are some differences in the intensity of the minima at 208

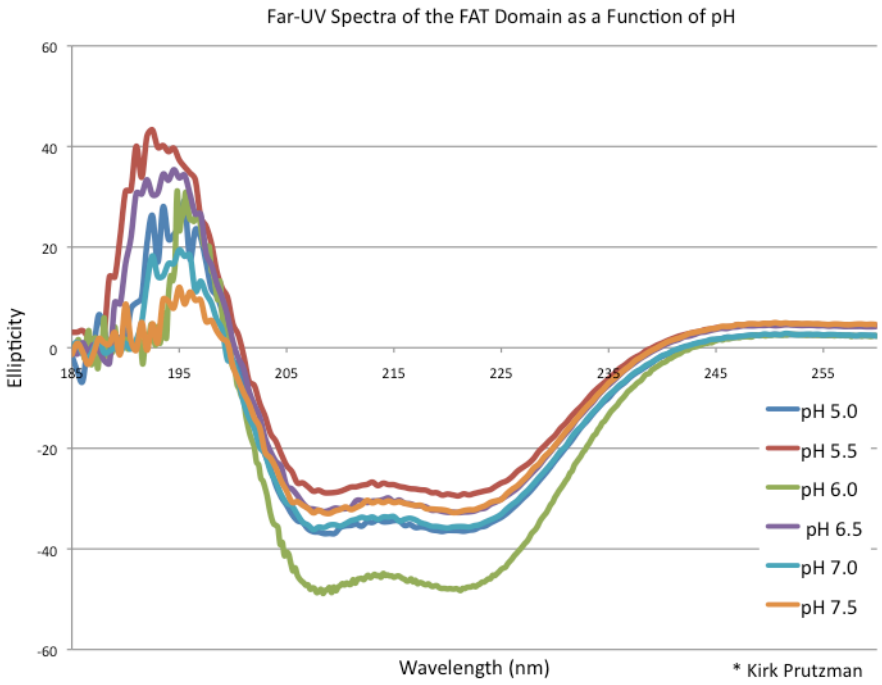

Figure 2.6: Far-UV Spectra of the FAT Domain as a Function of pH
Far-UV CD spectra of the FAT domain were collected at pH 5.0, 5.5, 6.0, 6.5, 7.0, and 7.5 from 260 – 185 nm. The minima at 222 and 208 nm are characteristic of a helical protein. These data show that the FAT domain retains its helical content as the pH is changed.

and 222 nm, the changes are subtle and do not show a trend as a function of pH. It is likely that these differences are a result of errors in concentration rather than changes in secondary structure. The CD signal is very sensitive to change in concentration; therefore, to determine whether pH affects the secondary structure of the FAT domain by CD, these data would have to be repeated and carefully adjusted for concentration. Overall, these data indicate that the FAT domain remains helical as the pH is changed.

We also investigated the pH-dependence of the thermal stability of the FAT domain by CD. **Figure 2.7** shows the thermal denaturation curves at pH 5.5, 6.0, 6.5, 7.0, and pH 7.5, and the T_m values obtained from fitting the denaturation curves are shown in **Table 2.1**. Interestingly, a sizable decrease in the T_m (approximately 16°C) is observed as the pH is increased from pH 5.5 to pH 7.5. Because the CD data indicate

that the FAT domain retains helical content at higher pH, the decrease in stability at higher pH is likely a result of changes in tertiary packing interactions rather than loss of secondary structure.

^{1}H-^{15}N HSQC of the FAT Domain as a Function of pH

To evaluate pH-dependent structural changes on a per-residue basis, we collected

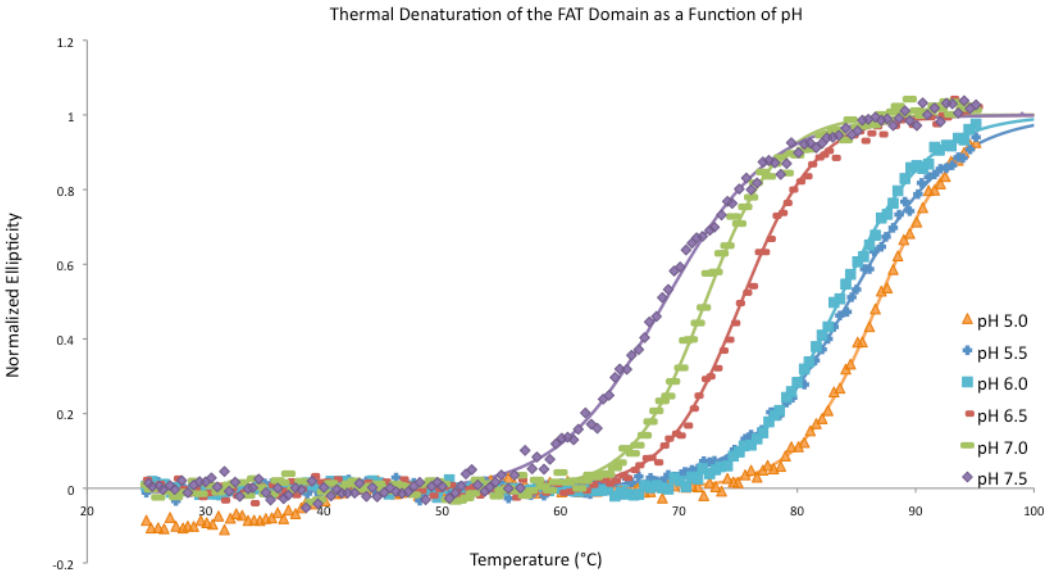

Figure 2.7: Thermal Denaturation of the FAT Domain as a Function of pH
Thermal denaturation was monitored by CD at 221 nm from 25-95°C at intervals of 0.5°C at pH 5.0, 5.5, 6.0, 6.5, 7.0, and 7.5. The melting curves show that the stability of the FAT domain is sensitive to pH; increasing the pH decreases the stability of the FAT domain.

Table 2.1: Melting Temperature of the FAT Domain as a Function of pH

	T_m (°C)
pH 5.0	86.9
pH 5.5	84.3
pH 6.0	83.4
pH 6.5	75.3
pH 7.0	72.2
pH 7.5	68.7

high-resolution ^{1}H-^{15}N HSQC spectra of ^{15}N-enriched FAT-domain at various pH values. The analysis of the ^{1}H-^{15}N HSQC spectra as a function of pH was performed by Dr. Kirk Prutzman, a former graduate student in the laboratory of Dr. Sharon Campbell at UNC-CH. **Figure 2.8A** shows an overlay of the ^{1}H-^{15}N spectra at pH 5.5, 6.0, 6.5, 7.0, and 7.5. While some of the NH resonances show significant pH-dependent chemical shift changes ($\delta > 0.05$ ppm) over the 5.5-7.5 pH range, other NH resonances remain unchanged. **Figure 2.4B** shows the weighted changes in chemical shift mapped onto the sequence of the protein. Of interest is that several residues with significant changes in chemical shift are in helix-1, which contains one of the sites of phosphorylation, Y926. In fact, one of the residues with the largest change in chemical shift is V928, which is near Y926. Furthermore, significant chemical shift changes are observed in the C-terminus of helix-1 and in the loop between helices-1 and 2. This region is of interest because dynamics in this region have been implicated in the regulation of phosphorylation of Y926 [48, 49]. The fact that regions that show pH-dependent changes in chemical shift correlate to regions near Y926 and regions thought to regulate phosphorylation of Y926 (the loop between helices-1 and -2) supports the MS data that phosphorylation of Y926 is affected by pH.

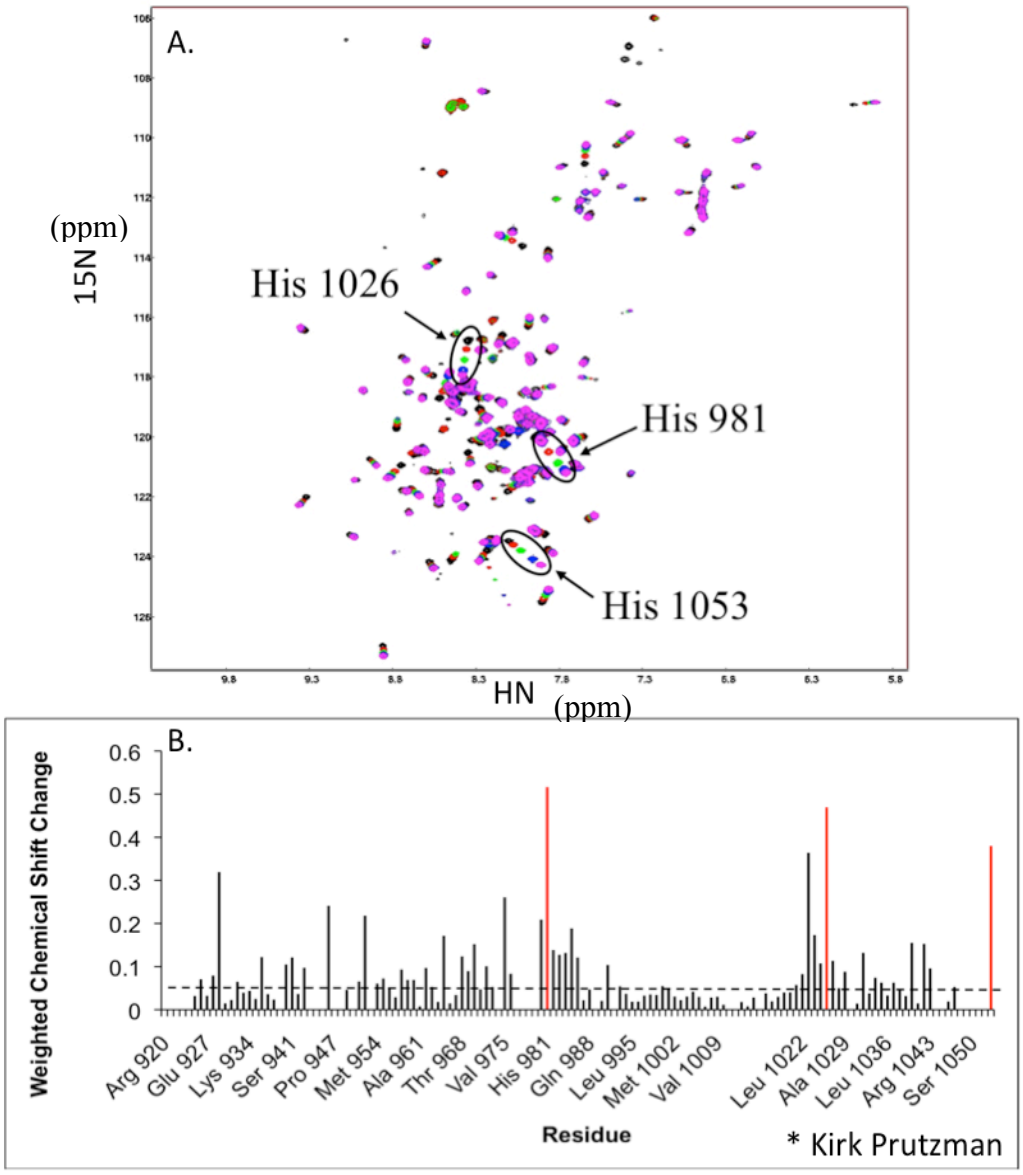

Figure 2.8: ^{1}H-^{15}N HSQC Spectra as a Function of pH:
A. Overlay of ^{1}H-^{15}N spectra collected at pH 5.5 (black), 6.0 (red), 6.5 (green), 7.0 (blue), and 7.5 (pink). The chemical shifts of several peaks are affected by pH whereas others do not change. The chemical shifts of the three histidine residues in the FAT domain (H981, H1026, and H1053) are circled. **B.** The weighted changes in chemical shift from pH 5.5 to 7.5 were calculated. Changes greater than 0.05 ppm (dashed line) were considered significant. The histidine residues are shown in red.

The largest chemical shift changes were observed for the three histidine residues (H981, H1026, H1053) in the FAT domain because histidine side chains typically have pK_a values in the range of 6.0-6.5. We were able to track the chemical shift changes of the NH resonances of the histidine residues as a function of pH to estimate the pK_a of

each histidine within the FAT domain. **Figure 2.9** shows the titration profiles used to estimate pK_a values for each histidine. Estimated pK_a values for H981, H1026, and H1053 are 5.8 ± 0.05, 6.2 ± 0.05, and 6.5, respectively. Because these pK_a values were distinct from each other, we proceeded to calculate the relative pK values of the residues that showed significant chemical shift changes. Chemical shift changes that resulted in a pK value ± 0.15 pH units to one of the histidine pK_a values were considered correlated to that histidine. **Figure 2.9** shows the residues whose pH-dependent changes in chemical shift correlated to specific histidine residues mapped onto the structure of the FAT domain. H981 and residues correlated to it are shown in blue while H1026 and residues correlated to it are shown in red. H1053 is shown in orange. Titration of H981, located at the beginning of helix-3 correlates with the pH-dependent NH chemical shift changes of nearby residues, as expected. However, there are also several residues distal to H981 whose pH-dependent NH resonances correlate with this residue, including residues all along helix-2 and in the amino-terminus of helix-1, which contains Y926. Titration of H1026, located in the middle of helix-4, correlates with the pH-dependent NH chemical shift changes of surrounding residues. Interestingly, however, there are several residues in the C-terminus of helix-1 (V936, S940, S941, and S943) that titrate with H1026. Although the side chain of H1026 is mostly exposed to the solvent, this region of helix-1 packs against helix-4 near H1026, and changes in helix-4 resulting from the titration of H1026 could affect residues in helix-1. These residues (V936, S940, S941, and S943) are near the loop between helices-1 and 2, which has been proposed to be involved in regulation of phosphorylation of Y926 [48, 49]. H1053, the last residue in FAK, does not appear to interact with other residues within the FAT domain, and titration of H1053 does

not seem to be correlated to nearby residues. There were also a number of peaks, notably in the N-terminal region of helix-2, whose pH-dependent chemical shifts do not track with a particular histidine residue. pH-dependent NH chemical shift perturbations for these residues may be a result of de/protonation of both H1026 and H981 or of another titrating residue, possibly an aspartate or glutamate residue.

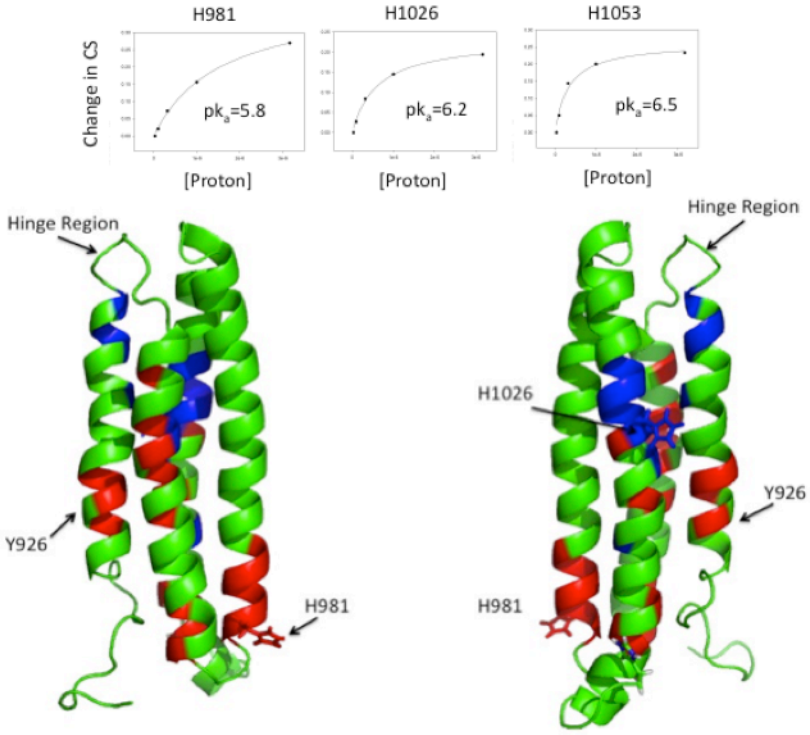

Figure 2.9: Titration of the Histidine Residues.
Titration profiles of each of the three histidine residues were used to calculate the pka of that residue (top). B. Residues that titrate with the histidines residues were mapped onto the structure of the FAT domain. Residues that titrate with H981 are shown in red. They include resides near H981 as well as residues spanning helix-2 and at the N-terminus of helix-1. Residues that titrate with H1026 are shown in blue. These residues localize to the region near H1026 in helix-4 as well as the C-terminus of helix-1.

Investigation of pH-dependent structural changes by NOEs

There are two possibilities for how pH could affect phosphorylation at Y926 and Y1008. First, pH could affect the structure near these tyrosine residues, affecting the accessibility of the side chain to Src. Second, pH could affect the dynamics of the FAT domain, which could render one site more susceptible to phosphorylation. Indeed, dynamics of the hinge region between helix-1 and -2 have been proposed to play a role in phosphorylation of Y926 [49]. To investigate whether pH alters the structure of the FAT domain, we collected ^{15}N- and ^{13}C-edited NOESY spectra at pH 6.0 and pH 7.5. **Figure 2.10** shows the carbon-based NOESY strips of the Cδ and Cε atoms of Y926 **(A-D)** and Y1008 **(E-H)** at pH 6.0 and pH 7.5. The NOEs observed from the Cδ and Cε atoms of Y926 and Y1008 are very similar at pH 6.0 and pH 7.5, suggesting that pH does not change the local environment of these tyrosine residues and therefore probably does not have a major effect on the structure of the FAT domain.

Investigation of pH-dependent structural changes by RDCs

To further investigate pH-dependent structural changes in the FAT domain, we collected NH RDCs at pH 6.0 and 7.5. **Figure 2.11** shows the correlation between RDC values of two datasets collected at pH 6.0, two datasets collected at pH 7.5, and a comparison of a dataset collected at pH 6.0 and at pH 7.5. The correlation between the RDC values at pH 6.0 and pH 7.5 was 0.85, which is not significantly different from the correlation between two datasets collected at pH 6.0 (0.88) or two datasets collected at pH 7.5 (0.90). Because neither the NOESY data nor the RDC data indicate that pH affects the structure of the FAT domain, we investigated the role of pH in altering the dynamics of the FAT domain.

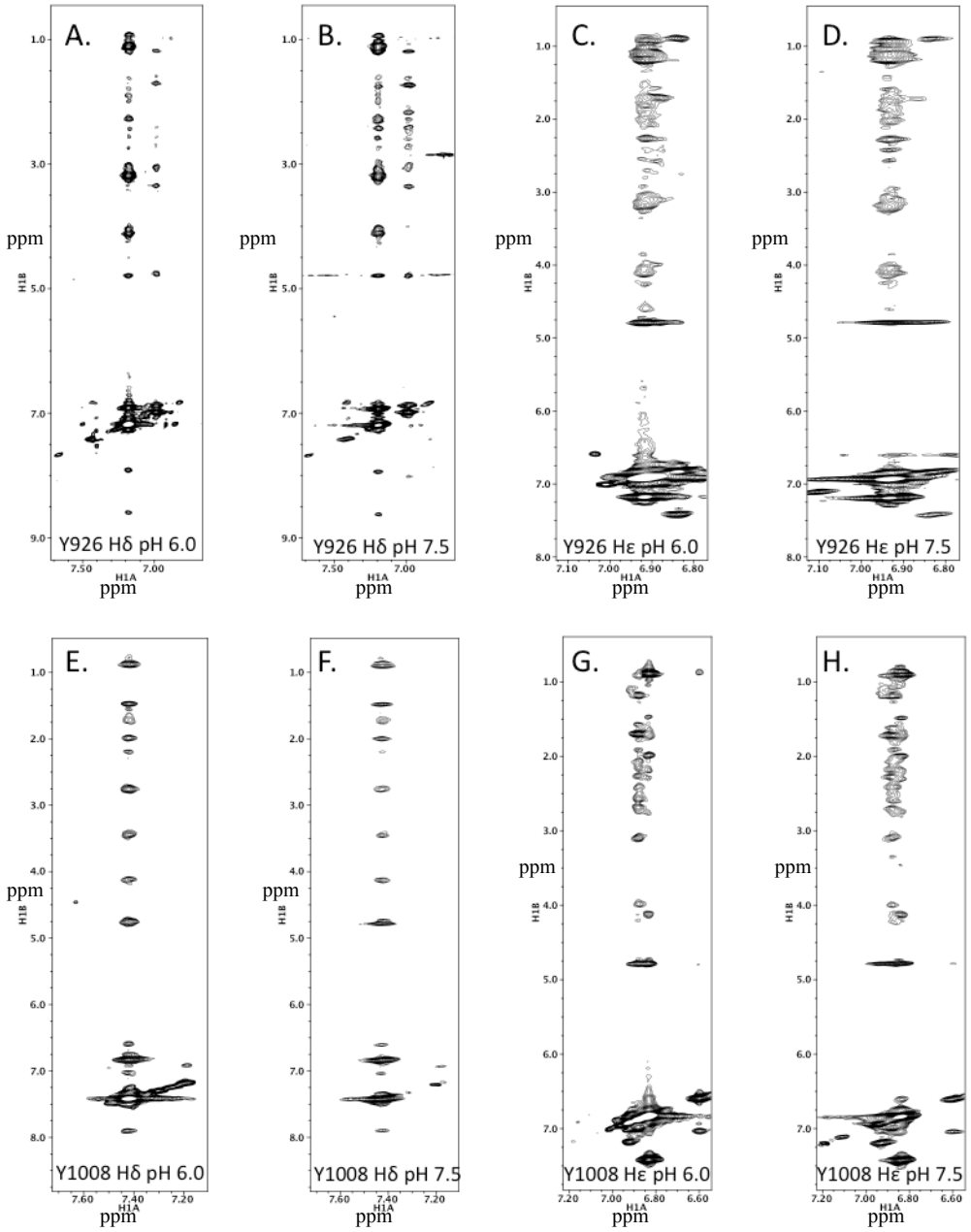

Figure 2.10: NOEs from the Sidechain of Y926 and Y1008:
^{13}C-edited NOEs were collected on the FAT domain at pH 6.0 and 7.5. **A.** NOEs from the Hδ of Y926 at pH 6.0. **B.** NOEs from the Hδ of Y926 at pH 7.5. **C.** NOEs from the Hε of Y926 at pH 6.0. **D.** NOEs from the Hε of Y926 at pH 7.5. **E.** NOEs from the Hδ of Y1008 at pH 6.0. **F.** NOEs from the Hδ of Y1008 at pH 7.5. **G.** NOEs from the Hε of Y1008 at pH 6.0. **H.** NOEs from the Hε of Y1008 at pH 7.5. There are no major differences in the NOEs between pH 6.0 and 7.5, indicating that pH does not cause a major structural change in these regions.

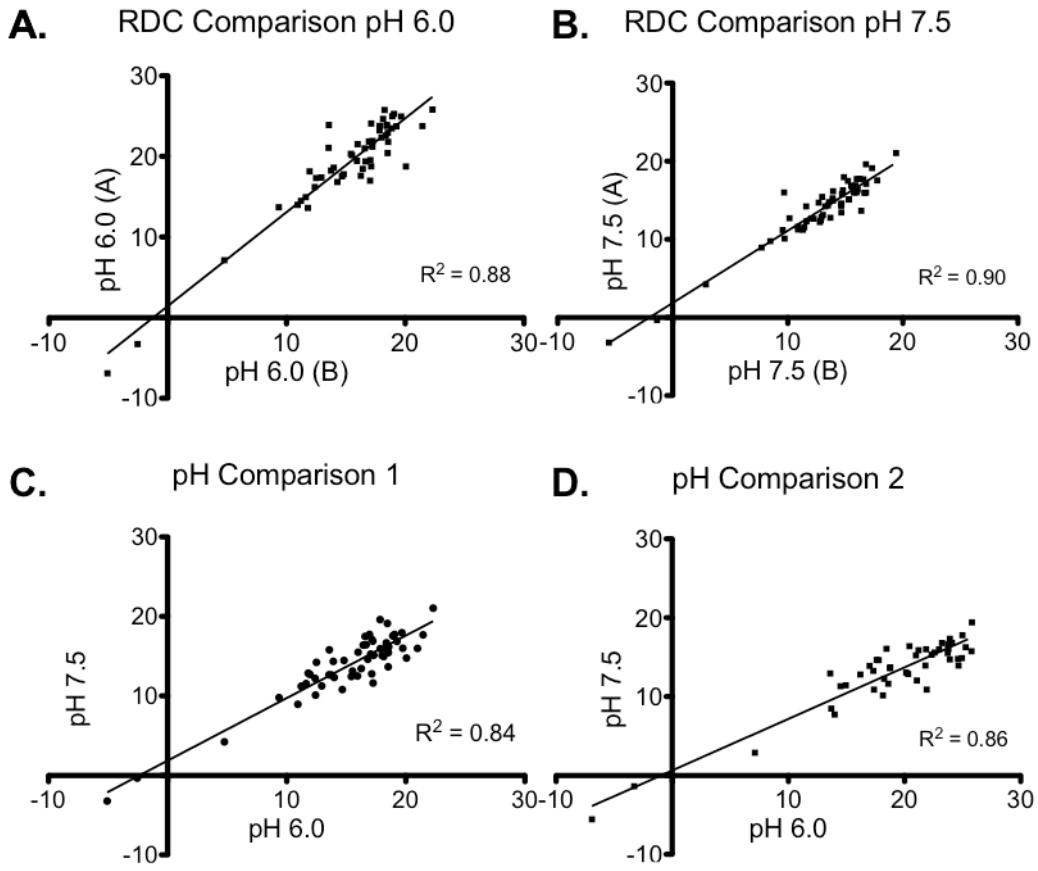

Figure 2.11: Residual Dipolar Couplings as a Function of pH:
Residual dipolar couplings were collected on the FAT domain at pH 6.0 and pH 7.5. **A.** Comparison of two independent datasets collected at pH 6.0. **B.** Comparison of two independent datasets collected at pH 7.5. **C.** Comparison of RDCs collected at pH 6.0 and pH 7.5. **D.** Comparison of second datasets collected at pH 6.0 and pH 7.5.

^{1}H-^{15}N HSQC Analyses Suggest pH-Dependent Changes in FAT Domain Dynamics.

While we were unable to detect any significant pH-dependent structural change, there are several residues in the ^{1}H-^{15}N HSQC spectra that show changes in NH peak intensity as a function of pH, suggesting a pH-dependent change in backbone dynamics. In particular, as the pH is increased from pH 6.0 to pH 7.5, several residues show significant decreases in intensity due to peak broadening. Broadening of the NH resonances as the pH is increased can be difficult to interpret because a variety of

mechanisms can contribute to this broadening, the most pertinent of which are pH-dependent differences in conformational dynamics (exchange between two or more states) and chemical exchange (an increase in exchange between the amide proton and the solvent). As expected, the N- and C-termini NH resonances are severely broadened at higher pH, likely due to an increase in base-catalyzed amide exchange. These residues are located in unstructured regions and consequently more exposed to the solvent. There are also several residues in the turn between helices-3 and -4 and in the N-terminus of helix 4 that broaden as the pH is increased. **Figure 2.12** shows the change in linewidth mapped onto the sequence of the FAT domain. In this figure, a negative change indicates broadening at pH 7.5 whereas a positive change indicates narrowing. Several resides near Y1008, one of the sites of phosphorylation, show an increase in linewidth as the pH is increased. However, as stated above, it is difficult to distinguish whether broadening in this region is due to an increase in solvent exchange, as these residues are in a turn and exposed to the solvent, or to changes in dynamics.

In addition to peaks that broaden as the pH is increased, there are also several peaks that increase in intensity due to a decrease in linewidth upon increasing the pH from 6.0 to 7.5. Interestingly, several peaks that localize to the end of helix-1, the beginning of helix-2, and the loop region in between these helices show a decrease in linewidth as the pH is increased (**Figure 2.12)**. There are also several peaks that span helix-3 that narrow as the pH is increased. **Figure 2.13** shows several peaks of interest as a function of pH. I943, A946, and M954 are all located in and around the hinge region. The observed narrowing of peaks in the hinge region of the FAT domain is likely due to a pH-dependent change in dynamics from the intermediate timescale where peaks are

broader, to a faster timescale, where peaks become sharper. Several of these residues were previously shown to be sensitive to temperature-dependent broadening [49], and dynamics in this region were postulated to affect phosphorylation of Y926 in helix-1 [48-50]. The fact that peaks in the hinge region show pH-dependent dynamics supports our phosphorylation data that shows that phosphorylation of Y926 is dependent on pH in the context of the full-length FAT domain.

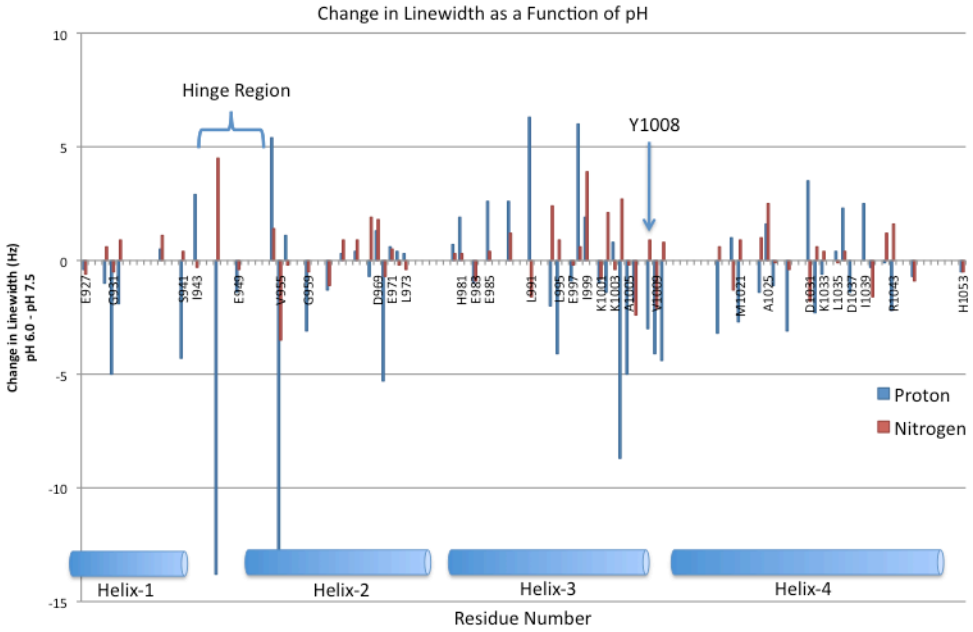

Figure 2.12: Changes in NH Linewidth as a Function of pH:
^{1}H-^{15}N spectra were collected at pH 6.0 an pH 7.5. The linewidths (proton and nitrogen) were measured using the program Sparky. Differences (pH 6.0 – pH 7.5) in linewidth are plotted on the sequence of the FAT domain. The secondary structure of the FAT domain is shown below the graph.

Investigation of pH-dependent dynamics – Backbone Relaxation

Because the pH-dependent ^{1}H-^{15}N HSQC data suggest changes in dynamics as a function of pH, we further investigated this effect by collecting T1, T2, and heteronuclear NOE (HetNOE) datasets at pH 6.0 and pH 7.5. These measurements are sensitive to backbone dynamics on the ps-ns timescale as well as the ms timescale. The relaxation

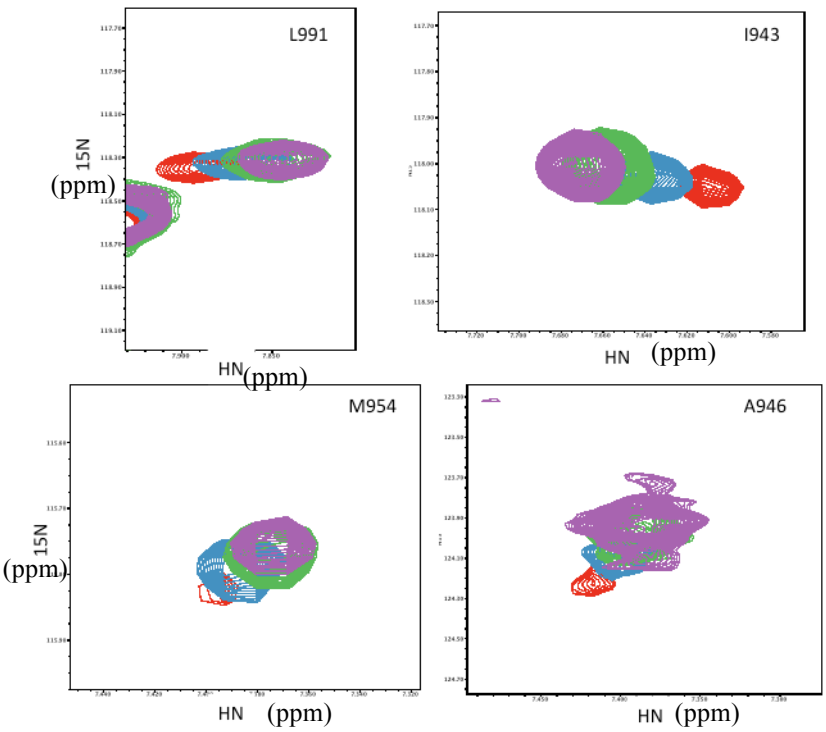

Figure 2.13: Representative Peaks that Narrow from pH 6.0 to pH 7.5:
Several peaks in the ^{1}H-^{15}N HSQC of the FAT domain increase intensity as the pH is raised from 6.0 to 7.5. Shown above are four such peaks at pH 6.0 (red), pH 6.5 (blue), pH 7.0 (green), and pH 7.5 (purple). M954, I943, and A946 are located in and around the hinge region between helices-1 and -2 whereas L991 is in helix-3. These data indicate that the hinge region experiences pH-dependent changes in backbone dynamics.

data was fit to a model-free formalism [75] to obtain the overall correlation time (τ_m) and the order parameters S^2 and τ_e, which measure the rigidity of the N—H bond and the internal correlation time, respectively. pH did not affect the overall correlation time (τ_m) of the protein, which is generally dependent on the overall size and shape of the molecule. The τ_m was determined to be 11.3 ns at pH 6.0 and pH 7.5. This value is slightly higher than expected for a protein this size (~9.5 ns). This discrepancy is likely due to the fact that the τ_m was determined assuming isotropic tumbling. However, the FAT domain is not a spherical molecule (60 Å x 20 Å x 20 Å [48]), and therefore some error would be expected in the isotropic τ_m. Our interest here is to compare the rotational correlation time at pH 6.0 and 7.5, thus a relative comparison indicates little change in τ_m.

No discernable difference was observed in the S^2 order parameter as a function of pH. As expected, the S^2 values are near 0.9 in the structured regions of the proteins and decrease to around 0.8 in the loops and turns. Residues in the N- and C-termini are not visible by NMR at pH 7.5 and have lower S^2 values at pH 6.0 (~0–0.6), as these residues are less structured relative to those in the helix bundle domain, are more exposed to the solvent, and likely undergo enhanced solvent-mediated chemical exchange. No difference in τ_e is observed as a function of pH.

It may not be surprising that we see little difference in S^2 or τ_e as a function of pH because these values are sensitive to backbone motions on faster timescales (ps-ns) than the overall correlation time of the FAT domain. Thus, it is possible that the dynamic changes that occur as a function of pH occur on a slower timescale (μs-s) and may involve the side chains.

While the ^{15}N-based T1, T2, and HetNOE relaxation measurements provide backbone dynamic information on the ps-ns timescale, the measurements are also sensitive to motions on slower timescales (μs-ms). Indeed, several residues appear to be undergoing motion on these slower timescales, as indicated by contributions by R_{ex} in the model-free fitting. At pH 6.0, there are three residues in helix-1, K924 (which is not visible at pH 7.5), I937, and A946, that experience slower μs-ms timescale dynamics. The intensity of the A946 NH resonance also increases in the ^{1}H-^{15}N HSQC spectrum as the pH is increased, which provides further evidence that dynamics in this region are susceptible to changes in pH. A946 is in a putative "hinge region", the loop between helices 1 and 2. It has been postulated that dynamics in this region due to strain caused

by a series of proline residues modulate a helix-coil transition in helix-1 that regulates phosphorylation of Y926 [49].

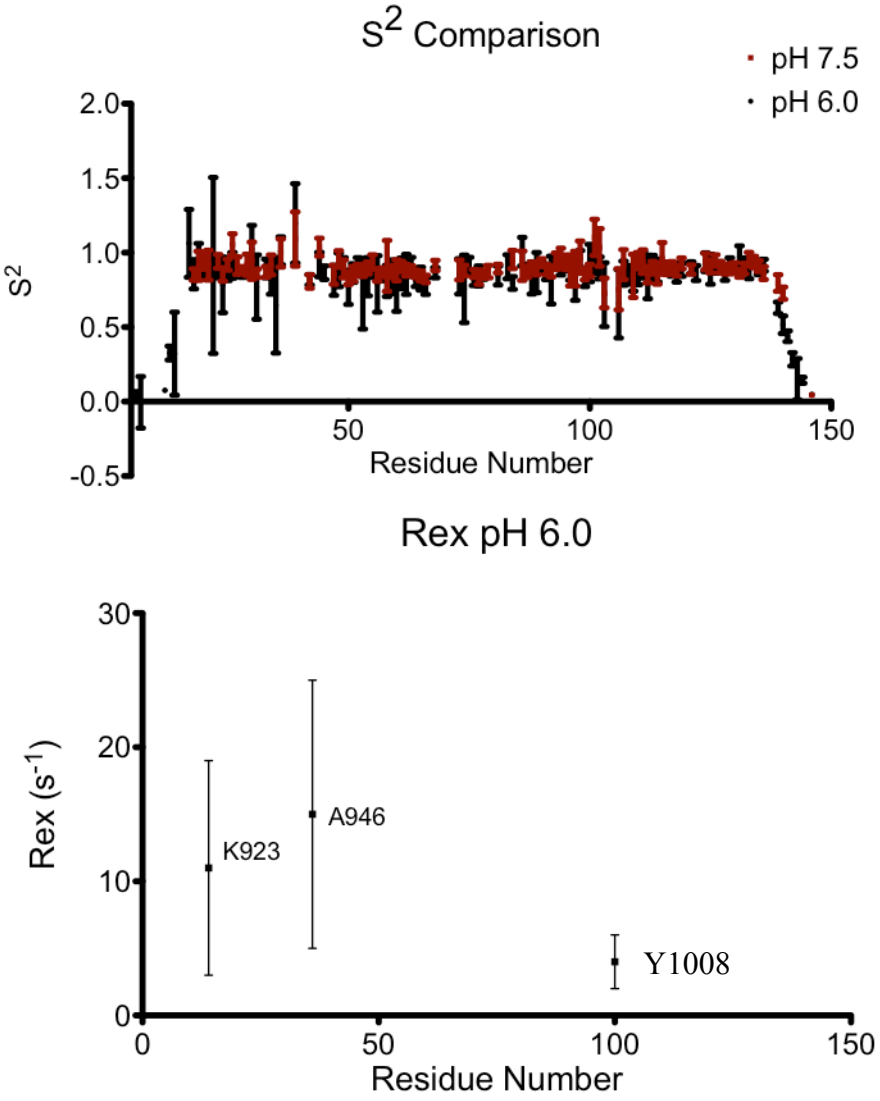

Figure 2.14: Backbone Dynamics of the FAT Domain as a Function of pH: ^{15}N-based T1, T2, and HetNOE data were collected at pH 6.0 and pH 7.5 and fit a model-free formalism to obtain S^2 order parameters (top). Three residues at pH 6.0 also showed evidence of µs-ms timescale motion, apparent in the R_{ex}

Investigation of pH-dependent dynamics by CPMG-based Relaxation Dispersion

Because it appears that dynamics in the FAT domain are sensitive to pH on the μs-ms timescale, we collected further NMR experiments that are sensitive to dynamics on this timescale. One method to quantify dynamics on the μs-ms timescale is by Carr-Purcell-Meiboom-Gill relaxation dispersion experiments. These ^{1}H-^{15}N HSQC-based experiments allow one to measure dynamics on the μs-ms timescale by introducing a series of spin-echoes into the sequence (τ - 180° - τ). If there are conformational dynamics in the protein that occur on the same order as the frequency of the spin-echo sequence, the 180° pulses become less effective at refocusing the magnetization, leading to a decay in the observed signal. By measuring peak intensity as a function of τ, one can obtain kinetic and thermodynamic information on the exchange process and on weakly-populated conformations of the protein, respectively. The ability to observe dynamics by relaxation dispersion depends on both the timescale of the dynamics and on the population of lowly-populated species (for review see [76]). We collected CPMG-based relaxation dispersion experiments at pH 6.0 and pH 7.5 at several temperature values (15°C, 25°C, 37°C, and 45°C) at τ = 0, 0.556, 5, and 10 ms. **Figure 2.15** shows the difference in $R_{2,eff}$ between τ_{10} and $\tau_{0.556}$. Generally, a difference of 8-10 Hz provides enough sensitivity to fit the relaxation curves. However, as seen in **Figure 2.15**, the differences in $R_{2,eff}$ are on the order of 2-3 Hz and are too small to quantify.

Investigation of pH-dependent dynamics by CLEANEX-PM

Another method to examine dynamics on the μs-ms timescale is hydrogen exchange measured by the CLEANEX-PM pulse sequence [77]. In this ^{1}H-^{15}N HSQC-

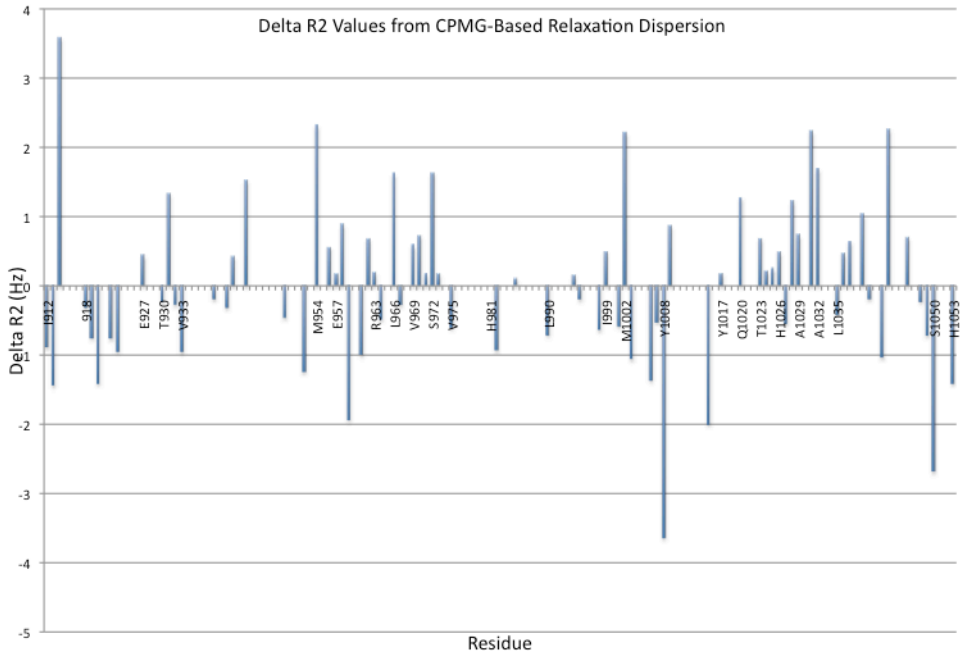

Figure 2.15: Delta R2 Values from CPMG-Based Relaxation Dispersion
CPMG-based relaxation dispersion data were collected at 37°C at pH 6.0 with delay times (τ) of 0, 0.556, and 10 ms. The R2 for each delay was calculated by the following equation: $R2 = -(1/0.04)\mathrm{Ln}(I_0/I_\tau)$. The delta R2 ($R2_{10} - R2_{0.556}$) was plotted as a function of the sequence of the FAT domain. The differences in R2 are too small to quantify relaxation dispersion

based experiment, the water signal is saturated, a short delay is applied (0-55 ms), and the protein signal is observed by an ^{1}H-^{15}N HSQC sequence. Only the residues that exchanged with water during the delay period will be observable. As the delay is increased, the intensity of the observable resonances will increase, and rates of exchange can be acquired. Processes that affect the solvent accessibility of a particular residue would be expected to have an effect on the rate of solvent exchange.

We collected CLEANEX-PM spectra at pH 6.0, 6.5, 7.0, and 7.5 to investigate dynamics on slower timescales. **Figure 2.16** shows the residues observed at each pH value. Many of the peaks observed in the CLEANEX-PM spectrum at low pH values (pH 6.0 and 6.5) are in the termini and loops, which are not visible at pH 7.5. This is expected because these residues are in unstructured regions and therefore readily

exchange with the solvent. Furthermore, many of the peaks in the CLEANEX-PM spectrum at pH 7.5 are not observed at pH 6.0. Interestingly, the peaks that appear at pH 7.5 are localized to helix-1, which was previously shown by conventional hydrogen exchange experiments to be less protected than the other three helices [50].

Hydrogen exchange is base catalyzed at pH values above 4.0; therefore, the increase in the observable peaks at pH 7.5 could be either a result of a change in solvent accessibility of these residues due to a change in dynamics or an increase in solvent exchange due to the increase in pH. To distinguish between these two processes, it is necessary to monitor the pH dependence of the rate of exchange for a particular residue and see if it deviates from the expected 10-fold increase in exchange per pH unit. A deviation in this dependence would suggest that there are other processes, i.e., changes in dynamics, that affect the solvent accessibility and therefore rate of solvent exchange of a particular residue. However, we were not able to conduct such a comparison because we were not able to visualize many peaks at more than one pH value.

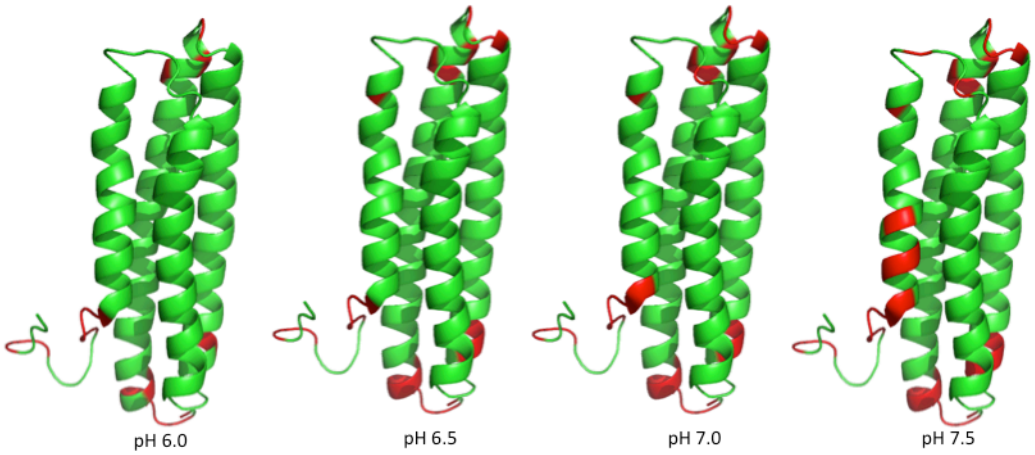

Figure 2.16: CLEANEX Experiments of the FAT Domain as a Function of pH: CLEANEX data were collected on the FAT domain at 37°C at pH 6.0, 6.5, 7.0, and 7.5. Shown in red are the residues that were detected in the CLEANEX spectrum at the indicated pH. Most of the residues localize to the termini and loops, and as expected, the number of residues detected increases as the pH is increased.

Identifying Residues Whose Titration Correlates with the pH-Dependent Stability

The pH-dependent changes in phosphorylation, stability, and dynamics that we observe in the FAT domain beg the question what is causing this pH sensitivity. To answer this question, we have mutated several residues in the FAT domain and assessed their sensitivity to pH by measuring the thermal stability by CD. First, because histidine side chains typically have a pK_a at about pH 6.0, these residues are likely candidates for the cause of the observed pH sensitivity. There are three histidine residues in our construct, and we have made single point mutations in which each of these residues has been mutated to alanine. The experimental work with the histidine mutants was conducted by Dr. Kirk Prutzman, a graduate student in the laboratory of Dr. Sharon Campbell at UNC-CH. Thermal melts monitored by CD at 221 nm indicate that none of single histidine mutants are able to completely compensate for the pH-dependent change in stability (data not shown). It is possible that the pH-dependent change in stability is caused by an additive effect of the titration of all three histidines.

Another explanation for the pH-dependent change in stability is anomalous titration of an aspartate or glutamate residue. This would be unusual, but not unheard of. While the canonical pK_a for the side chain of aspartate and glutamate is around pH 4, pK_a is very sensitive to the local environment, and a pK_a as high as 6.7 has been detected for an glutamate residue in the glycoprotein CD2 [78] and 6.6 for an aspartate residue in a mutant of PGB1 [79]. Based on the structure of the FAT domain, we individually mutated two asparate residues and one glutamate residue to alanine (D994A, E949A, D1040A). D994 is in the middle of helix-3 in the FAT domain. In the three-dimensional

structure of the FAT domain, D994 is in between E997 and D1031. We reasoned that the concentration of negative charge in this region might promote protonation of D994, which could allow it to form hydrogen bonds with the side chains of E997 or D1031. Second, we mutated E949, which is in the loop between helices-1 and -2. In the NMR structure of the FAT domain, solved at pH 6.0 [49], E949 is in an unstructured region and, in some of the models, the side chain is packed into the core of the helix bundle whereas in the crystal structure solved at pH 7.0 [48], E949 is in the beginning of helix-2 and the side chain is exposed to the solvent. If the side chain of E949 is able to pack into the core of the helix bundle, as observed in several of the NMR models, then burial of the negative charge would likely promote protonation of the side chain. However, it should be mentioned that the loop between helices-1 and -2 contains several proline residues; therefore, the NMR data in this area is sparse, and the conformational variability of E949 may be due to the lack of restraints in this region. Finally, we also mutated D1040 in helix-4 of the FAT domain. The side chain of D1040 faces helix-1 near Y926 and, in the crystal structure [48], is involved in a salt bridge with R920. In the NMR structure, however, this salt bridge is not observed, perhaps due to a lack of data near R920, which is unstructured, and the R920 resonance is broadened in the ^{1}H-^{15}N HSQC spectrum, making it difficult to acquire restraints in this region. However, in the NMR structure [49], the side chain of D1040 is buried by the N-terminus of the protein, which, due to the lack of NMR data in this region, may or may not be observed in the actual protein.

We individually mutated D994, D1040, and E949 to alanine and measured the thermal stability at pH 6.0 and pH 7.5 by CD. As observed for the histidine mutants, none of the aspartate/glutamate mutants were able to abrogate the pH-dependent stability.

Figure 2.17 shows the thermal denaturation curves for D994A, E949A, and D1040A at pH 6.0 and pH 7.5. The melting temperatures obtained from fitting the curves are shown in **Table 2.2**. Currently, the molecular basis for the pH sensitivity observed in the FAT domain remains elusive. It is possible that one of the aspartate or glutamate residues that we did not mutate is titrating and causing the pH sensitivity, or perhaps the pH sensitivity is not due to titration of a single residue and is the result of a more complex phenomenon. Finally, it should also be noted that whatever mechanism promotes the pH-dependent stability may not be the same mechanism that affects the dynamics and phosphorylation. Currently, we have only tested the histidine and aspartate/glutamate mutants with regard to pH-dependent stability as we do not have a straightforward method to assess phosphorylation, and it is possible that while these mutants do not abrogate the pH-dependent stability, they may affect the pH-dependent changes in phosphorylation.

Conclusion

Phosphorylation of Y926 in the FAT domain has been shown to play a role in FAK signaling and localization. In particular, phosphorylation has been linked to promoting cell adhesion, migration, and invasion *in vitro* and metastasis *in vivo* [47]. However, the mechanism by which phosphorylation is regulated *in vivo* remains to be elucidated. While it has been speculated that a conformational change is necessary for phosphorylation of Y926 [48, 49], what regulates this conformational change *in vivo* is unknown.

In this study, we have shown that phosphorylation of Y926 by Src is pH dependent *in vitro*. Furthermore, we have demonstrated that Src is able to phosphorylate

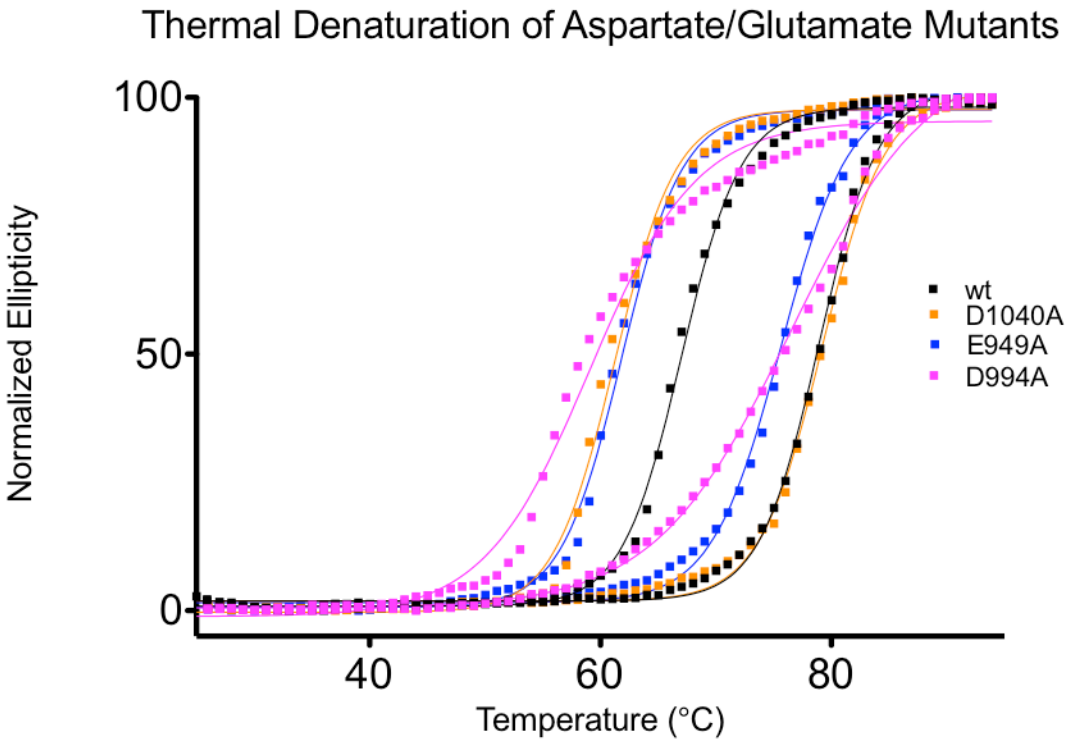

Figure 2.17: Thermal Denaturation of Aspartate and Glutamate Mutants:
The FAT domain and mutants were dialyzed in CD buffer at pH 6.0 (right) and pH 7.5 (left). Thermal denaturation was measured by monitoring the CD signal at 221 nm at intervals of 0.5°C.

Table 2.2: Melting Temperatures of Aspartate/Glutamate Mutants of the FAT Domain

	pH 6.0 (°C)	pH 7.5 (°C)	Difference (°C)
wt	78.93 ± 0.07	67.02 ± 0.08	11.91 ± 0.08
D1040A	79.22 ± 0.09	61.3± 0.1	17.9 ± 0.1
D994A	76.5 ± 0.2	59.12 ± 0.2	17.4 ± 0.2
E949A	75.63 ± 0.08	61.8 ± 0.1	13.8 ± 0.1

Y1008 *in vitro* and that phosphorylation at this site is also pH dependent.

Phosphorylation of peptides containing Y926 and Y1008 do not show the same pH dependence as phosphorylation of the full-length protein, suggesting that the observed pH dependence of phosphorylation is primarily a result of changes in the structure and/or dynamics of the FAT domain and not Src activity. Furthermore, in the context of the peptides, Y926 is phosphorylated approximately 100 times more than Y1008 whereas in

the context of the full-length protein, the levels of phosphorylation at the two sites are either comparable or favor Y1008, depending on pH. These results suggest that while the sequence surrounding Y926 is conducive to phosphorylation by Src, in the full-length FAT domain the conformation of Y926 is not. Y926 is in a helix, and it has been speculated that its conformation is not conducive to phosphorylation [48, 49]. Indeed, a construct containing helix-1 of the FAT domain fused to GST is phosphorylated to a greater extent *in vitro* than the full-length FAT domain [49], indicating that the conformation of Y926 in the full-length FAT domain does not favor phosphorylation. On the other hand, Y1008 is in a more appropriate conformation for phosphorylation in the full-length FAT domain even though the sequence is not as optimized for Src recognition as the sequence surrounding Y926. Y1008 is at the end of helix-3 and begins the turn between helices-3 and -4. Based on our phosphorylation results, the conformation of Y1008 in the full-length FAT domain is more favorable for recognition by Src than that of Y926. These results highlight the two basic determining factors for kinase recognition and subsequent phosphorylation: sequence and conformation. While it is well known that a potential site of phosphorylation must possess a suitable sequence and conformation for recognition by a kinase, our results present an interesting example in which one site (Y926) seems to be optimized for sequence but not conformation whereas the other site (Y1008) is optimized for conformation but not sequence. The fact that Y926 is the biological site of phosphorylation may suggest that, *in vivo*, sequence is more important than conformation for recognition by Src. However, the use of non-specific phosphorylation antibodies and peptide libraries to investigate sites of phosphorylation and determine kinase consensus sequences may have resulted in Y1008 being overlooked

as a possible substrate for Src. Further work is necessary to determine whether Y1008 is phosphorylated *in vivo*.

Our phosphorylation data suggest that the conformation of Y926 is sensitive to pH, which affects phosphorylation at that site. Our CD and NMR data suggest that the FAT domain does not experience a major structural change as a function of pH. Therefore, either the structural change is minor or pH primarily affects dynamics and not structure. The pH-dependent changes in linewidth observed in the ^{1}H-^{15}N HSQC spectra indicate that the backbone dynamics of the FAT domain are sensitive to pH. In particular, the region between helix-1 and -2, the hinge region, in which conformational dynamics have been proposed to regulate phosphorylation of Y926 [49], shows pH-dependent dynamics on the μs-ms timescale, supporting our data that show that phosphorylation of Y926 is pH dependent. We were not able to quantify the dynamics of the FAT domain by relaxation dispersion experiments. In order to quantify dynamics with these experiments, the dynamics must be in the proper time scale, and the lowly-populated state of the protein must be present at at least 0.5%. NMR-based hydrogen exchange studies of the excited state of the FAT domain estimate that the lowly-populated state is only present at about 0.1% [51]. Therefore, it may not be possible to quantify the dynamics in the hinge region.

We attempted to determine the titrating residue that was the cause of the pH dependent stability and dynamics. After individually mutating each histidine residue, two asparate residues, and one glutamate residue, we were unable to determine the cause of the pH sensitivity. It is possible that the pH dependent changes we see are due to titration of several residues, and therefore single point mutations cannot abrogate this

effect. Alternatively, the pH-dependent effects that we observe may be due to titration of a residue that we have not investigated. If we could determine the cause of the pH-dependent effect, we could potentially make a pH-insensitive mutant of the FAT domain that could be used *in vivo* to elucidate whether pH regulates the FAT domain *in vivo*. While more work remains to be done until we can test this hypothesis, our current pH-dependent phosphorylation data is consistent with the proposed function of phosphorylation at Y926. According to our data, phosphorylation of Y926 is weak under basic conditions; we observe the lowest levels of Y926 phosphorylation at pH 7.5. Therefore, at the leading edge of migrating cells, which is slightly more basic than the trailing edge, Y926 is less likely to be phosphorylated. The intracellular pH becomes more acidic towards the trailing edge of the cell, and according to our data, phosphorylation at Y926 increases as the pH is decreased from pH 7.5 to pH 7.0. Therefore, one might speculate that Y926 becomes phosphorylated at the trailing edge of cells due to the difference in pH between the leading and trailing edges. This hypothesis is consistent with data that demonstrate that Y926 delocalizes FAK from focal adhesions and promotes focal adhesion turnover [73]. In summary, our data support a model in which nonphosphorylated FAK localizes to focal adhesions at the leading edge of migrating cells where the pH is more basic than the overall intracellular pH. As the cell migrates, the leading edge becomes the trailing edge, and the pH becomes more acidic. These conditions promote phosphorylation of Y926 in the FAT domain, which causes delocalization of FAK from focal adhesions, focal adhesion turnover, and subsequently cell migration.

Methods

Expression and Purification of wild type and mutant FAT

The FAT domain construct used in these studies contains residues 920 to 1053 of chicken FAK plus a 12 amino acid N-terminal linker (bold): (**GSPGISGGGGGI**RSNDKVYENVTGLVKAVIEMSSKIQPAPPEEYVPMVKEVGL ALRTLLATVDESLPVLPASTHREIEMAQKLLNSDLAELINKMKLAQQYVMTSLQ QEYKKQMLTAAHALAVDAKNLLDVIDQARLKMISQSRPH). The FAT domain was expressed as a GST fusion protein as previously described. The pGEX-KG plasmid containing the GST-FAT sequence was transformed into BL21(DE3) *E. coli* cells for protein expression. Bacteria were grown in LB-Amp at 37°C to an OD_{600} ~ 0.6. Expression was then induced by the addition of 0.5 mM isopropyl β-D-1-thiogalactopyranoside (IPTG), and cells were grown for a further three to five hours before harvesting by centrifugation. Cells were resuspended in lysis buffer (20 mM Tris pH 7.5, 10% glycerol, 10 mM dithiothreitol (DTT), 150 mM NaCl) and lysed by sonication (5 sec. on 5 sec. off for a total of one hour). The lysate was centrifuged at 15k rpm for 70 min. to remove insoluble cell debris. The supernatant was added to glutathione-agarose (GSH) beads and incubated at 4°C overnight. The beads were washed once with lysis buffer and two times with thrombin cleavage buffer (50 mM Tris pH 8.0, 150 mM NaCl, 2.5 mM $CaCl_2$, 0.1% β-mercaptoethanol (BME)). Typically, about 0.5 units/mL of thrombin were added to the beads to cleave the fusion protein. The beads were incubated with thrombin at room temperature overnight and then washed three times with thrombin cleavage buffer. The supernatants of these washes were combined, and thrombin activity was inhibited by the addition of p-aminobenzamidine

agarose beads, which were subsequently removed by centrifugation. The protein was dialyzed into S-column buffer A (25 mM $NaPO_4$ pH 5.5, 0.01% NaN_3) and purified by cation-exchange chromatography on a mono S column and eluted with a gradient of 0 – 1 M NaCl over 200 mL. The protease inhibitors PPACK (1 μM) and pefablock (0.5 mg/mL) were added to the purified protein to prevent degradation.

Protein concentration was measured by diluting the protein in a final concentration of 6 M guanidinium hydrochloride and measuring the absorbance at 280 nm. The concentration was calculated using the calculated extinction coefficient at 280 nm (5120 $M^{-1}cm^{-1}$ for wild type and 4470 $M^{-1}cm^{-1}$ for the mutants) from the ProtParam tool on the ExPASy proteomics server [80].

Mutagenesis

The construct expressing the GST-wtFAT domain fusion protein has been described elsewhere [49]. The Quikchange mutagenesis protocol (Stratagene) was used to incorporate point mutations into positions 994, 1040, and 949. The following primers were used to make the desired mutants (bold indicates site of mutation):

D994A

5’ G AAA CTG CTG AAC TCT **GCG** CTG GCT GAG CTC ATT AAC 3’

D1040A

5’ CTG GAT GTC ATC **GCT** CAA GCC AGA CTG 3’

E949A

5’ AA ATA CAG CCA GCT CCG CCA **GCG** GAG TAC GTG CCA AT 3’

Quikchange reactions were digested with DpnI at 37°C to remove any template DNA and transformed into DH5α *E. coli* cells. Single colonies were chosen and

incubated in LB-Amp overnight, and plasmid DNA was purified using the Qiagen Miniprep kit. The mutation was verified by sequencing by GENEWIZ (USA) using the pGEX 5' sequencing primer (5' GGGCTGGCAAGCCACGTTTGGTG 3').

Src Expression and Purification

Several Src kinase constructs were received from various sources. Baculovirus-expressed full-length human Src was a gift from BioSource (PHO3131). Also, several bacterially-expressed constructs were used. Kinase domain (KD Src) only and full-length (FL Src) chicken c-Src constructs were received from the lab of Dr. John Kuriyan while full-length and ΔSH3 human Src constructs were received from Dr. Gonquin Sun [81]. Because of difficulties in purifying and achieving consistent phosphorylation with the full-length Src constructs, all studies reported in this paper were conducted with KD Src.

The expression and purification of the chicken c-Src constructs is similar to that in Seeliger et al. with a few modifications [82]. Bacteria were transformed with two plasmids. One plasmid contains the specified Src sequence while the other plasmid contains a YopH phosphatase sequence. Tyrosine kinases are notoriously difficult to express in bacteria. It is thought that expressing a phosphatase with the kinase will negate the effect of the kinase [81, 82]. Bacteria were grown in LB with 50 μg/mL kanamycin and 50 μg/mL streptomycin at 37°C to an $OD_{600} \sim 0.800$. The temperature was reduced to 18°C, and, after one hour, expression was induced by the addition of 0.2 mM IPTG. Cells were shaken at 18°C overnight and then harvested by centrifugation. Cells were resuspended in lysis buffer (50 mM Tris pH 8.0, 500 mM NaCl, 5% glycerol, 25 mM imidazole) and lysed by sonication. The lysate was centrifuged at 15,000 rpm for 70 min to remove cell debris, and the cleared lysate was loaded onto a Ni^{2+} affinity

column that had been pre-equilibrated with lysis buffer. The column was washed with two column volumes of lysis buffer with 50 mM imidazole, and protein was eluted with lysis buffer with 300 mM imidazole. Ten 5-mL fractions were collected from the Ni^{2+} column and analyzed by SDS-PAGE. The fractions containing Src were pooled and dialyzed into 20 mM Tris pH 8.0, 100 mM NaCl, 5% glycerol, and 1 mM DTT with tobacco etch virus (TEV) protease at 4°C overnight to cleave the 6X His tag. The protein was then re-loaded onto the Ni^{2+} affinity column pre-equilibrated with lysis buffer to remove the TEV, which contains a His tag. The first 20 mL of the flow-through were collected, and the presence of Src in the flow-through was verified by SDS-PAGE. Protein concentration was determined by measuring the absorbance at 280 nm (ε = 52745 $M^{-1}cm^{-1}$) as calculated by the ProtParam tool on the ExPASy proteomics server [80]. A 50% glycerol stock of the purified protein was made, and 5-10 μL aliquots were stored at -20°C until use.

In vitro Phosphorylation of the FAT domain and Synthetic Peptides

Purified full-length FAT domain was dialyzed into phosphorylation buffer (100 mM MES (pH 5.5, 6.0, 6.5) or 100 mM HEPES (pH 7.0, 7.5), 5.0 mM $MgCl_2$, 1 mM DTT, 0.01% NaN_3). Each reaction contained 0.5 mg/mL FAT domain, ~ 1 μM Src, and 0.5 mg/mL ATP. Reactions were incubated at 37°C overnight in an eppendorf tube with a 2 kDa MW cutoff bottom floating in 100 mL of phosphorylation buffer to ensure that the pH remained constant throughout the course of the reaction.

Two synthetic peptides (SNDKVYENVTGLVK-OH and MKLAQQYVMTSLQQEYK-OH, containing Y926 and Y1008, respectively) were synthesized by Dr. Krzysztof Krajewski in the laboratory of Dr. Brian Strahl at UNC-CH.

The peptides were dissolved in water and diluted with 10X phosphorylation buffer to a final concentration of 0.56 mg/mL in a final volume of 100 µL. Src (1 µL of 5 mg/mL) was added to each reaction, and the reactions were incubated at 37°C for one hour. In total, ten reactions were performed: peptide containing Y926 at pH 5.5, 6.0, 6.5, 7.0, and 7.5 and peptide containing Y1008 at pH 5.5, 6.0, 6.5, 7.0, and 7.5. Samples were kept at -20°C until analysis.

Detection of Phosphorylation in Full-Length FAT: Western Blot

After the reaction, phosphorylation reactions of the full-length FAT domain were separated by SDS-PAGE and transferred to a nitrocellulose membrane for 30 min. at 70 V. The membrane was blocked for one hour at room temperature with 5% bovine serum albumin (BSA) in tris-buffered saline plus tween (TBST) and then incubated with the primary antibody overnight at 4°C (1:5000 dilution, 5% BSA). Phosphorylation was detected by western blotting with a general phosphotyrosine antibody (4G10, Millipore) or a pY926-specific antibody (Santa Cruz). The membranes were washed three times in TBST and incubated with the appropriate secondary antibody at room temperature for one hour (1:5000 α-rabbit (pTyr) and α-goat (p-Y926)). Proteins were visualized using electrochemiluminescence (ECL) reagent (Pearce).

Mass Spectrometry of Phosphorylated FAT: FTICR

The site of phosphorylation was verified by microelectrospray fourier transform ion cyclotron resonance mass spectrometry (µESI-FTICR-MS) by Dr. Li Zhou in the laboratory of Dr. Xian Chen. Spectra were acquired on a hybrid Qe-FTICR mass spectrometer equipped with a 12.0 Tesla actively shielded magnet (Apex Qe-FTICR-MS, 12.0 T AS, Bruker Daltonics, Billerica, MA, USA) and an Apollo II µESI source. The

voltages on the μESI spray capillary, spray shield, capillary exit, deflector, ion funnel and skimmer were set at +4.2 kV, +3.6 kV, +340 V, +310 V, +185 V, and +25 V, respectively. The temperature of the μESI source was maintained at 180°C. Desolvation was carried out by using a nebulization gas flow (2.0 bar) and a countercurrent drying gas flow (4.0 L second^{-1}). cFAT samples were prepared by resuspending the lyophilized proteins in a mixture of acetonitrile/water/acetic acid (49.0:49.0:2.0 v/v/v) at a concentration of ~0.1 μg μL^{-1}, directly infused with a syringe pump (Harvard Apparatus, Holliston, MA, USA) and a 100-μL syringe (Hamilton, Reno, NV, USA), and electrosprayed at an infusion flow rate of 90 μL hour^{-1}. Before transfer, ion packets were accumulated inside the collision cell for a duration of 0.5 second. One hundred MS scans per spectrum were acquired in the ICR cell with a resolution of 580,000 at m/z 400 Da.

FTICR-electron capture dissociation (ECD) MS/MS was employed to fragment modified cFAT. Precursor ions were isolated with a quadrupole (Q1) and directly subjected to the ICR cell. The isolation window width was 2.0 Da. Before transfer, ion packets were accumulated inside the collision cell for a duration of 1.0 seconds. Low energy electrons were generated by the heated hollow dispenser cathode with a bias voltage of -2.5 V. The ECD lens voltage was set at +15.0 V. The electrons produced by the hollow dispenser cathode (operated at 1.7 A) were pulsed into the ICR cell with a length of 3.0 ms, which led to fragmentation of the ions that were already trapped in the ICR cell. One hundred MS/MS scans per spectrum were acquired with a resolution of 580,000 at m/z 400 Da.

Mass Spectrometry of Phosphorylated FAT: LC/MS

The site of phosphorylation was further verified by a bottom-up approach by LC/MS analysis of trypsin digest of the phosphorylation reaction by Dr. Harsha Gunawardena in the lab of Dr. Xian Chen. After overnight incubation with Src, samples were desalted using PepClean C18 spin columns (Pierce, Rockford, IL) according to the manufacturer's directions and re-suspended in an aqueous solution of 0.1% formic acid. Most of the samples were analyzed via reverse phase LC-MS/MS using a 2D-nanoLC ultra system (Eksigent Inc, Dublin, CA) coupled to an LTQ-Orbitrap XL system with electron transfer dissociation (ETD) (Thermo Scientific, San Jose, CA). The Eksigent system was configured to trap and elute peptides in 1D mode of operation via a sandwiched injection of sample. Trapping was performed on a 3-cm long 100-μm i.d. C18 column whereas elution was performed on a 15-cm long 75-μm i.d., 5 μm, 300 Å particle ProteoPep II integraFrit C18 column (New Objective Inc, Woburn, MA).

Analytical separation of all the tryptic peptides was achieved with a linear gradient of 2-40% buffer B (0.1% formic acid in acetonitrile) over 70 min at a 200 nL/min flow rate, where buffer A is 0.1% formic acid in an aqueous solution.

Mass spectrometric data acquisition was performed in a data-dependent manner on a hybrid LTQ-Orbitrap mass spectrometer. A full scan mass analysis on an Orbitrap (externally calibrated to a mass accuracy of < 1 ppm and a resolution of 60,000) was followed by intensity dependent MS/MS of the top six most abundant peptide ions in the linear ion trap. Collision activated dissociation (CAD)-MS/MS and ETD-MS/MS were used as complimentary methods to dissociate peptides. All CAD-MS/MS spectra were obtained for peptide ions that were subjected to 30 ms resonance activation at a

normalized collision energy of 35 eV in the presence of He bath gas atoms at a pressure of 1 mTorr. All ETD-MS/MS spectra were obtained by performing an ion/ion reaction between peptide cations and fluoranthene anions mutually stored for 100 ms within a linear ion trap. The MS/MS acquisition of a precursor m/z was repeated for a 30 sec duration and subsequently excluded for 60 sec. Monoisotopic precursor ion selection and charge state screening was enabled to trigger data-dependent MS/MS scans. A few neutral H_3PO_4 loss dependent CAD-MS^3 experiments and targeted peptide CAD-MS/MS experiments were also performed.

Mass spectra were processed, and peptide identification was performed using Mascot (Matrix Science Inc.) and Sequest (Thermo-Fisher Scientific) search algorithms against a human-IPI database (V3.63). Peptides were confidently identified using a target-decoy approach with a false discovery rate (FDR) of 1%. A precursor ion mass tolerance of 100 ppm and a product ion mass tolerance of 0.5 Da were used during the search with a maximum of two missed trypsin cleavages. Variable modifications included methionine oxidation and phosphorylation at serine, threonine, and tyrosine residues. The Ascore algorithm was used to confidently localize the phosphorylation site on the peptide.

Peptide quantitation

Quantitation of site-specific phosphorylation in the full-length FAT domain was performed on the peptides that contained the two identified phosphorylation sites of full-length FAT (pY-926 and pY-1008) via standard calibration. Four phosphopeptides containing a ^{13}C-labeled valine residue were synthesized to be used as internal standards by Dr. Krzysztof Krajewski in the laboratory of Dr. Brian Strahl at UNC-CH. The

sequences of the peptides are as follows: SNDKV(p^{926}Y)ENVTGL(V^{13}C5)K-OH, V(p^{926}Y)ENVTGL(V13C5)K-OH, LAQQ(p^{1008}Y)(V^{13}C5)MTSLQQEYK-OH, and MKLAQQ(p^{1008}Y)(V13C5)MTSLQQEYK-OH. The standardization was performed using a minimum of three-to-four standard concentrations (0.1, 0.2, 1, and 2 μg/mL) of the respective heavy stable isotope-labeled standard peptide. The raw peaks were processed, and extracted ion chromatograms (XIC) were generated from the full-scan MS using Xcalibur software. Peptide peaks of interests were normalized by their stable isotope-labeled heavy internal standard counterpart using an in-house Perl script. The integration of each analyte data point was performed using the Genesis algorithm (Thermo-Fisher Scientific, San Jose, CA). All deviations in retention times were corrected by peak alignment. The accuracy of the peak area ratios were validated by acquiring multiple chromatographic runs with the linear gradients described above. Label-free absolute quantitation was based on the relative peak area of the identified phosphopeptide and corresponding phosphopeptide heavy internal standard. A standard curve was generated by plotting the log of the normalized peak area (area of analyte/area of standard) versus the standard concentration. The curves were fit by linear regression in Excel; the x-intercept of the fit represents the analyte concentration. Both 3+ and 2+ charge states were quantified using these standard curves.

Quantification of the phosphorylation of the synthetic peptides as a function of pH was performed as described above except a single-point standard calibration was performed (0.5 μg/mL of heavy internal standard). Phosphorylation reactions of the peptide containing Y926 were diluted 100 fold before analysis by MS whereas reactions

of the peptide containing Y1008 were diluted 4 fold before analysis by MS so that the signal was in an appropriate dynamic range for quantitation.

Circular Dichroism

The CD experiments as a function of pH were conducted by Dr. Kirk Prutzman, a graduate student in the laboratory of Dr. Sharon Campbell at UNC-CH. The FAT domain was exchanged into a degassed phosphate buffer (10 mM K_2-HPO_4, 0.01% NaN_3) at pH 5.0, 5.5, 6.0, 6.5, 7.0, 7.5 and concentrated to 0.145 mg/mL. Far –UV CD spectra (185-260 nm) were collected at 25°C on an Applied Photophysics Pistar-180 spectropolarimeter at the UNC Macromolecular Interactions Facility. Thermal denaturation studies were conducted by monitoring the ellipticity at 221 nm over a temperature range of 25 to 95°C at increments of 0.5°C. Data points were collected after the temperature was constant (± 0.2°C) for 30 sec. After each thermal denaturation run, the temperature was reduced to 25°C for 15 min, and a far-UV spectrum was collected to verify that the FAT domain had refolded. After the far-UV spectrum was collected, a second thermal denaturation spectrum was collected and compared to the first spectrum to determine whether the thermal denaturation process was reversible.

Data analysis was conducted with the assumption that only populations of folded and unfolded species were being monitored and that any other species were not populated to any significant extent. The denaturation curves were first corrected for baseline and then fit to a four variable sigmoidal curve in SigmaPlot. The fit solves for the following variables: maximum, minimum, midpoint (T_m), and slope. The data were normalized from 0 to1 by the following equation: normalized value = (measured value – minimum)/(maximum – minimum).

NMR Spectroscopy

The FAT domain was expressed and purified as described above, except that cells were grown in M9 minimal media supplemented with 1 g/mL $^{15}NH_4$ Cl and 10 g/L ^{12}C glucose or 2 g/L ^{13}C glucose for double-labeled samples.

The purified FAT domain was exchanged into NMR buffer (25 mM Tris maleate pH 5.5, 6.0, 6.5, 7.0, or 7.5, 150 mM NaCl, 10% D_2O, 0.01% NaN_3) either by dialysis (MW cutoff 6,000-8,000 Da) or by an Amicon filtration device (MW cutoff 10,000 Da). Samples were concentrated by an Amicon filtration device (MW cutoff 10,000 Da). ^{1}H-^{5}N 2D HSQC spectra as a function of pH and a simultaneous 3D $^{13}C/^{15}N$-NOESY [83, 84] at pH 6.0 and 7.5 were collected on a Varian INOVA 800 MHz spectrometer at 37°C. While temperature changes in some buffered solutions can affect the pH, we used a tris-maleate buffer, which is relatively insensitive to temperature changes. The spectra were referenced to each other using peaks associated with the glycine linker. The backbone had been previously assigned at pH 6.0 and pH 7.5 by Dr. Kirk Prutzman, a graduate student in the laboratory of Dr. Sharon Campbell at UNC-CH. The data were processed with NMRPipe [85] and analyzed with NMRView [86].

^{15}N Backbone Relaxation Dynamics of the FAT Domain as a Function of pH

T1, T2, and HetNOE spectra were collected on a 0.4 mM sample of ^{15}N uniformly-labeled FAT domain on a Varian INOVA 600 MHz spectrometer at 37°C at pH 6.0 and pH 7.5. Prior to data collection, the temperature was calibrated using a 100% methanol standard sample. R1 and R2 relaxation rates were sampled with nine time points, three of which were collected in duplicate to estimate error. Delay values of 48, 136, 250, 385, 540, 708, 892, 1000, and 1300 ms were used for T1 experiments and 7, 15,

23, 39, 62, 78, 93, 109, and 125 ms were used for T2 experiments. Two experiments comprising the ^{1}H-^{15}N NOE were acquired in an interleaved fashioned with a recycle delay ~ 5 sec. For T1 and T2 analyses, the intensities of resolved amide peaks were fit to a single exponential decay using in-house programs provide by the laboratory of Andrew Lee (UNC-CH). For analysis of the HetNOE data, the difference in intensity between the irradiated and non-irradiated spectra was determined using in-house programs provided by the laboratory of Andrew Lee (UNC-CH).

T1, T2, and HetNOE data were used to evaluate motions on the ps-ns timescale using the model-free formalism. The isotropic rotational correlation times were determined using the approach described by Dellwo and Wand [87]. Backbone relaxation rates to fit to one- or two-parameter model-free models (S^2, $S^2 + \tau_e$, or $S^2 + R_{ex}$) using an in-house program provided from the laboratory of Andrew Lee (UNC-CH) [88, 89]. The values used for the effective N-H bond distance and ^{15}N chemical shift anisotropy were 1.02 Å and -170 ppm, respectively. Akaike's information criterion was used to select which model best describes the motion.

Residual Dipolar Couplings

Pf1 phage (Asla Biotech) was added to a sample of 0.4 mM ^{15}N-labeled FAT (in NMR buffer at pH 6.0 or pH 7.5) at a final concentration of 7.5 mg/mL. ^{1}H-^{15}N HSQC spectra were collected with and without Pf1 phage. No significant changes in chemical shift were observed upon the addition of phage, indicating that the phage does not interact with the FAT domain. ^{1}H-^{15}N IPAP HSQC spectra [90] were collected on a Varian INOVA 700-MHz spectrometer with and without phage to measure the $^{1}H^{N}$-^{15}N residual dipolar coupling constant. Two separate datasets were collected at pH 6.0, and

two datasets were collected at pH 7.5. The data were processed with NMRPipe [85] and visualized with NMRView [86]. Peaks were picked manually. We were able to measure 47 dipolar coupling constants out of a possible 138 (146 residues minus 8 prolines) that were common between the pH 6.0 and pH 7.5 datasets. The correlation between the RDC measurements was evaluated using the software Prism 5 (Graphpad).

CLEANEX

CLEANEX-PM [77] spectra were collected on a Varian INOVA 600-MHz spectrometer at 37°C on a sample of ^{15}N-labeled FAT domain at pH 6.0, 6.5, 7.0, and pH 7.5 with a delay period of 0, 10, 20, 30 and 55 ms. The data were processed by NMRPipe [85] and analyzed in NMRView [86].

Chapter 3

Characterization of Y926 Mutants of the FAT Domain

Introduction

Focal adhesion kinase (FAK) is a nonreceptor tyrosine kinase that localizes to focal adhesions upon integrin activation. FAK consists of an N-terminal FERM (4.1 protein, ezrin, radixin, moesin) domain, a central kinase domain, and a C-terminal focal adhesion targeting (FAT) domain. The FAT domain is responsible for proper localization and subsequent activation of FAK at least partially via its interaction with paxillin. Also, phosphorylation of Y926 in the FAT domain has been implicated in promoting delocalization of FAK from focal adhesions and focal adhesion turnover and in linking FAK to the mitogen-activated protein kinase (MAPK) pathway, thus promoting angiogenesis and cell migration [19]. The focus of this study is on investigating various Y926 mutants of the FAT domain.

Phosphorylation of Y926 in the FAT domain has been linked to angiogenesis [19] and tumor invasion and metastasis [47]. In these studies, the role of phosphorylation was probed by mutating Y926 to a nonphosphorylatable mutant, namely Y926F. Kaneda et al. demonstrated that a FAK Y926F mutant decreased migration and invasion *in vitro* and decreased metastasis *in vivo* [47]. However, they also reported that FAK Y926F is deficient in paxillin binding compared to wild type. There are two paxillin binding sites in the FAT domain. One site is located in a hydrophobic pocket between helices-1 and -4

whereas the other site is located between helices-2 and -3. While the integrity of both sites is important for maximal FAK activation, the 1,4 site is more important for localization of FAK to focal adhesions than the 2,3 binding site [39]. Because Y926 is in helix-1, mutation of this site would be expected to disrupt the 1,4 paxillin binding site. It has been shown that the Y926F mutant does localize to focal adhesions; however, these studies were not done quantitatively [19], and it is possible that the Y926F mutant reaches focal adhesions via an alternate paxillin-independent pathway [39]. Even if the Y926F mutant is successful at reaching focal adhesions, if it does so by using a secondary pathway, then one would expect a change in FAK/paxillin-mediated signaling pathways because paxillin is a substrate of FAK. Therefore, impairment of FAT/paxillin interactions may lead to decreased phosphorylation of paxillin, which could lead to changes in paxillin-mediated signaling pathways. Therefore, it is difficult to interpret *in vivo* data that rely on the Y926F mutant because it is difficult to distinguish whether effects of the mutation are due to a loss of phosphorylation at Y926 or a decrease in FAT/paxillin interactions.

While not as common, phosphomimetic mutants of the FAT domain have also been studied to investigate how phosphorylation at Y926 might alter the structure or dynamics of the FAT domain. Zhou et al. conducted NMR-based hydrogen exchange studies as a function of denaturant to study the folding mechanism of Y926E and detected an intermediate state in which helix-1 is less structured [51]. This state is similar to the intermediate detected in our lab in wild type FAT using hydrogen exchange-directed discrete molecular dynamics (DMD) [50]. However, it is unclear whether introducing a negative charge at position 926 with an aspartate mutation affects the probability of the

intermediate state because no studies were performed with both the wild type FAT domain and the phosphomimetic mutant.

Because the Y926F mutant affects paxillin binding and therefore may affect FAK localization and signaling, we characterized this mutant *in vitro* to see if the mutation alters the structure of the FAT domain, thus altering paxillin binding. Furthermore, because the Y926F mutant is known to be deficient in paxillin binding, we made a Y926A and Y926N mutant to determine whether a different mutation at Y926 would retain paxillin binding while still acting as a non-phophorylatable mutant, thus simplifying the analysis of *in vivo* studies. We also characterized the Y926D and Y926E phosphomimetic mutants to investigate how phosphorylation might affect the structure and function of the FAT domain.

We investigated the structural properties of the Y926 mutants described above (Y926F, Y926A, Y926N, Y926D, and Y926E) by circular dichroism (CD) and NMR and analyzed their ability to bind paxillin by fluorescence polarization and pull-down assays. The CD experiments revealed that all of the mutants retained helical content and that the non-phosphorylatable mutants Y926F and Y926A had similar stability to wild type whereas the nonphosphorylatable mutant Y926N and the phosphomimetic mutants Y926D and Y926E were less stable than wild type. Because we had evidence that the stability of the FAT domain is sensitive to pH (see pH chapter), we evaluated the stability of the Y926 mutants at pH 6.0 and pH 7.5. The nonphosphorylatable mutants Y926F, Y926A, and Y926N had a similar sensitivity to pH as wild type with regard to stability whereas the stability of the phosphomimetic mutants Y926D and Y926E was less sensitive to pH than wild type. The paxillin binding experiments revealed that none of

the mutants were able to bind to paxillin as well as wild type, suggesting that Y926 may be involved in key interactions between FAT and paxillin. Therefore, it does not appear that there is an ideal nonphosphorylatable mutant of Y926 that can retain paxillin binding.

Results/Discussion

Expression of Y926 FAT Mutants

We used site-directed mutagenesis to mutate Y926 in the FAT domain to phenylalanine, alanine, asparagine, serine, aspartate, or glutamate. We were not able to express or purify the serine mutant. The other mutants, however, expressed and purified similarly to wild type and were conducive to biophysical studies.

Circular Dichroism of Y926 Mutants

We first investigated whether mutation at Y926 affected the secondary structure of the FAT domain by CD. Analysis of secondary structure by CD indicates that each mutant is helical, similar to wild type (data not shown). We also analyzed the stability of these mutants by CD. We collected CD melting curves at pH 6.0 and pH 7.5 because we have evidence that the stability of the wild type FAT domain is sensitive to pH (see pH chapter). The melting curves of the Y926 mutants at pH 6.0 and 7.5 are shown in **Figure 3.1**. The values of the melting temperatures for each mutant at the two pH values are shown in **Table 3.1**.

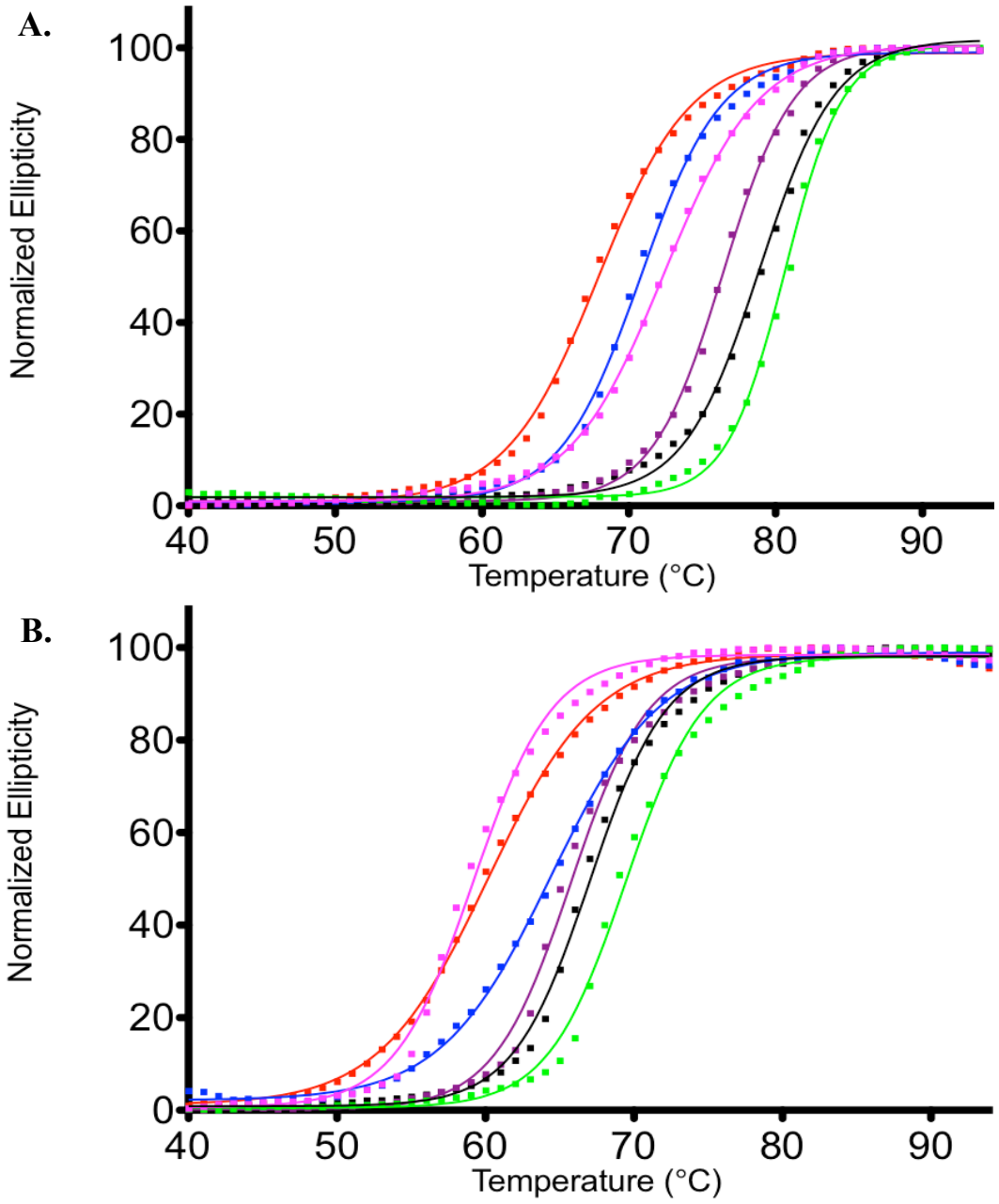

Figure 3.1: Thermal Denaturation of Y926 Mutants
A. Thermal denaturation melting profiles at pH 6.0 and **B.** at pH 7.5 of Y926F (green), wild type FAT (black), Y926A (purple), Y926E (blue), Y926D (red), and Y926N (pink).

The nonphosphorylatable mutants Y926F and Y926A have similar melting curve profiles at both pH 6.0 and pH 7.5 and show a similar sensitivity to pH compared to wild type, with a change in about 12°C between pH 6.0 and pH 7.5. However, the

nonphosphorylatable mutant Y926N and the phosphomimetic mutants (Y926D and Y926E) are less stable than wild type FAT at both pH 6.0 and pH 7.5. While the Y926N mutant has a similar sensitivity to pH as wild type, the Y926D and Y926E mutants are less sensitive to pH, with a change in about 7°C between pH 6.0 and pH 7.5. Therefore, introducing a negative charge at Y926 destabilizes the FAT domain and seems to partially counteract the observed pH sensitivity. Based on these data, one might speculate that if the FAT domain is regulated by pH *in vivo*, then upon phosphorylation, it is less sensitive to changes in pH.

Table 3.1: Melting temperatures of Y926 mutants of the FAT domain as a function of pH

	pH 6.0 (°C)	pH 7.5 (°C)	Difference (°C)
wt	78.93 ± 0.07	67.02 ± 0.08	11.91 ± 0.08
Y926F	80.64 ± 0.05	69.44 ± 0.09	11.20 ± 0.09
Y926A	76.42 ± 0.04	65.74 ± 0.09	10.68 ± 0.09
Y926N	72.41 ± 0.05	59.19 ± 0.09	13.22 ± 0.09
Y926E	70.80 ± 0.07	64.41 ± 0.07	6.39 ± 0.07
Y926D	67.92 ± 0.07	60.15 ± 0.08	7.77 ± 0.07

^{1}H-^{15}N HSQC Spectra of Y926 Mutants

To better ascertain whether various mutations at Y926 affect the structure of the FAT domain, we collected ^{1}H-^{15}N HSQC spectra on uniformly ^{15}N-labeled FAT constructs. **Figure 3.2** shows an overlay of the wild type spectrum (black) and the corresponding FAT mutant spectrum (color). There are considerable chemical shift changes between the HSQC spectra of wild type FAT and the mutants. These shifts are not localized to the site of mutation. Rather, chemical shift changes are seen throughout

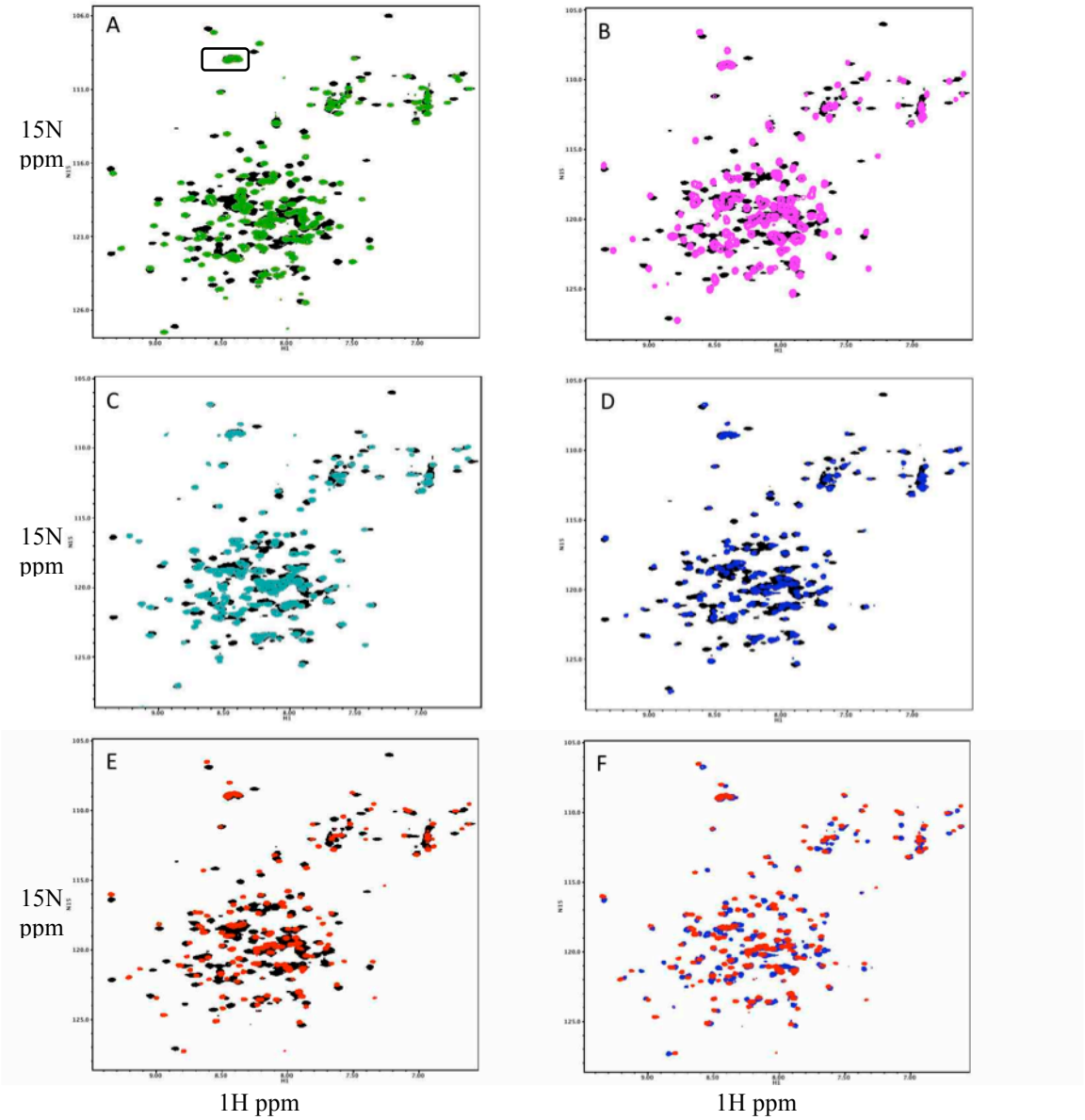

Figure 3.2: ^{1}H-^{15}N HSQC Spectra of the Y926 Mutants
Overlay of the ^{1}H-^{15}N HSQC spectra of wild type FAT with **A.** Y926F, **B.** Y926A, **C.** Y926N, **D.** Y926D, and **E.** Y926E. **F.** Overlay of the ^{1}H-^{15}N HSQC spectra of Y926D (blue) and Y926E (red). Data were collected at pH 6.0 at 37°C. The spectra were referenced by aligning the peaks of the glycine linker (in box in **A.**)

the 3D structure of the protein. Interestingly, there are also considerable chemical shift differences between the Y926D and Y926E spectra (**Figure 3.2F**). This is rather surprising because the Y926D and Y926E mutants differ by a single methylene group. Qualitative analysis of the Y926D and Y926E spectra suggests that the Y926D spectra is more similar to that of wild type FAT than the Y926E spectrum, perhaps suggesting that Y926E is a better phosphomimetic that Y926D, which is consistent with the fact that glutamate has a longer side chain than aspartate, which would be expected to more closely resemble the size of the tyrosine side chain.

A change in chemical shift suggests that the electrochemical environment of that residue has changed. It is therefore difficult to determine if changes in chemical shift are due to structural changes in the FAT domain or simply slight changes in the local environment that may propagate from the site of mutation. To better determine whether mutations at Y926 cause structural changes in the FAT domain, it will first be necessary to assign the HSQC spectra of the mutants. While a large number of the peaks can probably be assigned based on comparison with the wild type spectrum, the differences between the spectra are so pervasive that it is necessary to collect additional three-dimensional NMR data on the mutants to unequivocally assign the spectra. Once that is accomplished, further experiments, such as RDCs, will help to clarify whether there is a structural change.

Paxillin Binding of the Y926 Mutants

We also examined these mutants' ability to bind paxillin *in vitro*. We first pulled down endogenous full-length paxillin from REF52 lysates using GST-FAT and blotted for paxillin. **Figure 3.3** shows the results of a pull-down experiment. As expected, wild

type FAT shows robust paxillin binding. Similar to the results of Kaneda et al., we observed that Y926F does not bind to paxillin as well as wild type; however, among the Y926 mutants, the paxillin binding to the Y926F mutant is the most similar to that of wild type FAT. Some paxillin binding is observed with Y926A whereas paxillin binding is undetectable with the Y926N, Y926E, and Y926D mutants. These data are consistent with the thermal denaturation data in which the stabilities of the Y926F and Y926A mutants were more similar to wild type whereas the Y926D, Y926E, and Y926N mutants were significantly less stable than wild type.

The fact that Y926D and Y926E do not show any paxillin binding suggests that phosphorylation at Y926 may also disrupt paxillin binding. It has been speculated that phosphorylation at Y926 and paxillin binding are mutually exclusive because the paxillin binding site includes Y926; however, it has not been directly shown that this is the case. The fact that every mutation we have made so far at this site impairs paxillin binding suggests that Y926 may play a critical role in paxillin binding.

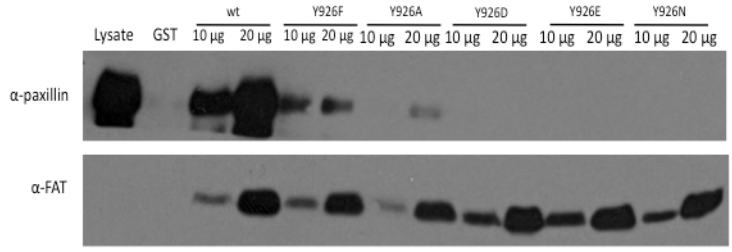

Figure 3.3: Paxillin Pull-Downs of the Y926 Mutants Endogenous paxillin was pulled down from REF52 cell lysates with the indicated amount of immobilized GST-FAT constructs. Paxillin and FAT were detected by Western blot.

To gain more quantitative information, we also analyzed paxillin binding to the FAT domain by fluorescence polarization. We used a 28-mer peptide conjugated to the fluorophore 5-carboxyfluorescein (5-FAM) designed to mimic the LD2 motif of paxillin, which has been shown to bind to the FAT domain at two sites, in a hydrophobic groove between helices-1 and -4 and between helices-2 and -3 [43]. The groove between

helices-1 and -4 contains Y926, and a perturbation at this site, for example mutation of Y926, might be expected to disrupt paxillin binding. **Figure 3.4** shows representative binding curves for wild type FAT and the Y926 mutants, and the K_d values are shown in **Table 3.2**. Wild type FAT has a K_d of approximately 7 μM, which is consistent with what has been previously observed by isothermal titration calorimetry (ITC) [43]. Similar to the pull-down experiments, none of the mutants were able to bind paxillin as well as the wild type protein. The K_d values for the mutants increased by about a factor of two compared wild type. It is somewhat difficult to compare these K_d values as they were fit assuming one binding site, and LD2 is known to bind to two sites on the FAT domain [40, 43]. However, we were hesitant to fit the binding curves of the Y926 mutants to a two-site model because we suspected that mutation of Y926 could eliminate binding to the 1,4 binding site. Therefore, the K_d values in **Table 3.2** should be interpreted as apparent binding affinities. Analysis by ITC would allow us to determine the stoichiometry of the binding interacting and to more appropriately fit the fluorescence polarization data.

It is interesting to note that paxillin binding to Y926N, Y926E, and Y926D was not observable in the pull-down assays whereas in the fluorescence polarization assay, the K_d only increases by a factor of two. As mentioned above, we are using a short (27-mer) peptide of paxillin in the fluorescence polarization assay, and, in the complex of this peptide and the FAT domain [43], Y926 is near the N-terminus of the peptide. Therefore, in the context of full-length paxillin, Y926 may be involved in interactions that are not possible in the context of the paxillin peptide. Thus, mutations of Y926 may not have as profound of an effect on binding the paxillin peptide as binding to full-length paxillin.

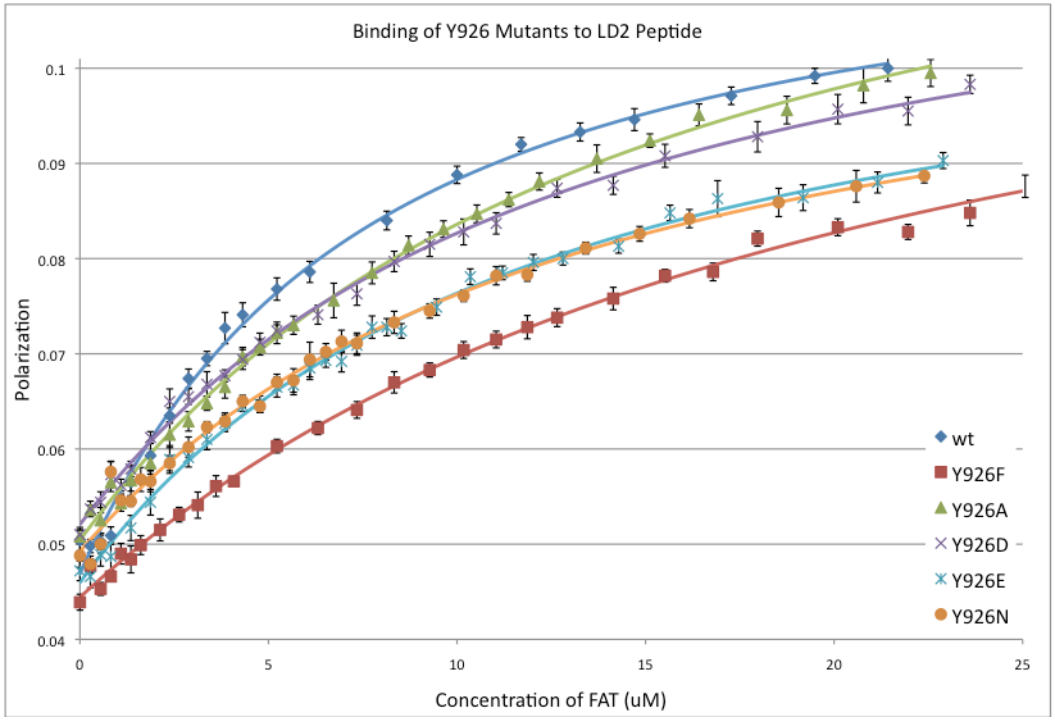

Figure 3.4: Binding of the Y926 Mutants to the LD2 Peptide:
Binding of the FAT domain to the LD2 paxillin peptide conjugated to the fluorophore 5-FAM was detected by fluorescence polarization. Each data point represents the average of nine measurements. Experiments were conducted at room termperature.

Table 3.2 Binding Affinities of Y926 Mutants to the LD2 peptide

	K_d (μM) (n=3)
wt	7.3 ± 0.3
Y926F	18.0 ± 0.8
Y926A	13.7 ± 0.5
Y926D	13.1 ± 0.7
Y926E	10.8 ± 0.4
Y926N	13.0 ± 0.9

Therefore, future studies should include a longer paxillin peptide construct to ensure that any interaction between position 926 and paxillin is taken into account. Also of interest is that whereas the Y926F mutant showed the highest paxillin binding among the Y926 mutants via the pull-down assay, it showed the weakest binding in the fluorescence

polarization assay. Again, this discrepancy is probably due to the fact that, in the pull-down assays, the FAT domain is binding to full-length paxillin whereas in the fluorescence polarization assays the FAT domain is binding to a short peptide. This discrepancy further highlights the need to test paxillin binding in the context of a longer paxillin peptide that is able to interact with Y926.

Conclusion

Phosphorylation of Y926 in the FAT domain of FAK is important for FAK signaling and has been shown to play a role in angiogenesis [19] and tumor invasion and metastasis [47]. In these studies, the effects of phosphorylation were probed by mutating Y926 to a non-phosphorylatable residue, namely phenylalanine. However, the Y926F mutant was also shown to be deficient in paxillin binding [47], which is important for proper localization and activation of FAK [34, 91]. Therefore, the results of *in vivo* experiments that use the Y926F mutant are difficult to interpret as they may be due to either defects in phosphorylation or paxillin binding.

In this study, we characterized the Y926F mutant of the FAT domain as well as two additional non-phosphorylatable mutants (Y926A and Y926N) and two phophomimetic mutants (Y926D and Y926E) to determine whether mutations at this site disrupt the structure of the FAT domain and to identify a mutation at this site that does not disrupt paxillin binding. Analysis of these mutants by thermal denaturation reveals that the Y926F and Y926A mutants have similar stability as the wild type FAT domain whereas the Y926N mutant is less stable than wild type. Y926 is located in the first turn of helix-1 in the FAT domain and is partially exposed to the solvent. It is unclear from the structure why mutation to asparagine would have such a profound effect on stability.

Analysis of these mutants by NMR reveals that widespread changes in chemical shift are present in the ^{1}H-^{15}N HSQC spectra of all the mutants compared to wild type. It is difficult to tell from the HSQC spectrum alone what type, if any, of structural change may be occurring upon mutation of Y926. If these analyses are to be taken further, these spectra must first be assigned using three-dimensional NMR techniques. Once that is accomplished, other experiments such as RDCs can better elucidate if a change in structure occurs upon mutation of Y926.

Whether mutation of Y926 causes a structural change in the FAT domain, it is known to have functional consequences, i.e., disruption of paxillin binding. We observed by pull-down assays and fluorescence polarization that the Y926F mutant does not bind to paxillin as well as wild type, which is consistent with previous reports [47]. Mutation of Y926 to alanine or aspargine did not rescue this deficiency in paxillin binding. In fact, of the mutants we tested, Y926F showed the highest paxillin binding. Therefore, it appears that there is not an ideal nonphosphorylatable mutant of the FAT domain that retains wild type levels of paxillin binding and that Y926F seems to be the best mutant available. However, because it does have a decreased affinity for paxillin compared to wild type FAT, the caveats of *in vivo* studies with this mutant should be taken into consideration when interpreting results from these studies.

We were unable to detect paxillin binding to the phosphomimetic mutants, Y926E and Y926D, by paxillin pull-downs. These mutants were made to mimic the negative charge of a phosphate group. Addition of a negative charge at Y926 destabilized the FAT domain and decreased its sensitivity to pH. The destabilization could be due to the fact that the side chain of D1040, located in helix-4 of the FAT domain, points toward

Y926. In the crystal structure of the FAT domain, D1040 is involved in a salt bridge with R920 [48], which is one of the interactions that tethers helix-1 to helix-4. In the NMR structure of the FAT domain [49], this salt bridge is not apparent. It is possible that the addition of a negative charge at Y926 could either interfere with this interaction or is simply destabilizing because of the introduction of negative charge near a negatively-charged residue (D1040). It is interesting to speculate that phosphorylation at Y926 may have a similar effect, which could have consequences on how phospho-Y926 is recognized by the SH2 domain of Grb2. It is difficult to speculate on the mechanism for the decrease in sensitivity to pH observed in the Y926D and Y926E mutants as we do not currently know what is causing this pH sensitivity. We have mutated D1040 to alanine and do not see a change in the pH sensitivity of the protein (see Chapter 2).

Methods

Mutagenesis

The construct expressing the GST-wtFAT domain fusion protein has been described elsewhere [49]. The Quikchange mutagenesis protocol (Stratagene) was used to incorporate point mutations into position 926. The following primers were used to make the desired mutants (bold indicates site of mutation):

Y926F

5’ CGC TCC AAT GAC AAA GTC **TTT** GAG AAT GTA AAC GGG CTG 3’

Y926D

5’ CGC TCC AAT GAC AAA GTC **GAT** GAG AAT GTA AAC GGG CTG 3’

Y926E

5’ CGC TCC AAT GAC AAA GTC **GAA** GAG AAT GTA AAC GGG CTG 3’

Y926A

5’ CGC TCC AAT GAC AAA GTC **GCG** GAG AAT GTA AAC GGG CTG 3’

Y926S

5’ CGC TCC AAT GAC AAA GTC **TCT** GAG AAT GTA AAC GGG CTG 3’ and

5’ CGC TCC AAT GAC AAA GTC **TCT** GAG AAT GTA AAC GGG CTG GTG 3’

Y926N

5’ CGC TCC AAT GAC AAA GTC **AAC** GAG AAT GTA AAC GGG CTG 3’

Quikchange reactions were digested with DpnI at 37°C to remove any template DNA and transformed into DH5α *E. coli* cells. Single colonies were chosen and incubated in LB-Amp overnight, and plasmid DNA was purified using the Qiagen Miniprep kit. The mutation was verified by sequencing at the UNC-CH Genome Analysis Facility using the pGEX 5’ sequencing primer (5’ GGGCTGGCAAGCCACGTTTGGTG 3’).

Expression and Purification of wild type and mutant FAT

The FAT domain construct used in these studies contains residues 920 to 1053 of chicken FAK plus a 12 amino acid N-terminal linker (bold): (**GSPGISGGGGGI**RSNDKVYENVTGLVKAVIEMSSKIQPAPPEEYVPMVKEVGL ALRTLLATVDESLPVLPASTHREIEMAQKLLNSDLAELINKMKLAQQYVMTSLQ QEYKKQMLTAAHALAVDAKNLLDVIDQARLKMISQSRPH). The FAT domain was expressed as a GST fusion protein as previously described [49]. The pGEX-KG plasmid containing the GST-FAT sequence was transformed into BL21(DE3) *E. coli* cells for protein expression. Bacteria were grown in LB-Amp at 37°C to an OD_{600} ~ 0.6. Expression was then induced by the addition of 0.5 mM IPTG, and cells were grown for a

further three to five hours before harvesting by centrifugation. Cells were resuspended in lysis buffer (20 mM Tris pH 7.5, 10% glycerol, 10 mM DTT, 150 mM NaCl) and lysed by sonication (5 sec. on 5 sec. off for a total of one hour). The lysate was centrifuged at 15k rpm for 70 min. to remove insoluble cell debris. The supernatant was added to glutathione-agarose (GSH) beads and incubated at 4°C overnight. The beads were washed once with lysis buffer and two times with thrombin cleavage buffer (50 mM Tris pH 8.0, 150 mM NaCl, 2.5 mM $CaCl_2$, 0.1% BME). Typically, about 0.5 units/mL of thrombin were added to the beads to cleave the fusion protein. The beads were incubated with thrombin at room temperature overnight and then washed three times with thrombin cleavage buffer. The supernatants of these washes were combined, and thrombin activity was inhibited by the addition of p-aminobenzamidine agarose beads, which were subsequently removed by centrifugation. The protein was dialyzed into S-column buffer A (25 mM $NaPO_4$ pH 5.5, 0.01% NaN_3) and purified by cation-exchange chromatography on a mono S column and eluted with a gradient of 0 – 1 M NaCl over 200 mL. The protease inhibitors PPACK (1 μM) and pefablock (0.5 mg/mL) were added to the purified protein to prevent degradation. All mutants were purified in a similar manner.

Protein concentration was measured by diluting the protein in a final concentration of 6 M guanidinium hydrochloride and measuring the absorbance at 280 nm. The concentration was calculated using the calculated extinction coefficient at 280 nm (5120 $M^{-1}cm^{-1}$ for wild type and 4470 $M^{-1}cm^{-1}$ for the mutants) from the ProtParam tool on the ExPASy proteomics server [80].

Circular Dichroism

Purified protein was dialyzed into CD buffer (10 mM $NaPO_4$) at the desired pH. Because Cl^- ions interfere with the CD signal, the desired pH was acquired by combining 10 mM Na_2HPO_4 and 10 mM NaH_2PO_4. The proteins were concentrated using an Amicon filtration device (MWCO 10 kDa), and the concentration was adjusted to 50 μM. CD spectra were collected at the Macromolecular Interactions Facility at UNC-CH on a Chirascan spectrometer. Wavelength scans were collected from 260 –180 nm with a 0.5 nm step size. Thermal denaturation was monitored at 222 nm from 25°C to 95°C with a ramp speed of 1°C/min and a tolerance of 0.2°C. The data were normalized from 0 to 100 and fit in Prism 5.0 to a sigmoidal curve with variable slope: y = minimum +(maximum-minimum)/(1+$10^{\log(Tm-x)\text{-slope}}$), where y is the normalized ellipticity, x is the temperature, Tm is the melting temperature, and slope is the Hill coefficient.

NMR Spectroscopy

The wild type FAT domain and mutants were expressed and purified as described above, except that cells were grown in M9 minimal media supplemented with 1 g/mL $^{15}NH_4$ Cl.

The purified FAT domain was exchanged into NMR buffer (25 mM tris maleate pH 6.0, 150 mM NaCl, 10% D_2O, 0.01% NaN_3) either by dialysis (MW cutoff 6,000-8,000 Da) or by an Amicon filtration device (MW cutoff 10,000 Da). Samples were concentrated by an Amicon filtration device (MW cutoff 10,000 Da). ^1H-^{15}N HSQC spectra were collected on either a Varian INOVA 500-, 600-, or 700-MHz spectrometer at 37°C. The data were processed with NMRPipe [85] and analyzed with NMRView

[86]. The mutants were referenced to the wild type ^{1}H-^{15}N HSQC spectrum using the peaks of the glycine linker.

Fluorescence Polarization

The FAT domain was dialyzed into 50 mM HEPES pH 7.0, 100 mM NaCl, 0.01% NaN_3 and concentrated with an Amicon filtration device (MWCO 10 kDa). The concentration was adjusted to 50 μM. The LD2 peptide, which mimics the LD2 motif of paxillin (^{133}MTSTSLGSNLSELDRLLLELNAVQHNP^{159}) was synthesized with the fluorophore 5-carboxyfluorescein (5-FAM) conjugated to the N-terminus by Dr. Krzysztof Krajewski in the laboratory of Dr. Brian Strahl at UNC-CH. The FAT domain was titrated into a quartz cuvette containing 1 mM of the LD2 peptide. The polarization was measured one minute after addition of the FAT domain to allow the system to reach equilibrium. Fluorescence polarization was collected on a Jobin Yvon Horiba Fluoromax-3 fluorimeter with dark value correction at room temperature. The slit width was set to 2 nm; the excitation wavelength was 492 nm, and the emission wavelength was 526 nm. The integration time was 1.0 sec, and each datapoint is the average of nine measurements. The data were fit using SigmaPlot.

Paxillin Pull-Downs

Rat embryo fibroblasts (REF52) were grown in Dulbecco's Eagle medium supplemented with 10% fetal bovine serum (FBS) and 0.1% antibiotic-antimyotic (PSF). Cells were placed on ice, washed with 1X phosphate buffered saline (PBS) and lysed in ice-cold RIPA buffer (150 mM NaCl, 50 mM Tris pH 7.6, 1% Triton X-100, 0.1% SDS, 0.25% deoxycholate, 200 μM orthovanadate, 1 μg/mL aprotinin, 1 μg/mL leupeptin, 1

mM PMSF). Lysates were centrifuged at 13,000 rpm at 4°C, and the supernatant was carefully collected and kept at -80°C until use.

GST-FAT fusion proteins were expressed and purified as described above. However, after incubation with GSH beads, the beads were washed three times with lysis buffer. GST-FAT concentration was estimated by a BCA assay (Pierce). The specified amount of immobilized GST-FAT was incubated with REF52 lysate for approximately two hours at 4°C. To keep the background consistent, blank GSH beads were added to the reaction so that the total amount of GSH beads was constant. After incubation, the beads were spun down and the supernatant removed. The beads were washed three times with RIPA buffer and once with PBS. Proteins were separated by SDS-PAGE and transferred to a polyvinylidene fluoride (PVDF) (Millipore) at approximately 85 V for one hour for western blotting analysis. The membrane was blocked with 5% milk for one hour at room temperature and then incubated with anti-paxillin (BD Transduction Laboratories Catalog # 610051) or anti-FAK antibodies (BC4 [5, 91], provided by Dr. Michael Schaller) (1:1000 dilution, 5% milk) for either one hour at room temperature or overnight at 4°C. After incubation with the primary antibody, the membrane was washed three times with TBST and incubated with the secondary antibody (anti-mouse IgG for paxillin and anti-rabbit IgG for FAK, 1:10000 dilution, 5% milk) for one hour at room temperature. The membrane was then washed three times with TBST, and proteins were visualized via SuperSignal West Pico Chemiluminescent Substrate (Pierce) and visualized using Kodak BioMax film (Kodak). For quantification of western blots, intensity values of bands were measured from three different repeats for each experiment using Image J software (NIH).

CHAPTER 4

FAT/TALIN INTERACTIONS

Introduction

FAK is a 125-kDa protein that is involved in cell adhesion and migration. FAK localizes to focal adhesions upon integrin activation and plays a key role in both focal adhesion assembly and disassembly. Localization of FAK to focal adhesions is mediated by the C-terminal focal adhesion targeting (FAT) domain [37, 38]. While it seems that there are several mechanisms by which the FAT domain can direct proper localization of FAK, the major mechanism seems to be the interaction of the FAT domain with paxillin [34, 39]. However, secondary mechanisms of localization have been proposed as there are mutants of the FAT domain that do not bind to paxillin that still localize to focal adhesions, albeit less than wild type [39].

One possibility for a paxillin-independent mechanism of localization is the interaction between the FAT domain of FAK and talin. Talin is a 270-kDa protein that consists of an N-terminal head domain and a C-terminal rod domain. The head domain is made up of a FERM domain (4.1/ezrin/radixin/moesin), which contains an F1, F2, and F3 lobe that mediates protein-protein interactions [92]. In particular, the F3 domain of talin binds to integrin tails whereas the rod domain of talin contains at least two actin binding sites. In this way, talin provides a physical link between integrins and the actin cytoskeleton at sites of focal adhesions [92]. Observations that talin co-

immunoprecipitates with FAK suggested an interaction between these two proteins *in vivo* [41, 42]. Furthermore, recombinant constructs of FAK were able to bind to immobilized talin that had been immunoprecipitated from SDS-denatured cell lysates to disrupt any talin/protein interactions that could mediate an indirect interaction with FAK, suggesting that the observed interaction between FAK and talin is indeed direct [41]. Attempts to localize the talin binding site of FAK revealed that deletion of residues 965-1012 of FAK, which are in the FAT domain, abrogate binding to talin, suggesting that talin binds to the FAT domain of FAK [41]. Interestingly, Pyk2, a close homolog of FAK that does not localize to focal adhesions does not bind to talin. However, a chimeric protein containing the N-terminal domains of Pyk2 and the C-terminal domain of FAK is able to bind talin and localize to focal adhesions [42]. These data suggest that talin binding to the FAT domain of FAK may be involved in localization to focal adhesions and that the FAK/talin interaction could be one mechanism that differentiates the functions of FAK from those of Pyk2. However, more recent studies have had difficulties detecting an interaction between FAK and talin [39], and a possible role for the FAK/talin interaction remains both controversial and elusive.

Unpublished data from the laboratory of Dr. David Schlaepfer at UCSD indicate that the FAT domain of FAK interacts with an F2F3 domain construct of talin, with the F3 domain containing the minimal necessary binding site. Attempts to purify the talin F2F3 domain construct were unsuccessful. Therefore, we tested whether we could detect an interaction *in vitro* between purified FAT and talin F3 domain constructs by gel filtration and NMR and were unable to detect an interaction under our conditions.

Results/Discussion

Purification of Talin Constructs

Several talin constructs were provided by Dr. Christine Lawson in the laboratory of Dr. David Schlaepfer at UCSD. First, two constructs containing the talin F2/F3 (206-405) and F3 domains (311-405) in pGEX-4T1 plasmids were expressed and purified from *E. coli*. While these proteins expressed well, they did not seem to be stable upon cleavage of the GST tag by thrombin. Therefore, these constructs were not considered to be conducive to NMR analyses. Next, a construct containing talin F2/F3 (209-400) in a pet28a vector was expressed and purified. While this construct expressed and purified well, we were not able to concentrate it to the levels need for NMR analyses (~ 100-400 μM), especially upon the addition of the FAT domain, as the protein precipitated out of solution. Finally, a talin F3 construct (309-405) in a pet28a vector was acquired that remained soluble at micromolar concentrations when combined with the FAT domain.

Gel Filtration of FAT/Talin

To determine whether the FAT domain interacts with the talin F3 domain *in vitro*, the two purified constructs were combined in a 1:1 ratio and run over an S75 column. **Figure 4.1A** shows an overlay of the traces from talin F3 alone, FAT alone, and FAT + talin F3. As expected, the talin F3 domain (11 kD) elutes slightly later than the FAT domain (16 kD). While the two individual proteins are not able to be resolved in the FAT + talin trace, there is no peak that corresponds to a FAT/talin complex (27 kD). **Figure 4.1B** shows the Coomassie-stained gel of the fractions from the FAT/talin run. The SDS-PAGE gel indicates that the two proteins elute separately and, as expected from the FAT alone and talin alone runs, the talin F3 domain elutes slightly later than the FAT domain.

While we were unable to detect an interaction between the talin F3 domain and the FAT domain by gel filtration, this method is not capable of detecting weak interactions. Therefore, we decided to investigate a possible interaction by NMR because this method is capable of detecting weak interactions ($k_d \sim$ mM).

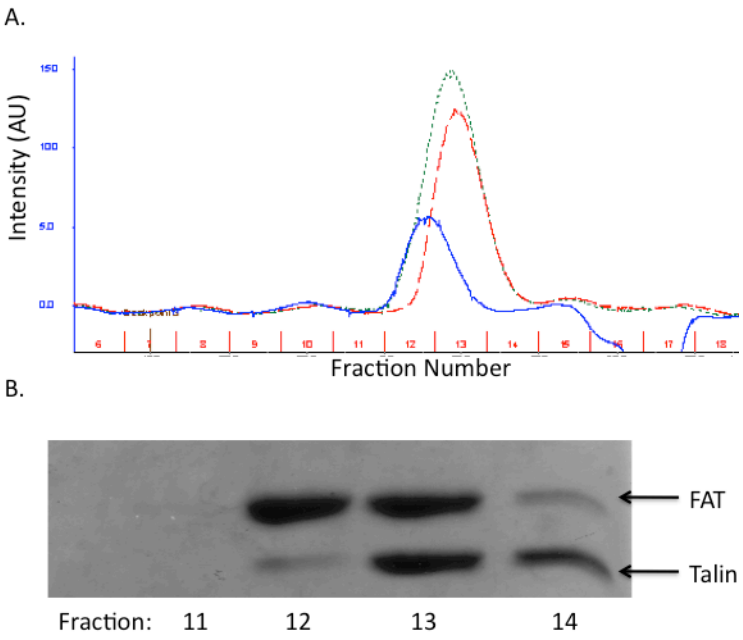

Figure 4.1: Gel Filtration of FAT/Talin
(A) Overlay of gel filtration chromatogram of FAT alone (blue, solid line), talin alone (red, dashed line), and FAT + talin (green, dotted line). (B) Coomassie-stained gel of fractions 11-14 showing the elutions profiles of the FAT + talin gel

HSQC Spectra of FAT/Talin

To further investigate whether we could detect a FAT/talin interaction *in vitro*, we combined ^{15}N-labeled FAT with unlabeled talin. ^{1}H-^{15}N HSQC spectra were collected under a variety of conditions: pH 6.0, 25°C with a 5-fold molar excess of talin; pH 6.0, 37°C with a 5-fold molar excess of talin; pH 7.5, 25°C with a 5-fold molar excess of talin; and pH 7.5, 25°C with a 10-fold molar excess of talin. Because the sample precipitated out of solution at 37°C at pH 6.0, we did not attempt to collect data at 37°C for the pH 7.5 sample. **Figure 4.2** shows the overlay of the ^{1}H-^{15}N HSQC spectra of the FAT domain alone (black) and with 5:1 molar excess of talin F3 (red) at pH 6.0. No changes in chemical shift are observed between the two spectra, indicating that the talin F3 domain does not interact with the FAT domain under

these conditions. Similar results were observed for the other conditions described above (data not shown).

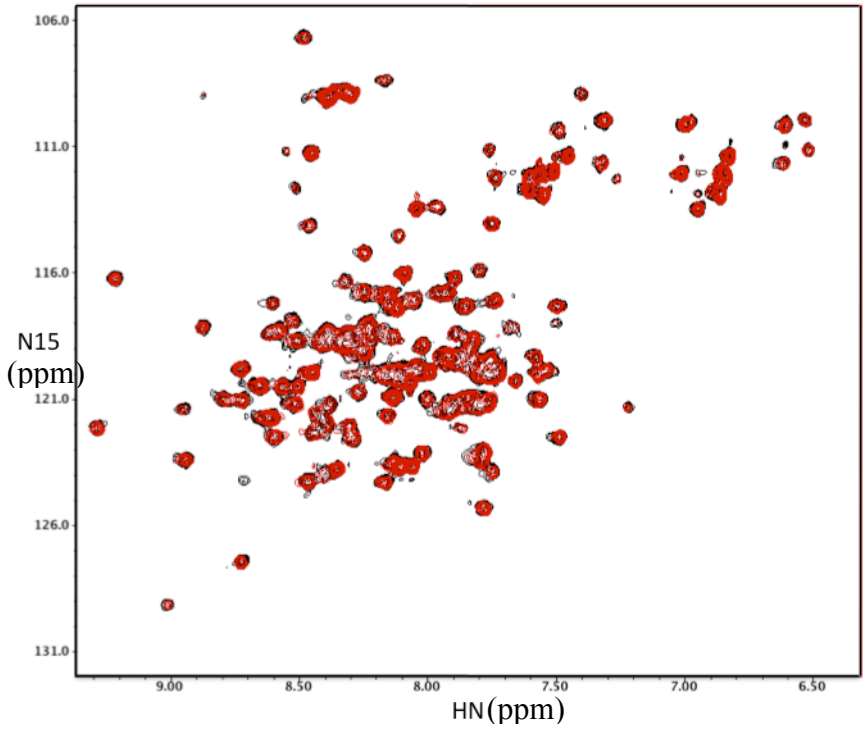

Figure 4.2: ^{1}H-^{15}N HSQC of the FAT Domain with Talin: Overlay of the ^{1}H-^{15}N HSQC of ^{15}N-labeled wild type FAT (black) and ^{15}N-labeled wild type FAT with a 5-fold molar excess of unlabeled talin F3 domain. These spectra were collected at pH 6.0 at 25°C. The lack of changes in chemical shift upon the addition of the talin F3 domain indicates that there is no interaction between these two proteins.

Conclusion

The FAT domain of FAK has been shown to bind to talin *in vivo* via co-immunoprecipitation; however, others have been unable to detect a direct interaction between talin and the FAT domain via several different methods [39]. In this paper, we investigated the interaction between the FAT domain of FAK and the F3 domain of talin. As described above, we had some difficulties finding a talin F3 or F2/F3 construct that was soluble at the concentrations necessary for NMR analyses. In particular, precipitation of the talin constructs appeared to be exacerbated upon addition of the FAT domain, possibly indicating that an interaction is occurring in solution but that the complex is not stable under our experimental conditions. No precipitation issues were

encountered with the talin F3 (309-405) construct upon addition of the FAT domain, and we were unable to detect an interaction between these two domains by either gel filtration or NMR. It is unclear whether our inability to detect a direct interaction between the FAT domain and the F3 domain of talin indicates that no so interaction exists or that the conditions we used were not conducive to FAT/talin binding. It is possible that the F2 domain of talin is necessary either for proper binding to the FAT domain or for proper folding of the F3 domain. A recent crystal structure of the talin head domain containing the F0, F1, F2, and F3 domains revealed several interactions including salt bridges, hydrogen bonds, and hydrophobic interactions between the F2 and F3 domains [93]. As stated earlier in the text, we attempted to purify several F2F3 domain constructs; however, none of these constructs were amenable to NMR analyses. However, an F2/F3 domain construct of talin has been used in crystallographic studies in which concentrations of up to 250 μM were achieved [94]. If this complex remains soluble upon addition of the FAT domain, it will be interesting to see whether an interaction can be detected between the FAT domain and the F2F3 domains of talin.

Methods

Expression and Purification of the FAT Domain

The FAT domain construct used in these studies contains residues 920 to 1053 of chicken FAK plus a 12 amino acid N-terminal linker (bold):

(**GSPGISGGGGGI**RSNDKVYENVTGLVKAVIEMSSKIQPAPPEEYVPMVKEVGL ALRTLLATVDESLPVLPASTHREIEMAQKLLNSDLAELINKMKLAQQYVMTSLQ QEYKKQMLTAAHALAVDAKNLLDVIDQARLKMISQSRPH). The FAT domain was expressed as a GST fusion protein as previously described [49]. The pGEX-KG

plasmid containing the GST-FAT sequence was transformed into BL21(DE3) *E. coli* cells for protein expression. Bacteria were grown in LB-Amp at 37°C to an OD_{600} ~ 0.6. Expression was then induced by the addition of 0.5 mM IPTG, and cells were grown for a further three to five hours before harvesting by centrifugation. Cells were resuspended in lysis buffer (20 mM Tris pH 7.5, 10% glycerol, 10 mM DTT, 150 mM NaCl) and lysed by sonication (5 sec. on 5 sec. off for a total of one hour). The lysate was centrifuged at 15k rpm for 70 min. to remove insoluble cell debris. The supernatant was added to glutathione-agarose (GSH) beads and incubated at 4°C overnight. The beads were washed once with lysis buffer and two times with thrombin cleavage buffer (50 mM Tris pH 8.0, 150 mM NaCl, 2.5 mM $CaCl_2$, 0.1% BME). Typically, about 0.5 units/mL of thrombin were added to the beads to cleave the fusion protein. The beads were incubated with thrombin at room temperature overnight and then washed three times with thrombin cleavage buffer. The supernatants of these washes were combined, and thrombin activity was inhibited by the addition of p-aminobenzamidine agarose beads, which were subsequently removed by centrifugation. The protein was dialyzed into S-column buffer A (25 mM $NaPO_4$ pH 5.5, 0.01% NaN_3) and purified by cation-exchange chromatography on a mono S column and eluted with a gradient of 0 – 1 M NaCl over 200 mL. The protease inhibitors PPACK (1 μM) and pefablock (0.5 mg/mL) were added to the purified protein to prevent proteolytic degradation.

Expression and Purification of the Talin F3 Domain

Several talin constructs were provided by Dr. Christine Lawson in the laboratory of Dr. David Schlaepfer at UCSD: mouse talin F2/F3 (206-405) in a pGEX-4T1 vector, mouse talin F3 (311-405) in a pGEX-4T1 vector, chicken talin F2/F3 (209-400) in a

pet28a vector, and mouse talin F3 (309-405) in a pet28a vector. While all of these constructs expressed well in *E. coli*, only the talin F3 (309-405) construct was amenable to purification and the concentrations needed for NMR analyses (~ 0.1 mM).

The talin F3 domain (309-405) was cloned into a pet28a vector by Dr. Christine Lawson in the laboratory of Dr. David Schlaepfer at UCSD. The plasmid was transformed into *E. coli* BL21 cells for protein expression. Cells were grown in LB-Kan to an OD_{600} ~ 0.6 at 37°C, at which time the temperature was reduced to 18°C for about an hour. Protein expression was then induced by the addition of 0.25 mM ITPG, and the cells were incubated overnight at 18°C. The cells were harvested by centrifugation, resuspended in lysis buffer (50 mM Tris pH 8.0, 500 mM NaCl, 5% glycerol, 5 mM imidazole), and lysed by sonication. The lysate was cleared by centrifugation and applied to a Ni^{2+} affinity column that had been pre-equilibrated with lysis buffer. The column was washed with two column volumes of lysis buffer followed by two column volumes of lysis buffer with 50 mM imidazole. Protein was eluted with lysis buffer with 300 mM imidazole. Ten 5-mL fractions were collected, and the presence of the talin F3 domain was verified by SDS-PAGE. Fractions containing the F3 domain were combined and dialyzed against thrombin cleavage buffer (50 mM Tris pH 8.0, 150 mM NaCl, 2.5 mM $CaCl_2$, 0.1% BME) with 5-10 units of thrombin at room temperature overnight. Thrombin activity was inhibited by the addition of p-aminobenzamidine agarose beads, which were subsequently removed by centrifugation. The protein was then loaded onto a mono-S column and eluted with a gradient of 150 – 1000 mM NaCl over 200 mL. The presence and purity of the F3 domain was verified by SDS-PAGE.

Gel Filtration of the Talin F3 Domain

The talin F3 domain and wild type FAT domain were dialyzed into 25 mM Tris-Maleate, pH 6.0, 150 mM NaCl, and 0.01% NaN_3 overnight at 4°C. The proteins were concentrated with an Amicon filtration device (MW cutoff 3 kDa). Two milliliters of 1 mg/mL of the talin F3 domain, 1 mg/mL of wild type FAT domain, and 1 mg/mL talin F3 + 1 mg/mL FAT were run over an S75 column (void volume ~ 23 mL) at a flow rate of 0.3 mL/min. Fractions containing protein were analyzed by SDS-PAGE.

NMR of FAT/Talin Interactions

The talin F3 domain and wild type ^{15}N-labeled FAT domain were dialyzed into NMR buffer (25 mM Tris-Maleate, pH 6.0 or pH 7.5, 150 mM NaCl, and 0.01% NaN_3) overnight at 4°C. The proteins were concentrated with an Amicon filtration device (MW cutoff 3 kDa (talin), MW cutoff 10 kDa (FAT)), and the concentration was measured using the calculated extinction coefficient at 280 nM. Two samples were made up for each pH value. One sample contained a final concentration of 40 μM ^{15}N-labeled FAT domain whereas the other sample contained a final concentration of 40 μM ^{15}N-labeled FAT domain and 200 μM unlabeled talin F3 domain to achieve a 5:1 talin:FAT ratio.

^{1}H-^{15}N HSQC spectra were collected on a Varian INOVA 500-MHz spectrometer equipped with a cold probe at 25°C and 37°C. The data were processed by NMRPipe [85] and visualized with NMRView [86].

CHAPTER 5

CONCLUSIONS AND FUTURE DIRECTIONS

Summary

Focal adhesion kinase (FAK) is a non-receptor tyrosine kinase that localizes to focal adhesions upon integrin activation. It plays a key role in focal adhesion assembly and disassembly and is therefore intimately associated with cell migration and adhesion. Overexpression of FAK has been observed in several types of cancer, and increased overexpression often correlates with increased metastasis and poor prognosis. FAK has recently become a target for cancer therapeutics. Therefore, understanding the mechanisms by which FAK is regulated could prove vital in designing therapies that target specific functions of FAK. The focus of this study was on the C-terminal focal adhesion targeting (FAT) domain of FAK as it plays a key role in FAK function.

Various studies have shown that the interaction between the FAT domain and the protein paxillin is the major mechanism by which FAK localizes to focal adhesions [34, 39]. However, secondary paxillin-independent mechanisms for localization have been proposed because mutants of FAK that cannot bind to paxillin are still able to localize to focal adhesions, albeit at levels about 10% that of wild type FAK [39]. One mechanism put forth for paxillin-independent localization is via an interaction between the FAT domain and the protein talin. While several studies have shown an interaction between the FAT domain and talin, others have had difficulties detecting this interaction [39], and

the existence and possible role for a FAK/talin interactions remains both controversial and elusive.

The FAT domain of FAK is not only necessary for proper localization of FAK to focal adhesions but also plays a key role in proper activation of FAK and signaling pathways involved in cell migration and cell proliferation. In particular, phosphorylation of Y926 in the FAT domain has been suggested to promote angiogenesis, cell migration, and cell metastasis [19, 47]. Because of its role in these processes, therefore, phosphorylation of Y926 may represent an important mechanism by which FAK exerts its metastatic effect. Several studies have addressed the role of phosphorylation of Y926 by mutating the tyrosine to a nonphosphorylatable residue, namely phenylalanine. While this is a common approach to investigate the role of phosphorylation, mutation could affect other processes in addition to preventing phosphorylation. For example, it has been shown that mutating Y926 to a phenylalanine disrupts paxillin binding both *in vitro* and *in vivo* [47]. Because paxillin binding is the major mechanism by which FAK localizes to focal adhesions and paxillin is a substrate of FAK, disruption of paxillin binding could affect FAK localization, activation, and signaling. Because of its proposed role in cell migration and metastasis, understanding how phosphorylation of Y926 is regulated and how phosphorylation affects the structure of the FAT domain will increase our understanding of FAK's role in cancer. Furthermore, because of the complications with the Y926F mutant, new tools are needed to assess the role of phosphorylation of Y926 *in vivo*.

In this study, we conducted a series of biochemical and biophysical experiments to better understand regulation of the FAT domain at the molecular level. In particular,

we investigated phosphorylation of Y926, paxillin binding to FAT mutants, and talin binding. We have addressed the following specific topics:

1. **The effect of pH on the structure, dynamics, and phosphorylation of the FAT domain.**
2. **The effect of mutation of Y926 on the structural features and paxillin binding of the FAT domain.**
3. **A possible interaction between the FAT domain and the F3 domain of talin.**

The Effect of pH on the FAT domain

Summary of Results

a. The FAT domain is phosphorylated by Src at two sites *in vitro*, Y926 and Y1008.
b. Phosphorylation at Y926 and Y1008 is pH dependent, with the two sites showing a different pH-dependent profile. In particular, the optimum pH for phosphorylation at Y926 is 6.0 whereas the optimum pH for phosphorylation at Y1008 is 6.5.
c. Phosphorylation of linear peptides that contain Y926 and Y1008 suggest that it is the structure of the FAT domain and not Src specificity that is dependent on pH.
d. Analysis by CD reveals that the stability of the FAT domain is sensitive to pH.
e. NMR studies suggest that pH affects the dynamics, but not the structure, of the FAT domain.

Implications

The results described in Chapter 2 are the first evidence that Y1008 is a substrate of Src. While phosphorylation of Y1008 has been observed before [74], it was not identified as a Src substrate. Furthermore, the results suggest that phosphorylation of Y926 and Y1008 is differentially regulated by pH. Under our conditions *in vitro*, optimum phosphorylation of Y926 occurs at pH 6.0 whereas optimum phosphorylation of Y1008 occurs at pH 6.5. These data suggest that pH affects the accessibility of Y926 and Y1008 to Src. Our NMR data suggest that pH affects the dynamics, and not the structure, of the FAT domain, which may affect phosphorylation of Y926 and Y1008 although we have not been able to fully characterize the pH-dependent dynamics.

Previous evidence has shown that because Y926 is in a helical conformation, it is not inherently conducive to recognition by Src, and a conformational change must occur in order for phosphorylation to occur [48, 49]; however, what causes this conformational change has yet to be determined. Y1008, on the other hand, is in a more unstructured region of the FAT domain. In some structures, Y1008 is in the beginning of helix-4 whereas in others it is at the end of the loop between helices-3 and -4. Our data suggest that changes in pH may represent one mechanism by which phosphorylation of Y926 is regulated. While the data also suggest that phosphorylation of Y1008 may be regulated by pH, further experiments are needed to determine whether phosphorylation of Y1008 occurs *in vivo*.

It remains to be determined whether the FAT domain of FAK is regulated by pH *in vivo*; however, our results are consistent with recent data that demonstrated a pH gradient in migrating cells (from 0.05 to 0.16 pH units depending on cell type) [63]. The

leading edge of migrating cells is slightly basic due to the ion-exchange activity of the sodium/proton exchanger NHE1. According to our data, phosphorylation of Y926 is prohibited under basic conditions, and indeed, we observe the lowest levels of Y926 phosphorylation at pH 7.5. Therefore, one might speculate that at the leading edge of cells, Y926 is less likely to be phosphorylated. The intracellular pH becomes more acidic towards the trailing edge of the cell, and according to our data, phosphorylation at Y926 increases as the pH is decreased from pH 7.5 to pH 7.0. Therefore, one might speculate that Y926 becomes phosphorylated at the trailing edge of cells due to the difference in pH between the leading and trailing edges. This hypothesis is consistent with data that demonstrate that Y926 delocalizes FAK from focal adhesions and promotes focal adhesion turnover [73]. In summary, our data support a model in which nonphosphorylated FAK localizes to focal adhesions at the leading edge of migrating cells where the pH is more basic than the overall intracellular pH. As the cell migrates, the leading edge becomes the trailing edge, and the pH becomes more acidic. These conditions promote phosphorylation of Y926 in the FAT domain, which causes delocalization of FAK from focal adhesions, focal adhesion turnover, and subsequently cell migration.

Future Directions

In this study, we demonstrated that pH affects the dynamics of the FAT domain; however, these dynamics have not been fully characterized. Attempts to characterize the pH-dependent dynamics by CPMG-based relaxation dispersion and hydrogen exchange methods were unsuccessful. It will be of interest to determine whether the pH-dependent dynamics can be characterized via other NMR techniques such as T1 rho-based

experiments or zz exchange-based experiments, which can provide information on dynamics in the ms-sec timescale. In addition, all of the experiments performed so far have investigated the backbone dynamics. It may be of use to investigate side chain dynamics as well.

Determining the titrating residue that is causing these pH-dependent changes in dynamics will provide a better picture of the pH-dependent dynamics in the FAT domain. We have individually mutated the three histidine residues, two aspartate residues, and one glutamate residue in the FAT domain and were not able to abrogate the pH-dependent stability. Further experiments would mutate the other aspartate and glutamate residues in the FAT domain and/or monitor the carboxyl carbon of aspartate and glutamate residues as a function of pH by NMR to determine if these residues are titrating within the pH 5.5 – 7.5 range.

If it is discovered that titration of a particular residue is responsible for the observed pH-dependent dynamics, the next step would be to confirm that mutation of this residue also alters the pH-dependent phosphorylation of the FAT domain *in vitro*. Finally, if the pH dependence of phosphorylation is altered upon mutation of the titrating residue, this mutant would be a good tool to verify whether pH regulates phosphorylation of Y926 *in vivo*.

On a separate note, we have shown that Y1008 is a substrate for Src *in vitro*. Future work should determine whether this site is phosphorylated *in vivo* or whether it is simply a product of our *in vitro* conditions. If Y1008 is phosphorylated *in vivo*, it will be of great interest to investigate a possible biological function of phosphorylation of Y1008. One possibility for this function could involve talin binding. As mentioned in

Chapter 4, there is preliminary evidence that the F2/F3 domain of talin binds to the FAT domain. While we were unable to detect an interaction between the F3 domain and the FAT domain, it is possible that the F2 domain is necessary for the interaction. Data from the laboratory of Dr. David Schleapfer has localized the talin binding site on the FAT domain to a region that encompasses Y1008. Therefore, it would be interesting to determine whether phosphorylation of Y1008 affects talin binding.

Finally, the original goal of this project was to determine how phosphorylation at Y926 affects the structure, dynamics, and ligand binding properties of the FAT domain. However, because we were unable to generate a singly phosphorylated species at Y926, we were unable to investigate the effect of phosphorylation at Y926. One way to circumvent this issue would be to mutate Y1008. We have been hesitant about mutating Y1008 because we did not want the mutation to affect the structural or functional properties of the FAT domain, and we wanted to wait until we had data on the relative levels of phosphorylation at Y1008 versus Y926. However, since it now appears that we are unable to preferentially phosphorylate Y926 *in vitro*, mutation of Y1008 is probably the only means to investigate the role of phosphorylation of Y926. Any Y1008 mutant would have to be characterized *in vitro* to ensure that the mutation does not change the structure, stability or paxillin binding of the FAT domain. Once an appropriate Y1008 mutant is found, it should be fairly straightforward to phosphorylate the FAT domain *in vitro.* Previous work by Dr. Kirk Prutzman in the Campbell lab has demonstrated that we can purify the phosphorylated form of the FAT domain from the nonphosphorylated form by ion exchange chromatography. Therefore, it should be relatively straightforward to

purify a Y926-phosphorylated species, which can be characterized by CD, NMR, and paxillin binding.

Characterization of Y926 Mutants

Summary

1. We created several nonphosphorylatable (Y926F, Y926A, Y926N) and phosphomimetic (Y926E, Y926D) mutants.
2. Analysis by CD reveals that Y926F and Y926A show similar stability and similar pH sensitivity to wild type FAT. The Y926N mutant is less stable than wild type but shows similar pH sensitivity. The Y926D and Y926E mutants are also less stable than wild type and are less sensitive to pH.
3. The ^{1}H-^{15}N HSQC spectra of these mutants show considerable changes in chemical shift compared to wild type. Therefore, further NMR experiments are required to assess any structural change in the FAT domain upon mutation of Y926.
4. All the Y926 mutants show decreases paxillin binding compared to wild type, with the Y926F mutant being most similar to wild type.

Implications

The results described in Chapter 3 demonstrate that mutation of Y926 in the FAT domain disrupts paxillin binding. These results are consistent with those of Kaneda et al., which showed that the Y926F mutant was deficient in paxillin binding [47]. However, these are the first results to show that introducing a negative charge at Y926 via mutation to a glutamate or aspartate virtually eliminates paxillin binding. These results suggest that phosphorylation at Y926 may have similar consequences, and while it has been

suggested that phosphorylation at Y926 is incompatible with paxillin binding, it has not been demonstrated.

Furthermore, the fact that every mutation at Y926 that we have tested disrupts paxillin binding suggests that Y926 may play an important role in recognizing paxillin. The current structural data on a possible interaction between Y926 and paxillin is lacking because structures have only been solved with paxillin peptides. Again, if Y926 is essential for recognition of paxillin by the FAT domain, either via hydrophobic or hydrogen bonding interactions, perturbation at this site via phosphorylation would be expected to disrupt paxillin binding, which would not only affect FAK localization but also FAK signaling as paxillin is a substrate of FAK and phosphorylation at Y926 creates a binding site for the SH2 domain of Grb2.

Finally, we have observed by CD that the stabilities of the Y926E and Y926D mutants are less sensitive to pH than wild type. As described in Chapter 2, we have put forth a model in which phosphorylation of the FAT domain may be regulated by pH *in vivo*. While this model remains to be tested, if the FAT domain is regulated by pH *in vivo*, our results with the Y926E and Y926D mutants suggest that phosphorylation may alter the way pH affects the FAT domain and may decrease the sensitivity of the FAT domain to pH. Therefore, according to our model, the FAT domain is phosphorylated at the trailing edge of the cell where the pH is more acidic than the leading edge. Once phosphorylated, FAK delocalizes from focal adhesions and participates in MAPK signaling via its interaction with Grb2 and pH no longer plays a role in regulation of the phosphorylated FAT domain.

Future Directions

Our data suggest that Y926 plays a key role in paxillin binding and that any perturbation at this site would disrupt paxillin binding. Further studies need to be done to validate this hypothesis. First, our fluorescence polarization binding studies with the FAT domain were conducted with a short peptide designed to mimic the LD2 motif of paxillin. As explained in Chapter 3, the N-terminus of this peptide is near Y926 in the FAT domain. Therefore, these experiments may not be sensitive to interactions between Y926 and paxillin. One solution is to repeat these experiments with a longer paxillin construct. We would probably only need to extend the paxillin peptide by five or six amino acids to capture the interaction between Y926 and paxillin. Fluorescence polarization may not be the best experiment to test the longer paxillin construct as our dynamic range with the experiment is already on the low side, and increasing the size of the peptide will further limit the dynamic range. ITC would be more suited for these experiments as the size of the peptide would not affect the dynamic range of the signal. Furthermore, ITC has several advantages over fluorescence polarization in that it provides information on stoichiometry and energetics of binding in addition to affinity. Since we know that the LD2 peptide binds to two sites on the FAT domain [43] and Y926 is expected to effect one the sites but not the other, information regarding the stoichiometry of binding would be useful in interpreting the change in paxillin binding observed upon mutation of Y926.

Further characterizing the structure of the Y926 mutants by NMR will also help us interpret the change in paxillin binding of these mutants. To accomplish this, we must first assign the ^{1}H-^{15}N HSQC spectra of the mutants by collecting a 3D HNCACB dataset

for each mutant. Once that is accomplished, we can assess structural changes in the Y926 mutants by collecting NH RDCs and Hα-Cα RDCs. If any of these mutations appear to be causing a structural change, we may acquire further structural data such as NOEs. In particular, the Y926E mutant may be of interest as it may mimic the effects of phosphorylation; also, the Y926F mutant may also be of interest as it has been used in several studies in vivo to assess the role of phosphorylation.

Finally, to assess the role of Y926 in paxillin binding, we could model the interaction between the LD2 peptide of paxillin and the FAT domain in silico. This process would consist of starting from one of the solved structures of the LD2 peptide and the FAT domain, extending the paxillin peptide in silico, assessing the interaction between Y926 and LD2, and mutating Y926 to phenylalanine, aspartate, glutamate, alanine, and asparagine to determine how mutation might affect specific interactions between the FAT domain and paxillin. Furthermore, it may be possible to model in a phosphorylated tyrosine at Y926 to assess how phosphorylation might change specific interactions between the FAT domain and paxillin and to help us determine whether mutation to aspartate or glutamate would mimic the effects of phosphorylation. These studies would shine new light on the role of Y926 in paxillin binding and hopefully provide perspective on how phosphorylation of Y926 might affect paxillin binding.

FAT/Talin Interactions

Summary

1. We were unable to detect an interaction between the FAT domain and the F3 domain of talin *in vitro* by either gel filtration or NMR.

Implications

The possibility of an interaction between the FAT domain of FAK and talin has been a controversial issue with some groups detecting an interaction [41, 42] and other groups unable to detect an interaction [39]. There are several explanations for this discrepancy. First, the interaction between talin and the FAT domain may be indirect. While attempts were made to distinguish between a direct and indirect interaction, and the data suggested a direct interaction [41], no binding studies have been conducted with purified components. Second, post-translational modifications may be necessary for the interaction between the FAT domain and talin. We would not expect phosphorylation of Y926 to promote talin binding as talin binding is associated with focal adhesion localization and phosphorylation of Y926 is associated with delocalization. However, there may be other sites of post-translational modification on either the FAT domain or talin that promote binding between these two proteins. One possibility is phosphorylation of Y1008 in the FAT domain, which we described in Chapter 2. Data from the Schlaepfer laboratory has localized the talin binding site on the FAT domain to a region encompassing Y1008 (personal communication). Therefore, it will be interesting to see how phosphorylation at Y1008 might affect talin binding, if at all.

Future Directions

We were unable to detect an interaction between the FAT domain of FAK and the F3 domain of talin *in vitro* via gel filtration and NMR. While the F3 domain of talin is the minimal domain necessary for binding to the FAT domain (Dr. David Schlaepfer, personal communication), most of the binding assays were performed with a construct containing the F2 and F3 domains of talin. While we have had trouble finding an F2/F3

construct of talin that remained soluble at ~100 μM upon addition of the FAT domain, other groups have had success crystallizing an F2/F3 domain construct [94], which they were able to concentrate to 250 μM. Therefore, future studies should attempt to purify the F2/F3 domain describe in Anthis el al. [94] and repeat the gel filtration and NMR experiments described in Chapter 4.

If we are able to detect an interaction between the FAT domain of FAK and the F2/F3 domain of talin, then a whole world of possibilities is opened up. First, we would want to characterize the binding by either pull-down experiments, ITC, SPR. We would also attempt to structurally characterize the complex by NMR. If we could gain structural information on the complex, we could potentially design mutants in FAK that would disrupt talin binding to be used in cells to assess the role of talin binding. Furthermore, the structure between the FAT domain and talin would provide information on whether phosphorylation of Y1008 would be expected to disrupt, or perhaps promote, this interaction, which could support the notion that phosphorylation of Y1008 is relevant *in vivo*.

WORKS CITED

1. Cornillon, J., L. Campos, and D. Guyotat, *Focal Adhesion Kinase (FAK), une proteine aux fonctions multiples.* Medecine Sciences, 2003. **19**: p. 743-752.

2. Hauck, C.R., D.A. Hsia, and D.D. Schlaepfer, *The Focal Adhesion Kinase - A Regulator of Cell Migration and Invasion.* IUBMB Life, 2002. **53**: p. 115-119.

3. Mitra, S.K., D.A. Hanson, and D.D. Schlaepfer, *Focal Adhesion Kinase: In Command and Control of Cell Motility.* Nature Reviews, 2005. **6**: p. 56-68.

4. Petit, V. and J.-P. Thiery, *Focal Adhesions: Structure and Dynamics.* Biology of the Cell, 2000. **92**: p. 477-494.

5. Schaller, M.D., et al., *pp125FAK, a structurally distinctive protein-tyrosine kinase associated with focal adhesions.* PNAS, 1992. **89**: p. 5192-5196.

6. Hanks, S.K., et al., *Focal adhesion protein-tyrosine kinase phosphorylated in response to cell attachment to fibronectin.* PNAS, 1992. **89**: p. 8487-8491.

7. Ilic, D., et al., *Reduced cell motility and enhanced focal adhesion contact formation in cells from FAK-deficient mice.* Nature 1995. **377**: p. 539-544.

8. Webb, D.J., et al., *FAK-Src signalling through paxillin, ERK and MLCK regulates adhesion disassembly.* Nature Cell Biology, 2004. **6**: p. 154-161.

9. Hungerford, J., et al., *Inhibition of pp125FAK in cultured fibroblasts results in apoptosis.* J Cell Biol, 1996. **135**(5): p. 1383-90.

10. Ryu, S.J., et al., *Role of Src-specific phosphorylation site on focal adhesion kinase for senescence-associated apoptosis resistance.* Apoptosis, 2006. **11**: p. 303-313.

11. Ilic, D., et al., *Extracellular Matrix Survival Signals Transduced by Focal Adhesion Kinase Suppresses p53-mediated Apoptosis.* J Cell Biol, 1998. **143**(2): p. 547-560.

12. Xu, L., et al., *Attenuation of the expression of the focal adhesion kinase induces apoptosis in tumor cells.* Cell Growth Differ, 1996. **7**(4): p. 413-8.

13. Cary, L., J. Chang, and J. Guan, *Stimulation of cell migration by overexpresison of focal adhesion kinase and its association with Src and Fyn.* J Cell Sci, 1996. **109**: p. 1787-94.

14. Crowe, D.L. and A. Ohannessian, *Recruitment of focal adhesion kinase and paxillin to B1 integrin promote cancer cell migration via mitogen activated protein kinase activation.* BMC Cancer, 2004. **4**(18).

15. Peng, X., et al., *Overexpression of focal adhesion kinase in vascular endothelial cells promotes angiogenesis in transgenic mice.* Cardiovascular Research, 2004. **64**(421-430).

16. McLean, G.W., et al., *The Role of Focal Adhesion Kinase in Cancer - a New Therapeutic Opportunity.* Nature Reviews, 2005. **5**: p. 505-515.

17. Parsons, J.T., *Focal Adhesion Kinase: the First Ten Years.* Journal of Cell Science, 2003. **116**: p. 1409-1416.

18. Rothhut, B., et al., *Epidermal Growth Factor Stimulates Matrix Metalloproteinase-9 Expression and Invastion in Human Follicular Thyroid Carcinoma cells Through Focal Adhesion Kinase.* Biochimie, 2007. **89**: p. 613-624.

19. Mitra, S., et al., *Intrinsic FAK Activity and Y925 Phosphorylation Facilitate an Angiogenic Switch in Tumors.* Oncogene, 2006: p. 1-16.

20. Decaestecker, C., et al., *Can Anti-Migratory Drugs Be Screened In Vitro? A Review of 2D and 3D Assays for the Quantitative Analysis of Cell Migration.* Medicinal Research Reviews, 2006. **27**(2): p. 149-176.

21. Hauck, C.R., et al., *Inhibition of Focal Adhesion Kinase Expression or Activity Disrupts Epidermal Growth Factor-stimulated Signaling Promoting the Migration of Invasive Human Carcinoma Cells.* Cancer Res, 2001. **61**: p. 7079.

22. Smith, C., et al., *Effect of focal adhesion kinase (FAK) downregulation with FAK antisense oligonucleotides and 5-fluorouracil on the viability of melanoma cell lines.* Melanoma Res, 2005. **15**(5): p. 357-62.

23. Han, E., et al., *Functional anaylsis of focal adhesion kinase (FAK) reduction by small inhibitory RNAs.* Anitcancer Res, 2004. **24**: p. 3899-905.

24. Schultze, A. and W. Fiedler, *Therapeutic potential and limitations of new FAK inhibitors in the treatment of cancer.* Expert Opin. Investig. Drugs, 2010. **19**(6): p. 777-88.

25. Bantscheff, M., et al., *Quantitative chemical proteomics reveals mechanisms of action of clinical ABL kinase inhibitor.* Nature Biotechnology, 2007. **25**: p. 1035-1044.

26. Ko, B.-S., T.-C. Chang, and J.-Y. Liou, *Focal adhesion kinase as a therapeutic target of bortezomib.* Anticancer Agents Med Chem, 2010. **10**(10): p. 747-52.

27. Ko, B.-S., et al., *Bortezomib suppresses focal adhesion kinase expression via interrupting nuclear factor-kappa B.* Life Sciences, 2010. **86**: p. 199-206.

28. Schlaepfer, D.D. and S.K. Mitra, *Multiple Connections link FAK to Cell Motility and Invasion.* Current Opinion in Genetics and Development, 2004. **14**: p. 92-101.

29. Dunty, J.M., et al., *FERM domain interaction promotes FAK signaling.* Molecular and Cellular Biology, 2004. **24**: p. 5353-5368.

30. Lietha, D., et al., *Strucutural basis for the autoinhibition of focal adhesion kinase.* Cell, 2007. **129**: p. 1177-1187.

31. Cooper, L.A., T.L. Shen, and J.L. Guan, *Regulation of focal adhesion kinase by its amino-terminal domain through an autoinhibitory interaction.* Molecular and Cellular Biology, 2003. **23**: p. 8030-8041.

32. Cohen, L.A. and J.L. Guan, *Residues within the first subdomain of the FERM-like domain in focal adhesion kinase are important in its regulation.* Journal of Biological Chemistry, 2005. **280**: p. 8197-8207.

33. Schlaepfer, D.D. and T. Hunter, *Evidence for in vivo phosphorylation of the Grb2 SH2-domain binding site on focal adhesion kinase by Src-family protein-tyrosine kinases.* Mol Cell Biol, 1996. **16**(10): p. 5623-33.

34. Tachibana, K., et al., *Direct Assocation of $pp125^{FAK}$ with Paxillin, the Focal Adhesion-Targeting Mechanism of $pp125^{FAK}$.* Journal of Experimental Medicine, 1995. **182**: p. 1089-1100.

35. Katz, B.Z., et al., *Targeting membrane-localized focal adhesion kinase to focal adhesions: roles of tyrosine phosphorylation and SRC family kinases.* J Biol Chem, 2003. **278**(31): p. 29115-20.

36. Schlaepfer, D.D. and T. Hunter, *Focal Adhesion Kinase Overexpression Enhances Ras-dependent Integrin Signaling to ERK2/Mitogen-activated Protein Kinase through Interactions with and Activation of c-Src.* The Journal of Biological Chemistry, 1997. **272**(20): p. 13189-13195.

37. Hildebrand, J.D., M.D. Schaller, and J.T. Parsons, *Identification of Sequences Required for the Efficient Localization of the Focal Adhesion Kinase, pp125FAK, to Cellular Focal Adhesions.* The Journal of Cell Biology, 1993. **123**(4): p. 993-1005.

38. Schaller, M., C. Borgman, and J. Parsons, *Autonomous expression of a noncatalytic domain of the focal adhesion-associated protein tyrosine kinase pp125FAK.* Mol Cell Biol, 1993. **13**(2): p. 785-91.

39. Scheswohl, D.M., et al., *Multiple paxillin binding sites regulate FAK function.* Journal of Molecular Signaling, 2008. **3**(1).

40. Bertolucci, C.M., C.D. Guibao, and J. Zheng, *Structural Features of the Focal Adhesion Kinase-Paxillin Complex give Insight into the Dynamics of Focal Adhesion Assembly.* Protein Science, 2005. **14**: p. 644-652.

41. Chen, H.-C., et al., *Interaction of Focal Adhesion Kinase with Cytoskeletal Protein Talin.* The Journal of Biological Chemistry, 1995. **270**(28): p. 16995-16999.

42. Zheng, C., et al., *Differential Regulation of Pyk2 and Focal Adhesion Kinase (FAK) The C-Terminal Domain of FAK Confers Response to Cell Adhesion.* The Journal of Biological Chemistry, 1998. **273**(4): p. 2384-2389.

43. Gao, G., et al., *NMR Solution Structure of the Focal Adhesion Targeting Domain of Focal Adhesion Kinase in Complex with a Paxillin LD Peptide: Evidence for a two-site binding model.* The Journal of Biological Chemistry, 2004. **279**(9): p. 8441-8451.

44. Hayashi, I., K. Vuori, and R.C. Liddington, *The Focal Adhesion Targeting (FAT) Region of Focal Adhesion Kinase is a Four-Helix Bundle that Binds Paxillin.* Nature Structural Biology, 2002. **9**(2): p. 101-106.

45. Deramaudt, T.B., et al., *FAK phosphorylation at Tyr-925 regulates cross-talk between focal adhesion turnover and cell protrusion.* Molecular Biology of the Cell, 2011. **22**(7): p. 964-75.

46. Songyang, Z., et al., *SH2 Domains Recognize Specific Phosphopeptide Sequences.* Cell, 1993. **72**: p. 767-778.

47. Kaneda, T., et al., *Mutation of Y925F in focal adhesion kinase (FAK) suppresses melanoma cell proliferation and metastasis.* Cancer Letters, 2008.

48. Arold, S.T. and M.K. Hoellerer, *The Structural Basis of Localization and Signaling by the Focal Adhesion Targeting Domain.* Structure, 2002. **10**: p. 319-327.

49. Prutzman, K.C., et al., *The Focal Adhesion Targeting Domian of Focal Adhesion Kinase Contains a Hinge Region that Modulates Tyrosine 926 Phosphorylation.* Structure, 2004. **12**: p. 881-891.

50. Dixon, R.D.S., et al., *New Insights into FAK Signaling and Localization Based on Detection of a FAT Domain Folding Intermediate.* Structure, 2004. **12**: p. 2161-2171.

51. Zhou, Z., H. Feng, and Y. Bai, *Detection of a Hidden Folding Intermediate in the Focal Adhesion Targetin Domain: Implications for its Function and Folding.* Proteins: Structure, Function, and Bioinformatics, 2006. **65**: p. 259-265.

52. Bergdoll, M., et al., *Proline-dependent oligomerization with arm exchange.* Structure, 1997. **5**: p. 391-401.

53. Rousseau, F., et al., *Three-dimensional domain swapping in p13suc1 occurs in the unfolded state and is controlled by conserved proline residues.* PNAS, 2001. **98**(10): p. 5596-5601.

54. Donato, A.D., V. Cafaro, and G. D'Alessio, *Ribonuclease A Can Be Transformed into a Dimeric Ribonuclease with Antitumor Activity.* The Journal of Biological Chemistry, 1994. **269**: p. 17394-17396.

55. Hoellerer, M.K., et al., *Paxillin LD4 motif bound to the Focal Adhesion Targeting (FAT) domain of the Focal Adhesion Kinase.* Structure, 2003. **11**: p. 1207-1217.

56. Liu, G., C.D. Guibao, and J. Zheng, *Structural Insight into the Mechanisms of Targeting and Signaling of Focal Adhesion Kinase.* Molecular and Cellular Biology, 2002. **22**(8): p. 2751-2760.

57. Bose, R., et al., *Protein tyrosine kinase-substrate interactions.* Current Opinion in Structural Biology, 2006. **16**: p. 668-675.

58. Hubbard, S.R., *Crystal Structure of the Activated Insulin Receptor Tyrosine Kinase in Complex with Peptide Substrate and ATP Analog.* The EMBO Journal, 1997. **16**(18): p. 5573-5581.

59. Gaul, B.S., et al., *Substrate Recognition by the Lyn Protein-tyrosine Kinase.* The Journal of Biological Chemistry, 2000. **275**(21): p. 16174-16182.

60. Ettmayer, P., et al., *GRB2-SH2 Domain in Complex with Cyclo-[N-alpha-acetyl-L-thialysyl-O-phosphotyrosyl-valyl-asparagyl-valyl-prolyl] (PKF273-791).* Journal of Medicinal Chemistry, 1999. **42**: p. 971-980.

61. Rahuel, J., et al., *Structural basis for specificity of GRB2-SH2 revealed by a novel ligand binding mode.* Nature Structural and Molecular Biology, 1996. **3**: p. 586-589.

62. Ogura, K., et al., *Solution Structure of the SH2 Domain of Grb2 Complexed with the Shc-derived Phosphotyrosine-containing Peptide.* J. Mol. Biol., 1999. **289**: p. 439-445.

63. Martin, C., et al., *Intracellular pH gradients in migrating cells.* Am J Physiol Cell Physiol, 2010.

64. Stock, C. and A. Schwab, *Protons make tumor cells move like clockwork.* Pflugers Arch - Eur J Physiol, 2009. **458**: p. 981-992.

65. Denker, S. and D. Barber, *Cell migration requires both ion translocation and cytoskeletal anchoring by the Na-H exchanger NHE1.* J Cell Biol, 2002. **159**(6): p. 1087-96.

66. Grinstein, S., et al., *Focal localization of the NHE-1 isoform of the Na+/H+ antiport: assessment of effects on intracellular pH.* EMBO J, 1993. **12**(13): p. 5209-18.

67. Ilic, D., et al., *Focal Adhesion Kinase Controls pH-Dependent Epidermal Barrier Homeostasis by Regulating Actin-Directed Na^+/H^+ Exchanger 1 Plasma Membrane Localization.* The American Journal of Pathology, 2007. **170**(6): p. 1-13.

68. Pouyssegur, J., et al., *Cytoplasmic pH, a key determinant of growth factor-induced DNA synthesis in quiescent fibroblasts.* FEBS Letters, 1985. **190**(1): p. 115-119.

69. Schelling, J. and B.A. Jawdeh, *Regulation of cell survival by Na+/H+ exchanger-1.* Am J Physiol Renal Physiol, 2008. **295**(3): p. F625-32.

70. Casey, J.R., S. Grinstein, and J. Orlowski, *Sensors and regulators of intracellular pH.* Nature Reviews Molecular Cell Biology, 2010. **11**: p. 50-61.

71. Srivastava, J., D.L. Barber, and M.P. Jacobson, *Intracellular pH Sensors: Design Principles and Functional Significance.* Physiology, 2007. **22**: p. 30-39.

72. Srivastava, J., et al., *Structural model and functional significance of pH-dependent talin-actin binding for focal adhesion remodeling.* PNAS, 2008. **105**(38): p. 14436-14441.

73. Katz, B.-Z., et al., *Targeting Membrane-localized Focal Adhesion Kinase to Focal Adhesions: Roles of Tyrosine Phosphorylation and Src Family Kinases.* The Journal of Biological Chemistry, 2003. **278**: p. 29115-29120.

74. Ciccimaro, E., J. Hevko, and I.A. Blair, *Analysis of phosphorylation sites on focal adhesion kinase using nanospray liquid chromatography/multiple reaction monitoring mass spectrometry.* Rapid Communications in Mass Spectrometry, 2006. **20**: p. 3681-3692.

75. Lipari, G. and A. Szabo, *Model-free approach to the interpretation of nuclear magnetic resonance relaxation in macromolecules. 2. Analysis of experimental results.* Journal of the American Chemical Society, 1982. **104**(17): p. 4559.

76. Korzhnev, D.M. and L.E. Kay, *Probing Invisible, Low-Populated States of Protein Molecules by Relaxation Dispersion NMR Spectroscopy: An Application to Protein Folding.* Accounts of Chemical Research, 2008. **41**(3): p. 442-451.

77. Hwang, T., P. van Zijl, and S. Mori, *Accurate quantitation of water-amide proton exchange rates using the phase-modulated CLEAN chemical EXchange (CLEANEX-PM) approach with a Fast-HSQC (FHSQC) detection scheme.* J Biomol NMR, 1998. **11**(2): p. 221-226.

78. Chen, H.A., et al., *Determination of pKa Values of Carboxly Groups in the N-Terminal Domain of Rat CD2: Anomalous pKa of a Glutamate on the Ligand-Binding Surface.* Biochemistry, 2000. **39**: p. 6814-6824.

79. Lindman, S., et al., *pKa Values for Side-Chain Carboxyl Groups of a PGB1 Variant Explain Salt and pH-Dependent Stability.* Biophysical Journal, 2007. **92**: p. 257-266.

80. Gasteiger, E., et al., *Protein Identification and Analysis Tools on the ExPASy Server*, in *The Proteomics Protocols Handbook*, J.M. Walker, Editor. 2005, Humana Press. p. 571-607.

81. Wang, Y., et al., *A new strategy to produce active human Src from bacteria for biochemical study of its regulation.* Biochem Biophys Res Commun, 2006. **346**(2): p. 606-11.

82. Seeliger, M.A., et al., *High Yield Bacterial Expression of Active c-Able and c-Src Tyrosine Kinases.* Protein Science, 2006. **14**: p. 3135-3139.

83. Pascal, S.M., et al., *Simultaneous acquisition of 15N and 13C NOE spectra of proteins in H2O.* J. Magn. Reson. Series B, 1994. **103**: p. 197-201.

84. Grzesiek, S. and A. Bax, *Correlating backbone amide and side chain resonances in larger proteins by multiple relayed triple resonance nmr.* J. Am. Chem. Soc., 1992. **114**(16): p. 6291-6293.

85. Delaglio, F., et al., *NMRPipe: a multidimensional spectal processing system based on UNIX pipes.* J. Biom. NMR, 1995. **6**: p. 277-293.

86. Johnson, B.A., *Using NMRView to visualize and analyze the NMR spectra of macromolecules.* Methods Mol Biol., 2004. **278**: p. 313-52.

87. Dellwo, M.J. and A.J. Wand, *Model-independent and model-dependent analysis of the global and internal dynamics of cyclosporin A.* J Am Chem Soc, 1989. **111**(13): p. 4571-4578.

88. Clarkson, M.W., et al., *Dynamic coupling and allosteric behavior in a nonallosteric protein.* Biochemistry, 2006. **45**(25): p. 7693-9.

89. Lee, A.L., P.F. Flynn, and A.J. Wand, *Comparison of H-2 and C-13 NMR relaxation techniques for the study of protein methyl group dynamics in solution.* J Am Chem Soc, 1999. **121**(12): p. 2891-2902.

90. Ottiger, M., F. Delaglio, and A. Bax, *Measurement of J and dipolar couplings from simplified two-dimensional NMR specra.* J Magn Reson, 1998. **131**(2): p. 373-8.

91. Shen, Y. and M. Schaller, *Focal adhesion targeting: the critical determinant of FAK regulation and substrate phosphorylation.* Mol Biol Cell, 1999. **10**(8): p. 2507-18.

92. Critchley, D.R., *Biochemical and Structural Properties of the Integrin-Associated Cytoskeletal Protein Talin.* Annu. Rev. Biophys., 2009. **38**: p. 235-54.

93. Elliott, P.R., et al., *The Structure of the Talin Head Reveals a Novel Extended Conformation of the FERM Domain.* Structure, 2010. **18**(10): p. 1289-1299.

94. Anthis, N.J., et al., *The structure of an integrin/talin complex reveals the basis of inside-out signal transduction.* EMBO, 2009. **28**(22): p. 3623-3632.